Homebuilt 4, 12 and 20 GHz Microwave Radiometers

by
Norman Grody (ngantique@hotmail.com)

This paper describes the construction and measurements of ground-based microwave radiometers. However, some of its most unique applications involves satellite observations.
This talk therefore contains two parts.

1. Satellite microwave radiometer applications in earth remote sensing.

   (a) Measuring earth's surface (snow cover, sea ice, soil moisture, etc.,)

   (b) Measuring earth's atmosphere (temperature, water vapor, rain rate, etc.,)

2. Ground-based radiometer construction & measurements (4, 12, 20 GHz)

   (a) Stability, calibration issues (detector linearity, dynamic range, temperature)

   (b) Measurements (temperature, soil moisture, rain rate, clouds, water vapor)

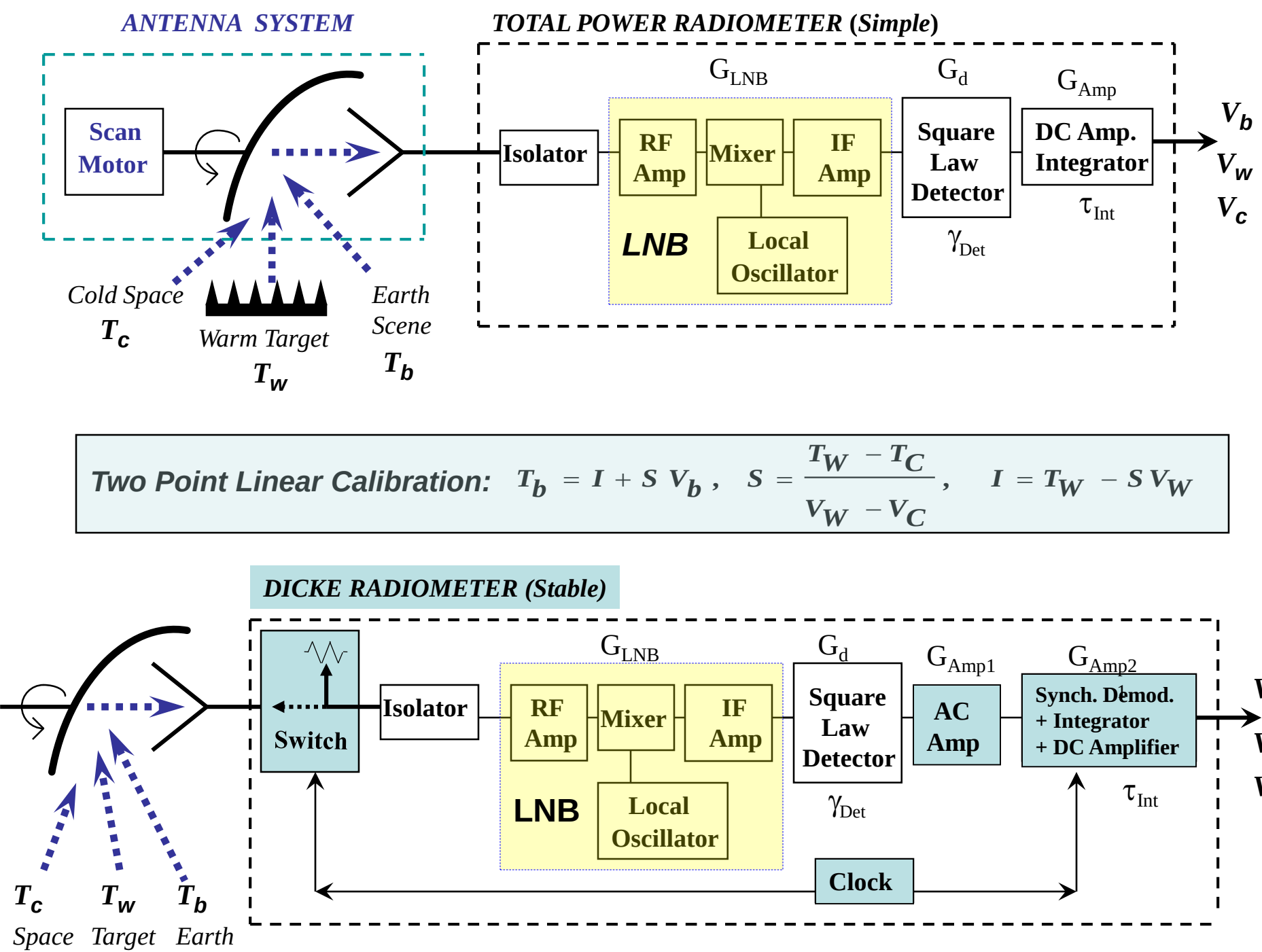
ANTENNA SYSTEM
TOTAL POWER RADIOMETER (Simple)
Scan Motor
Isolator
RF Amp
Mixer
IF Amp
LNB
Local Oscillator
Square Law Detector
DC Amp. Integrator
G_{LNB}
G_d
G_{Amp}
τ_{Int}
γ_{Det}
V_b
V_w
V_c
Cold Space
T_c
Warm Target
T_w
Earth Scene
T_b
Two Point Linear Calibration: $T_b = I + S\,V_b$, $S = \frac{T_W - T_C}{V_W - V_C}$, $I = T_W - S\,V_W$
DICKE RADIOMETER (Stable)
Switch
Isolator
RF Amp
Mixer
IF Amp
LNB
Local Oscillator
Square Law Detector
AC Amp
Synch. Demod. + Integrator + DC Amplifier
Clock
G_{LNB}
G_d
G_{Amp1}
G_{Amp2}
τ_{Int}
γ_{Det}
V_b
V_w
V_c
T_c Space
T_w Target
T_b Earth

Generic LNB Block Diagram

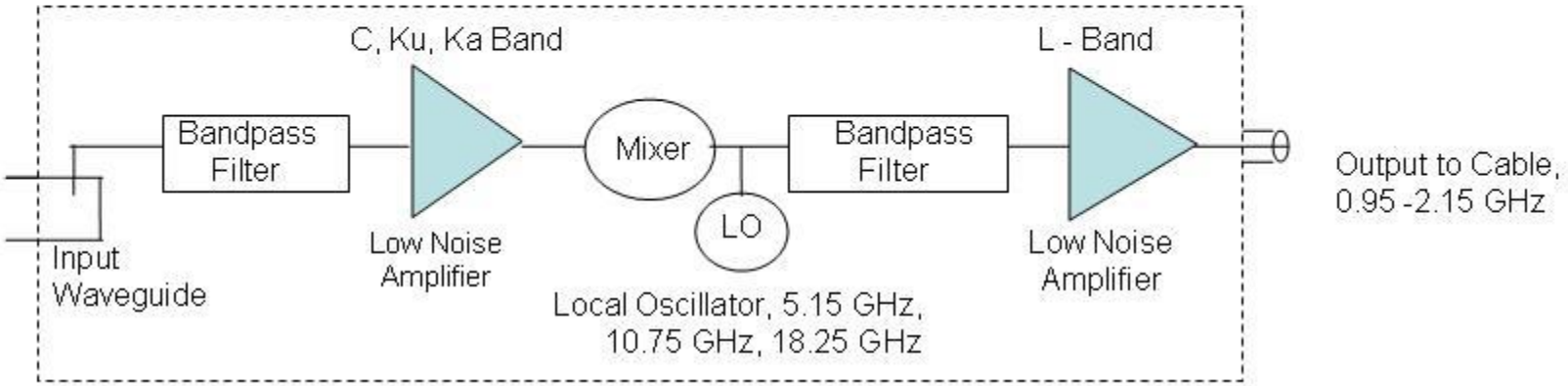

C - Band =	3.4 – 4.2 GHz	(4 GHz)	LO= 5.15 GHz
Ku - Band =	10.7 – 12.7 GHz	(12 GHz)	LO= 10.75 GHz
Ka - Band =	18.3 – 20.2 GHz	(19 GHz)	LO= 18.25 GHz

LNB's are the Key Radiometer Component

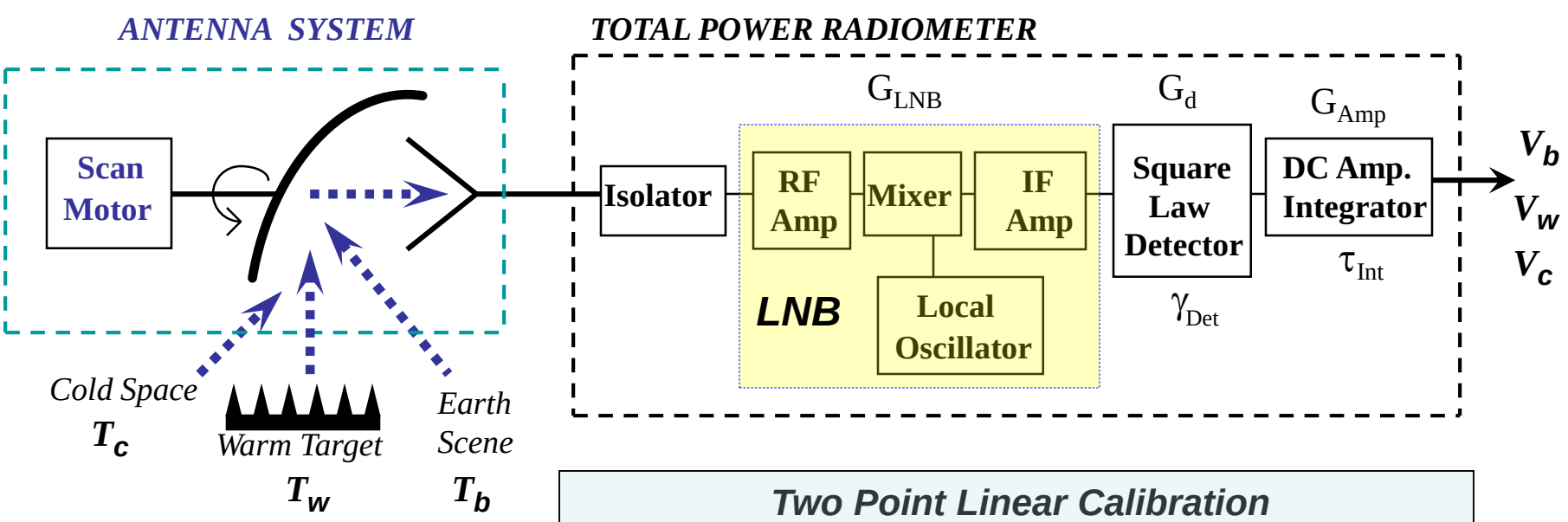

Two Point Linear Calibration

$$T_b = I + S\,V_b\,, \quad S = \frac{T_W - T_C}{V_W - V_C}\,, \quad I = T_W - S\,V_W$$

RADIOMETER NOISE EQUIVALENT TEMPERATURE (NEΔT)

$$\Delta T_b\big]_{\text{Total Power}} = \sqrt{\frac{(T_b + T_N)^2}{B_{IF}\ \tau_{\text{int}}} + \left(\frac{\Delta G}{G}\right)^2} \quad \text{where} \quad G = \underbrace{G_{LNB} G_{Amp} G_d}_{G'}\ \gamma_{det}$$

RADIOMETER DRIFT DUE TO TEMPERATURE CHANGE

$$V_b = k\,(G'\,\gamma_{det})\,B_{IF}\,T_b\,, \qquad \frac{\Delta V_b}{\Delta t} = k\,B_{IF}\,T_b\left[G'\underbrace{\left(\frac{\Delta \gamma_{det}}{\Delta T}\right)}_{\text{Detector}} + \gamma_{det}\underbrace{\left(\frac{\Delta G'}{\Delta T}\right)}_{\text{LNB \& DC Amplifiers}}\right]\left(\frac{\Delta T}{\Delta t}\right)$$

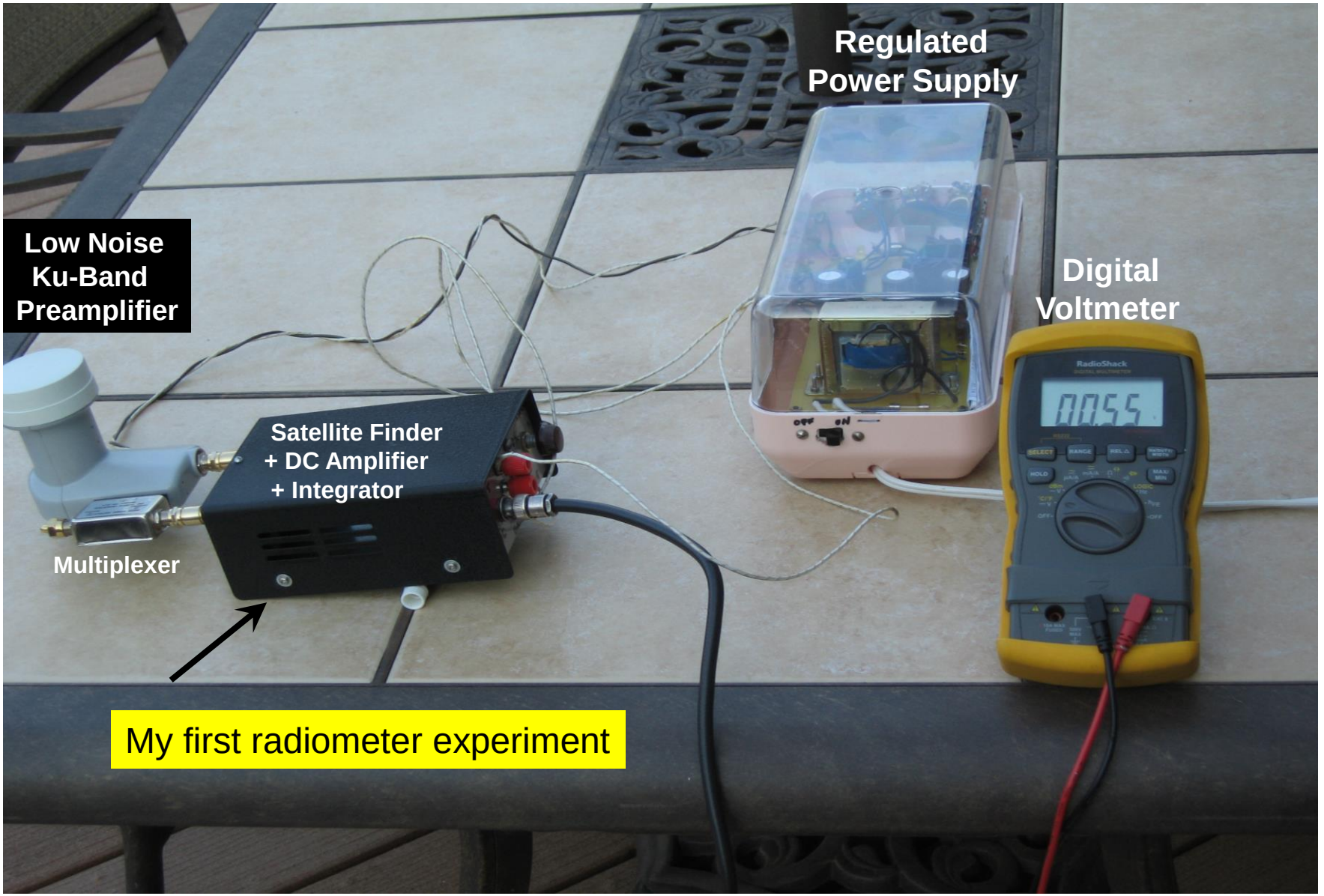

Total Power Radiometer using a Ku band (11 - 12 GHz) Low Noise Preamplifier. Note the low voltage reading (0.55 v) as it views space. The radiometer is adjusted so that the output voltage increases to about 10.5 V maximum when viewing earth. The sensitivity is therefore 10 V/330 K or 30 millivolts/ K .

Total Power Microwave Radiometer

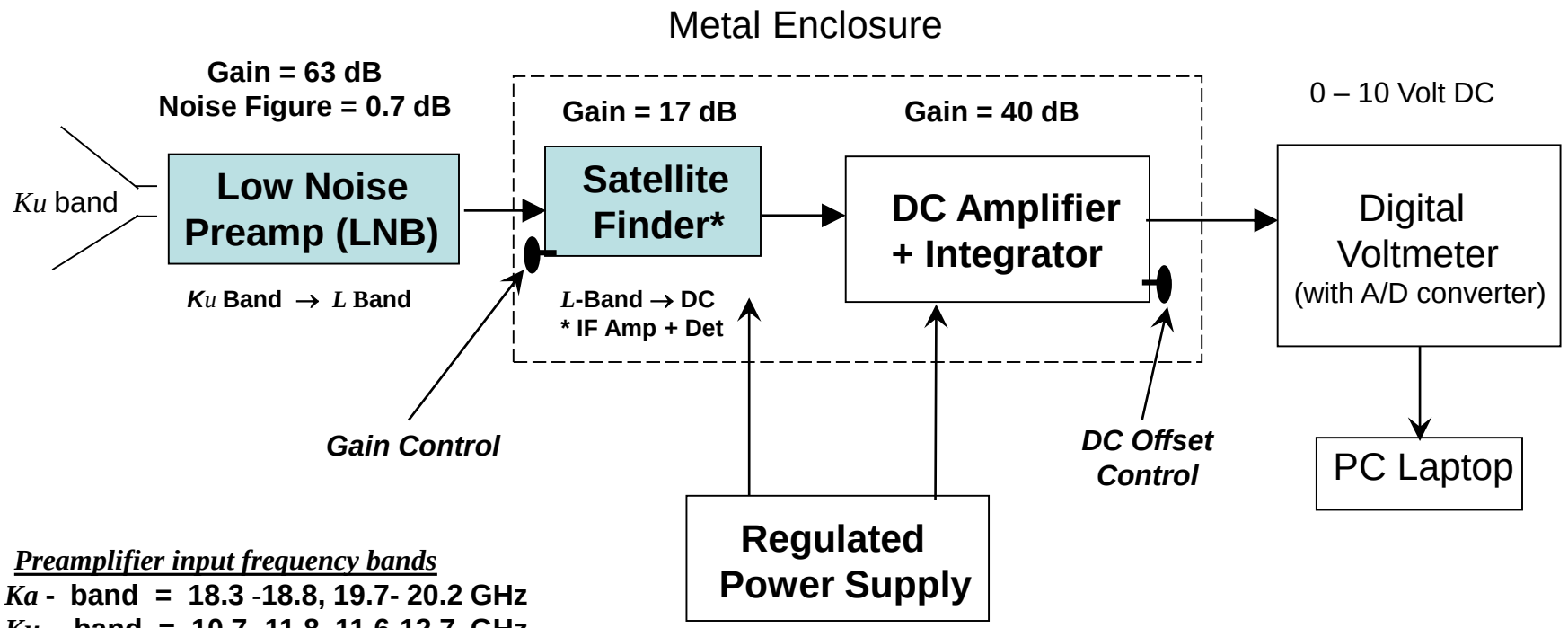

Preamplifier input frequency bands

Ka **- band = 18.3 -18.8, 19.7- 20.2 GHz**
Ku **- band = 10.7- 11.8, 11.6-12.7 GHz**
C **- band = 3.40 - 4.20 GHz**

Preamplifier output frequency bands

L **- band = 0.95 - 2.15 GHz (*Ku* - band)**
L **- band = 0.95 - 1.75 GHz (*C* - band)**

Wide band *Ku* band radiometer built using a Direct TV satellite receiver (*LNB*), satellite finder (*IF* amplifier + detector) and DC amplifier. It's sensitivity is 30 mvolts/*K*. The radiometer also works at *C* - and *Ka* band by changing the *LNB*.

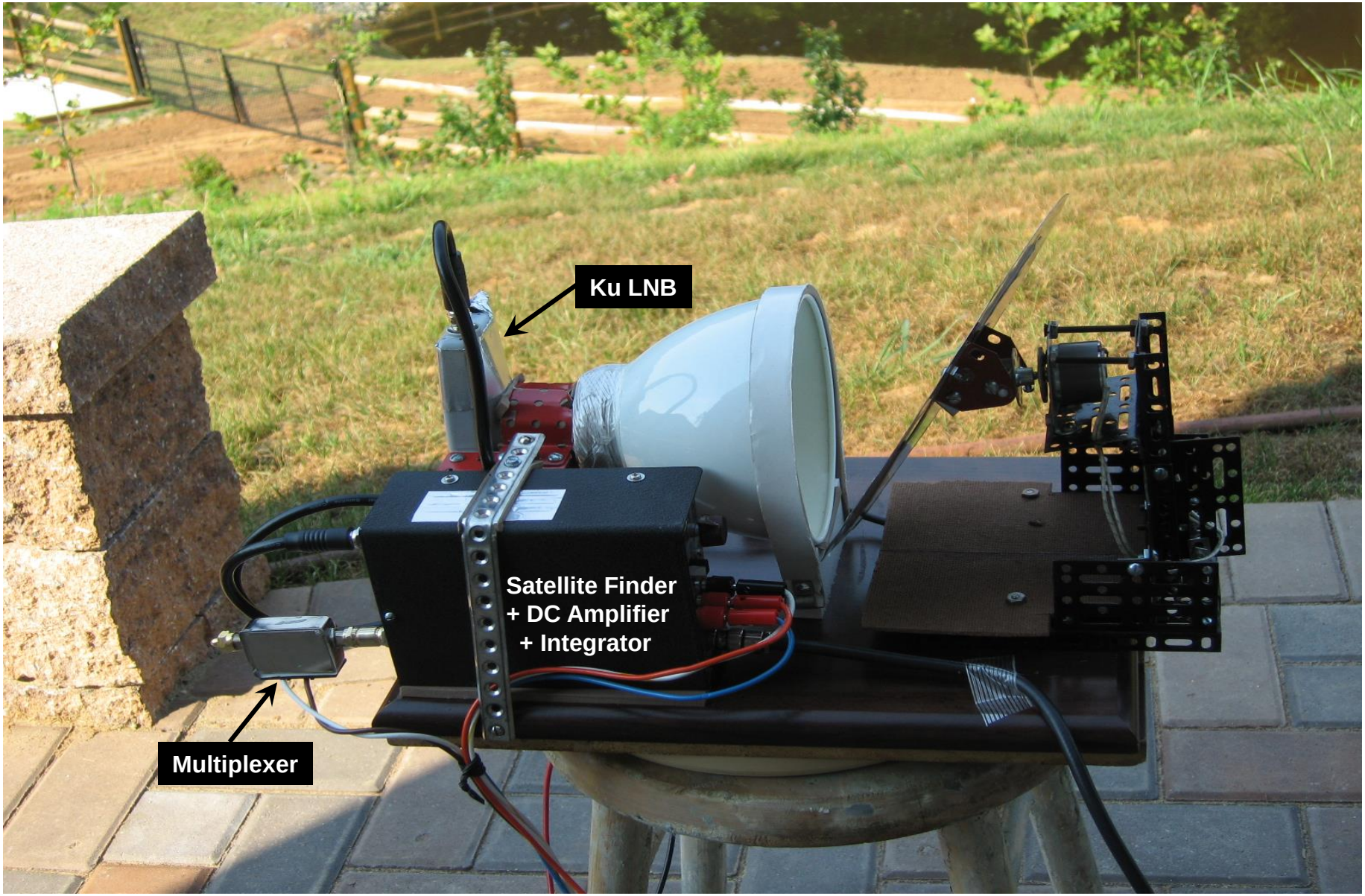

12 GHz Total Power radiometer uses an *LNB* , Satellite Finder (*IF* amplifier + detector), DC Amplifier and Integrator

Rain Simulation using a Garden Sprinkler

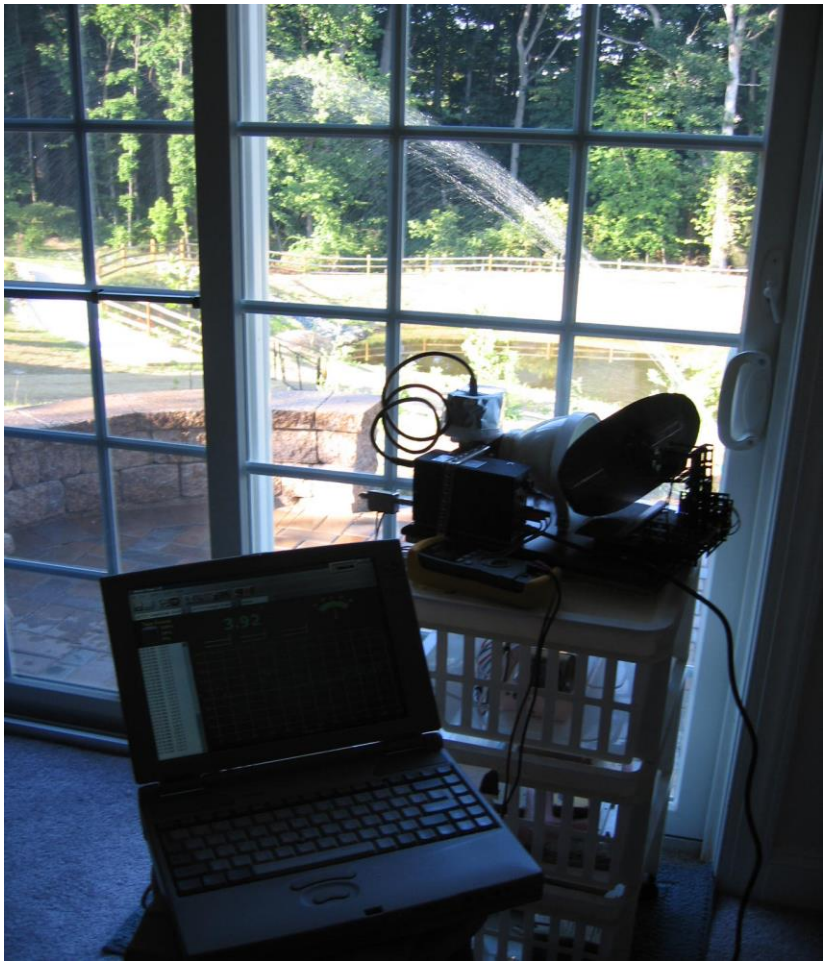

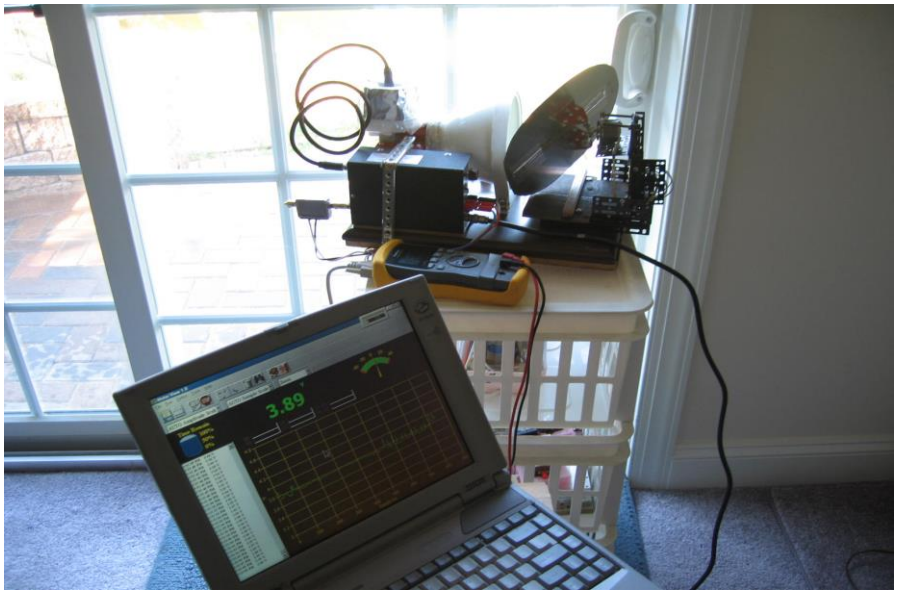

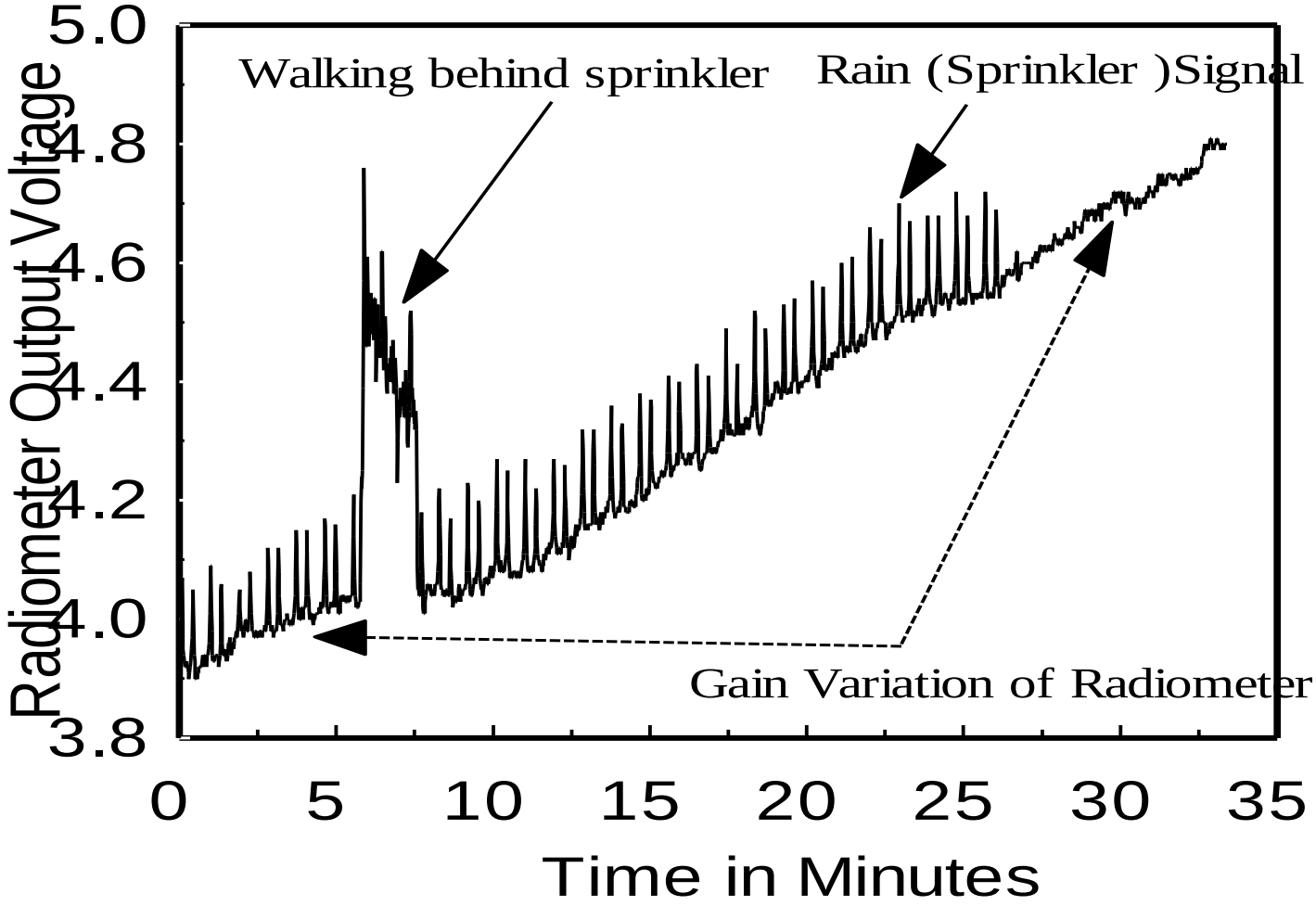

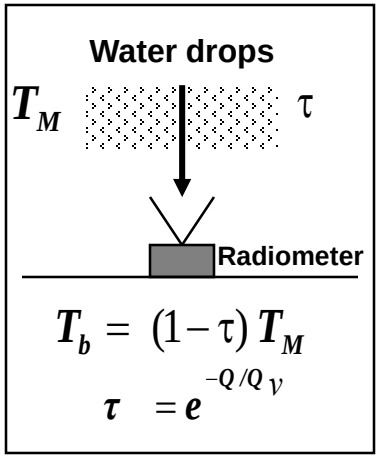

Shown is the increased 12 GHz radiometer voltage due to thermal emission, $(1-\tau)\,T_M$ by water drops from the sprinkler. Also seen is the gradual increase due to gain variation of the radiometer amplifiers, *i.e., LNB*, *IF* Amplifier and DC Amplifier. *To reduce effects due to gain variation, the Total Power radiometer must be calibrated every minute or less*.

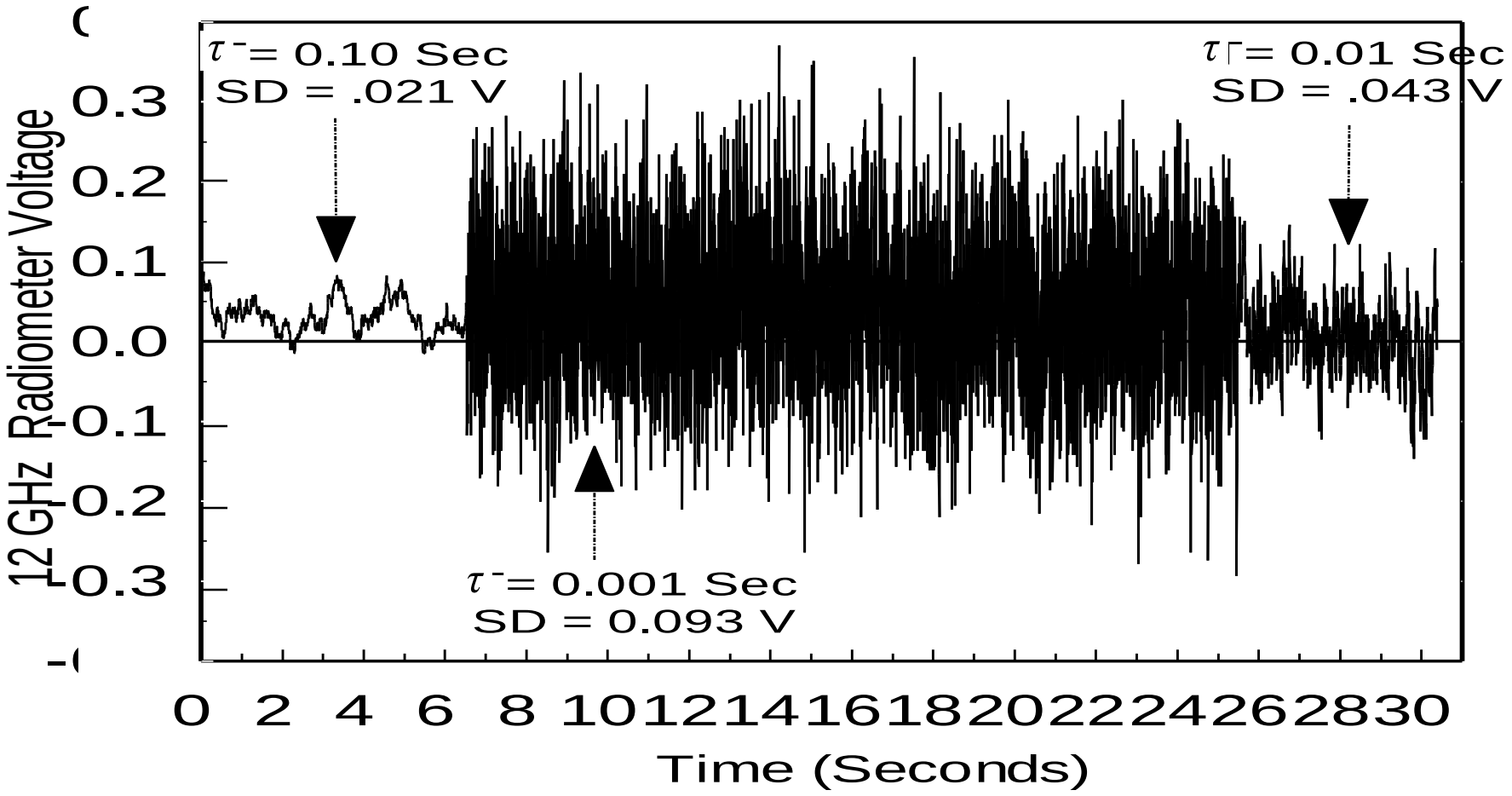

Total Power Radiometer output for different integration times, τ.

The standard deviation (SD) of the noise varies approximately as $\sqrt{\Delta V^2} \cong .015 + \frac{.0025}{\sqrt{\tau}}$

DICKE RADIOMETER

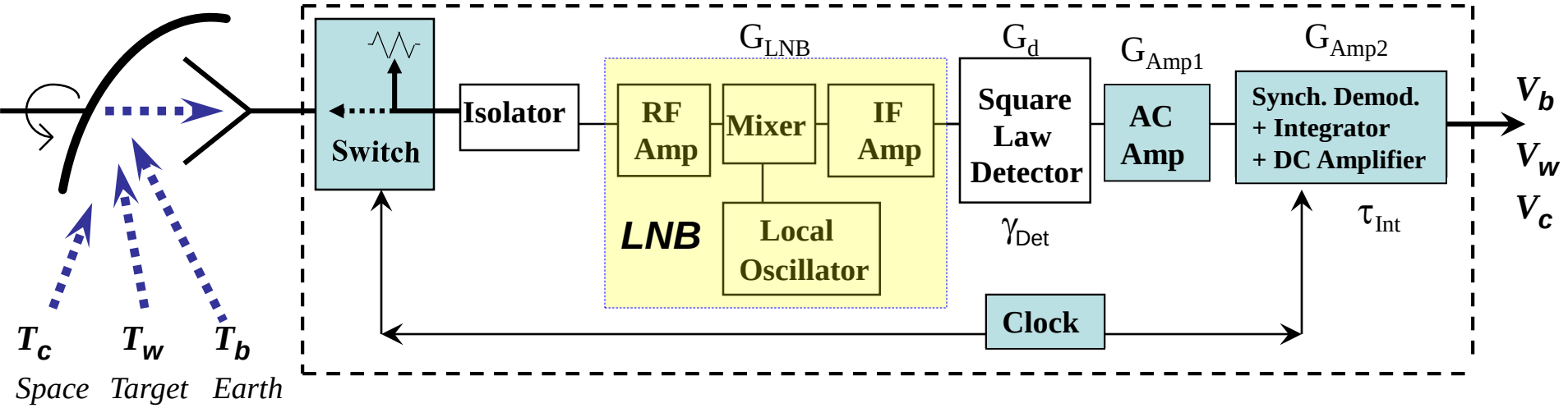

Two Point Linear Calibration

$$T_b = I + S\,V_b\,, \quad S = \frac{T_W - T_C}{V_W - V_C}\,, \quad I = T_W - S\,V_W$$

NOISE EQUIVALENT TEMPERATURE (NEΔT)

$$\Delta T_b\big]_{\text{Dicke}} = \sqrt{\frac{(T_b + T_N)^2 + (T'_R + T_N)^2}{B_{IF}\,(\tau_{\text{int}}/2)} + \left(\frac{\Delta G}{G}\right)^2 (T_b - T'_R)^2}$$

where $G = \overbrace{G_{LNB} G_{Amp1} G_{Amp2} G_d}^{G'}\ \gamma_{Det}$

DRIFT IS MAINLY DUE TO DETECTOR TEMPERATURE

$$V_b = \tfrac{1}{2} k (G' \gamma_{\text{det}}) B_{IF} [T_b - T'_R]\,, \qquad \frac{\Delta V_b}{\Delta t} = \tfrac{1}{2} k\, G' B_{IF} [T_b - T'_R] \left(\frac{\Delta \gamma_{\text{det}}}{\Delta T_{\text{det}}}\right) \frac{\Delta T_{\text{det}}}{\Delta t}$$

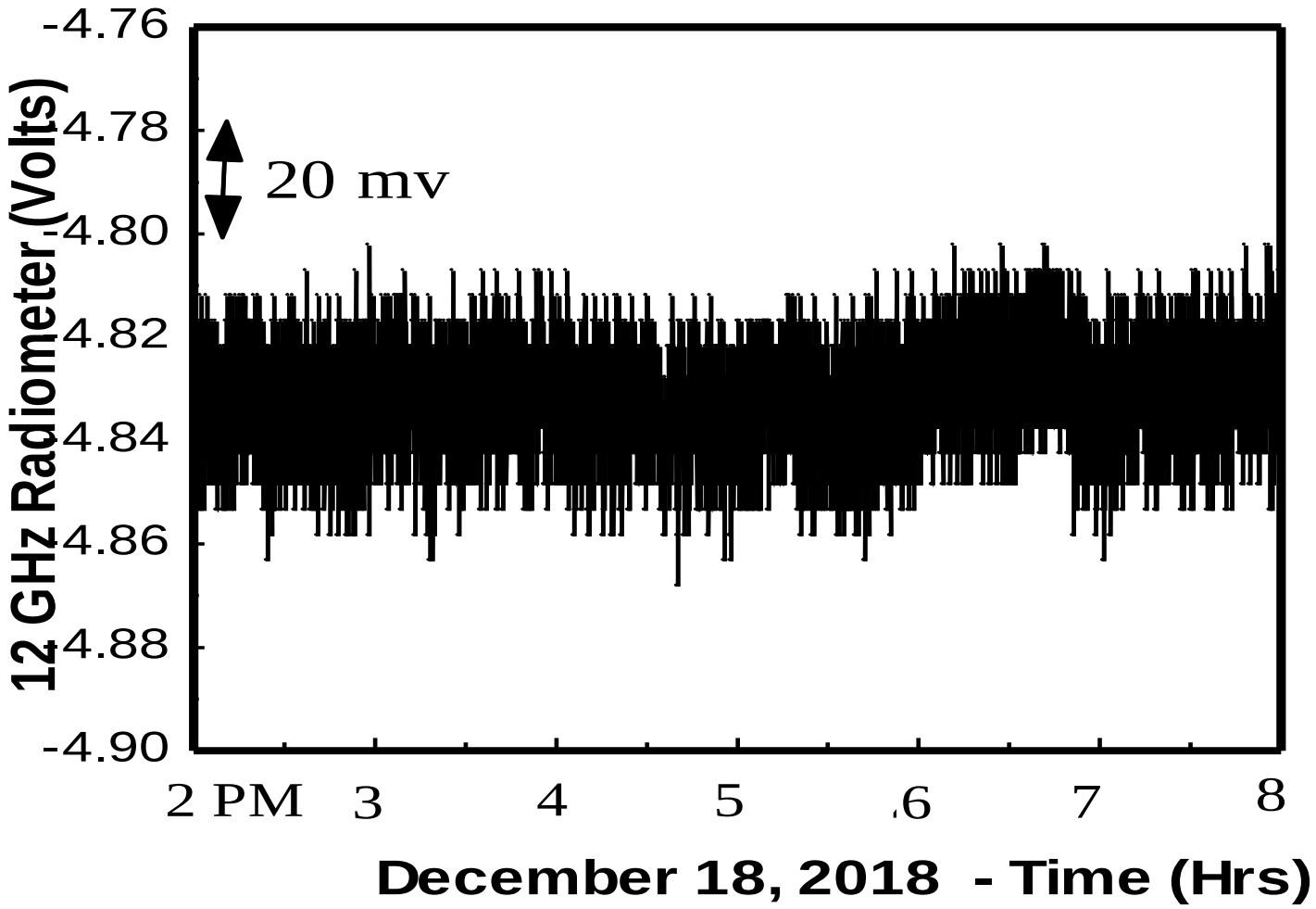

Clear sky 12 GHz Dicke radiometer measurements on Dec. 18, 2018 between 2 and 8 pm. The minimum integration time of 0.1 seconds was used for these measurements.

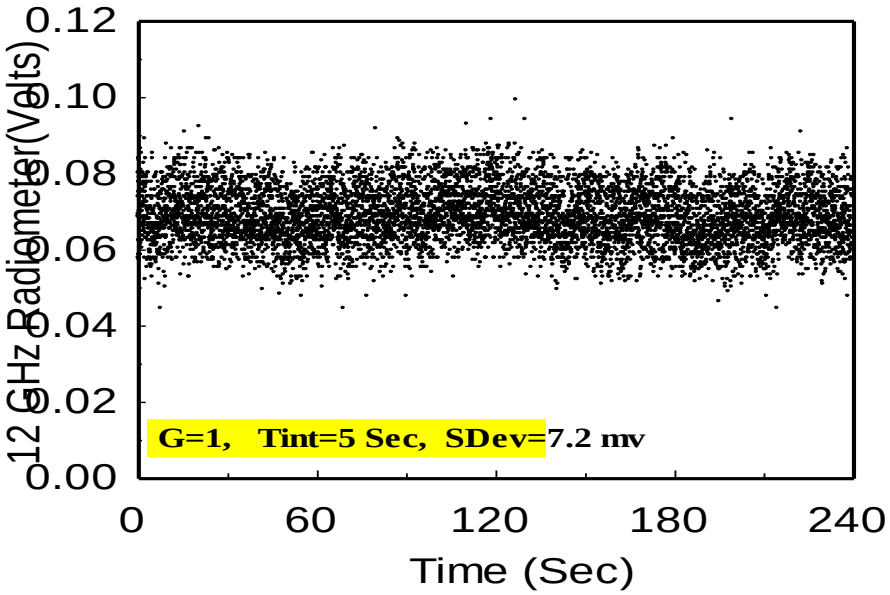

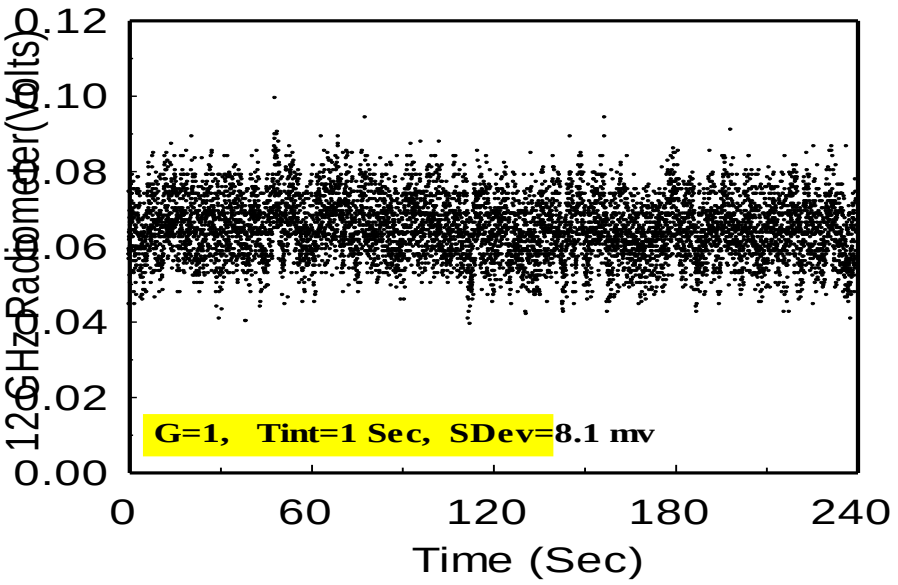

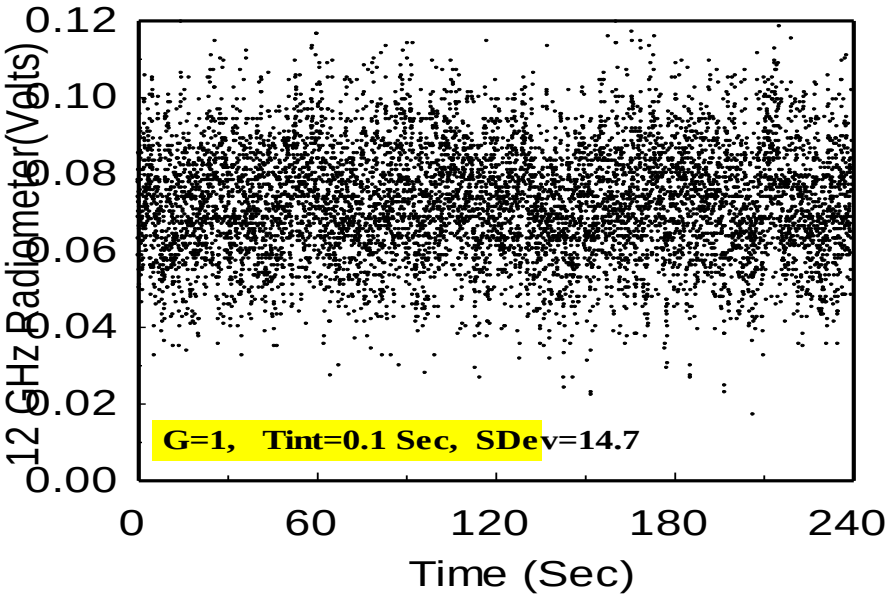

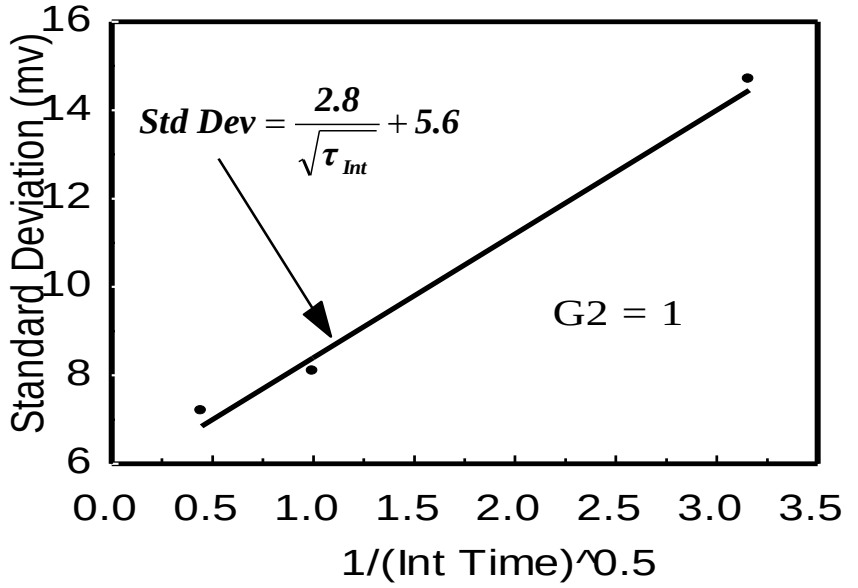

Time series of a 12 GHz Dicke radiometer output when viewing an ambient temperature target. The synchronous detector gain is set to unity and the integration time is changed from 0.1 to 5 seconds.

4 GHz Radiometer Block Diagram

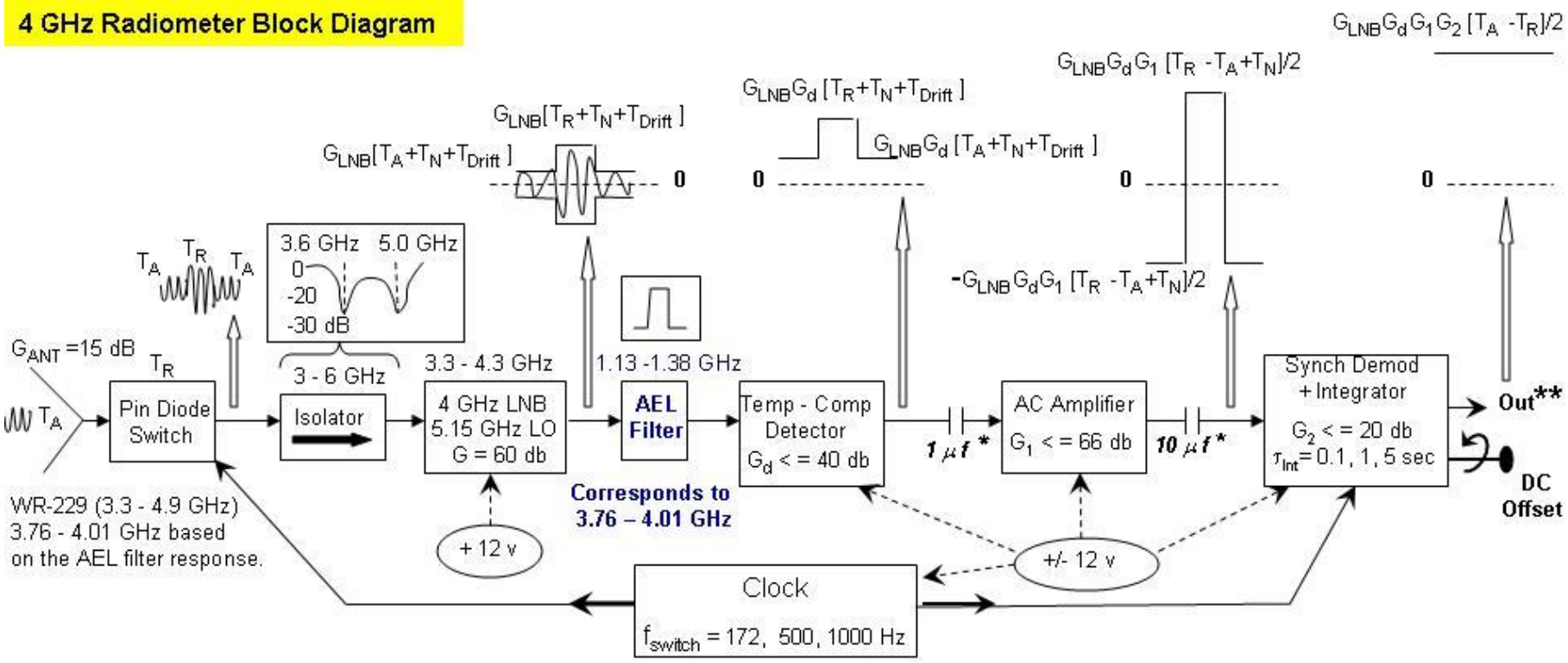

1 - The wideband isolator reduces* (a) *LO leakage out of the antenna and* (b) *reflections between pin diode switch output & LNB input.

2 - Narrow band IF* filter reduces interference *from Radar, Altimeter, WiFi.

3.4 - 4.2 GHz

AEL Bandpass Filter
1135 – 1385 MHz

12 GHz Radiometer Block Diagram

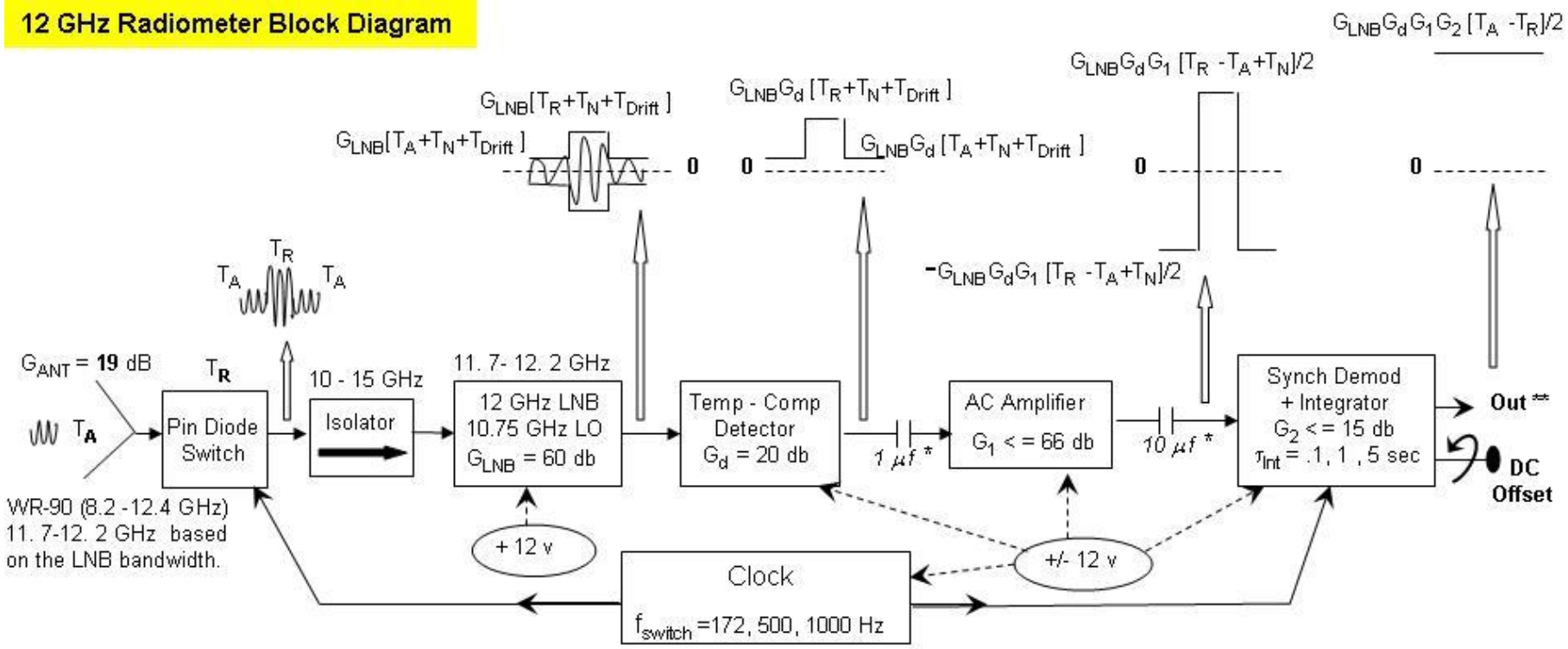

1. ***Isolator reduces* (a) *LO leakage out of the antenna and* (b) *reflections between pin diode switch output and LNB input.***

2. **No interference found.**

11.7 – 12.2 GHz

20.5 GHz Radiometer Block Diagram

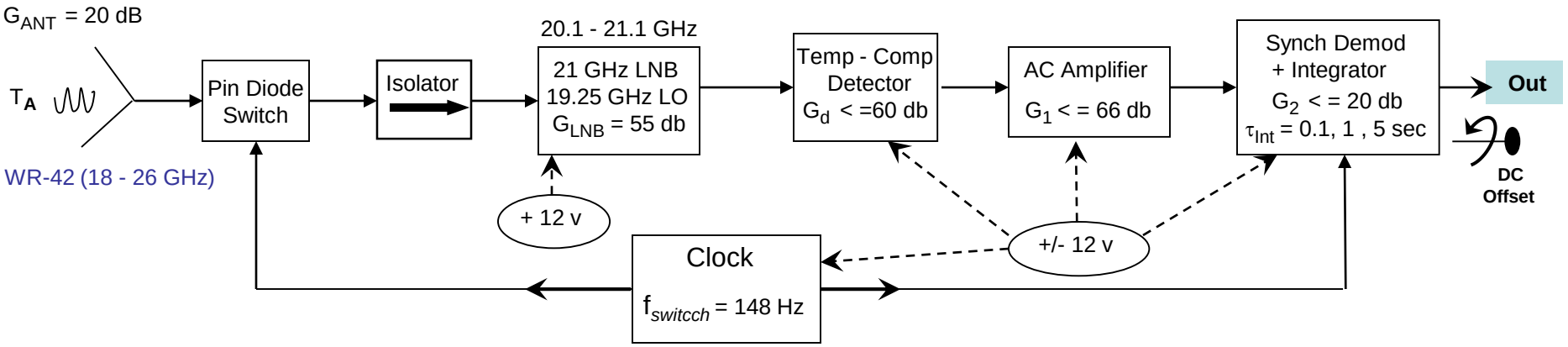

1. Isolator reduces (a) LO leakage out of the antenna and (b) reflections between pin diode switch output and LNB input.

2. Unknown step-wise interference during the evening by satellite transmission?

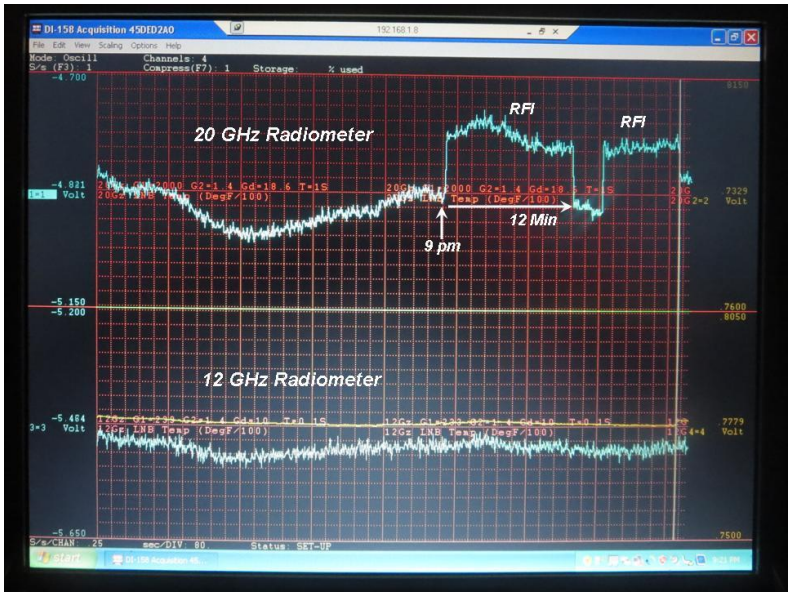

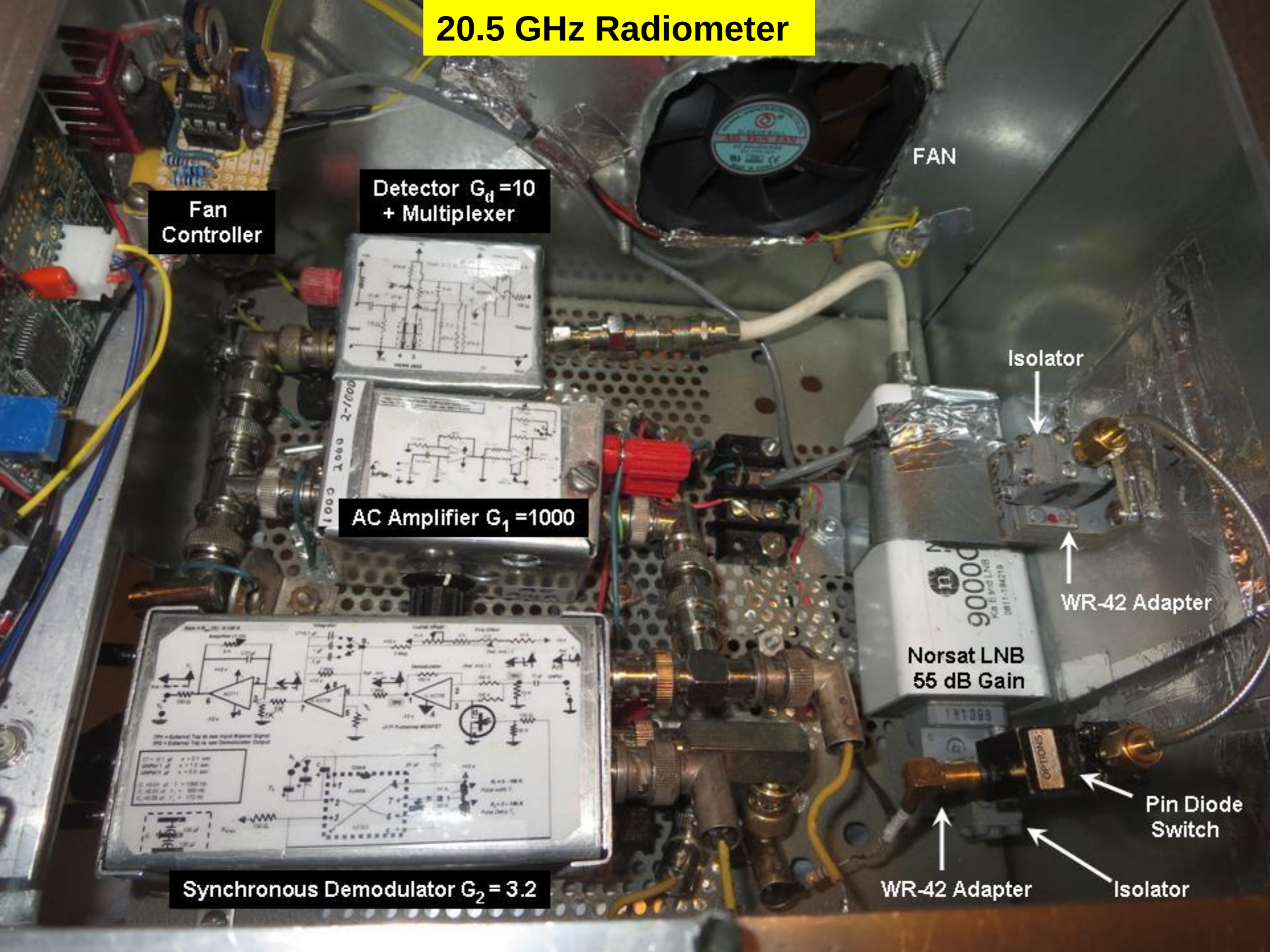
20.5 GHz Radiometer
FAN
Fan Controller
Detector G_d =10 + Multiplexer
Isolator
AC Amplifier G_1 =1000
WR-42 Adapter
Norsat LNB 55 dB Gain
Pin Diode Switch
WR-42 Adapter
Isolator
Synchronous Demodulator G_2 = 3.2

Evolution of Satellite Microwave Radiometers in the United States

To obtain high spatial resolution, radiometers are flown on low earth orbiting satellites (800 - 1100 km)

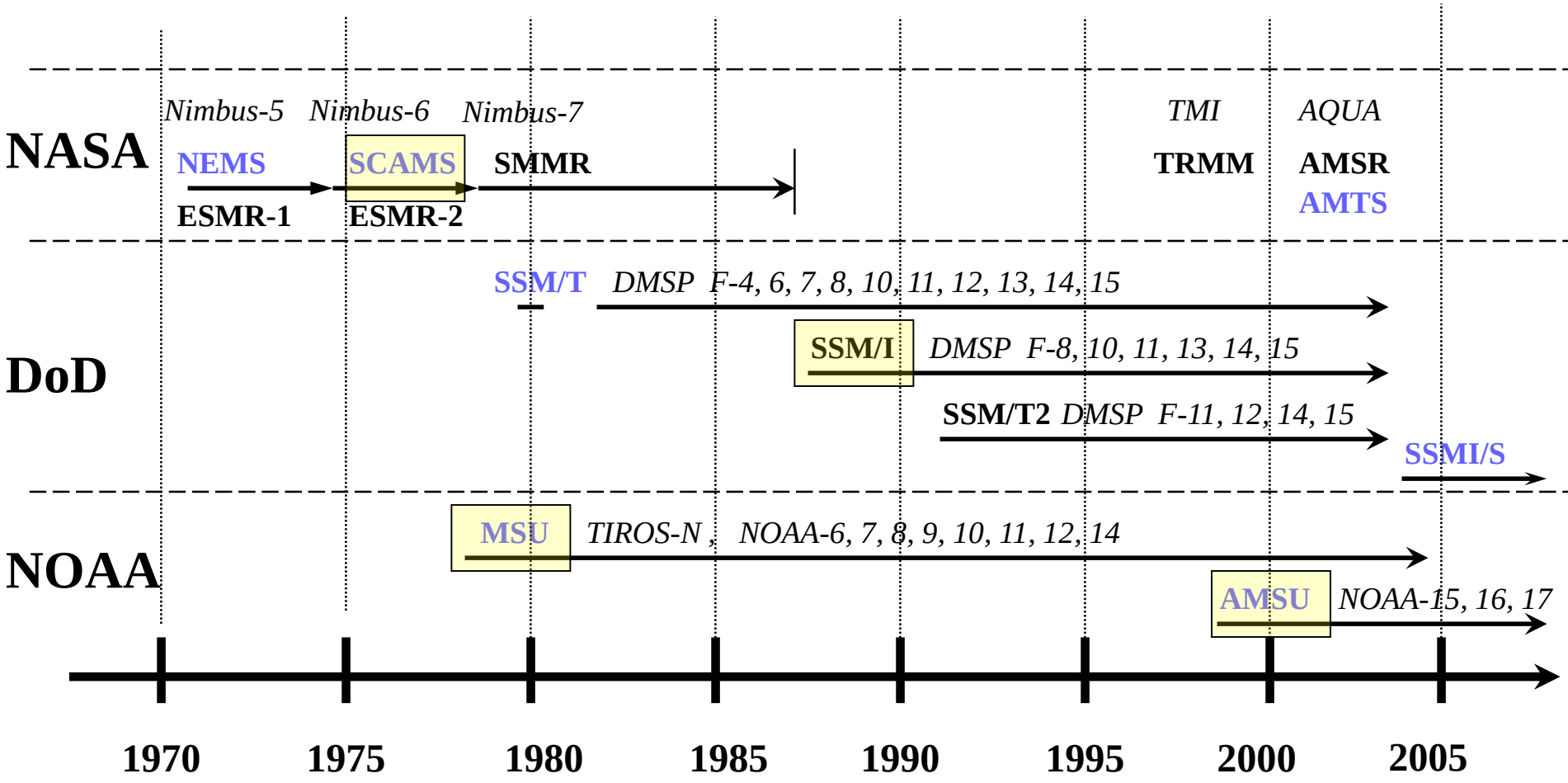

Contains 50-60 GHz Temperature Sounding Channels

Contains Transparent “Window” Channels

Unique Microwave Properties

1. **Good *Cloud Penetration***
2. **Large *Spectral Separation* between O_2 and H_2O**
3. **High *Spectral Resolution***
4. **Linear *Temperature Response***
5. **Large *Emissivity Difference* between Surface Types**

Applications of Microwave Radiometers

Atmospheric Measurements

1. Vertical Temperature Soundings
2. Climatic Temperature Trends
3. Warm Core Temperature Structure for Hurricanes
4. Rain Rate and Cloud Liquid Water

Surface Measurements

1. Surface Temperature
2. Snow Cover and Sea Ice Concentration
3. Ocean Wind Speed and Sea Surface Temperature
4. Soil Moisture

Applications of Satellite Microwave Radiometers

Frequency	Polarization	Application
2 - 3 GHz	V, H	Ocean Salinity & Soil Moisture
10 GHz	V,H	Sea Surface Wind Speed & Temperature
19 GHz	V,H	Sea Ice Concentration & Surface Wetness
20 - 22 GHz	V	Total Water Vapor (TPW) over Ocean
31 GHz	V	Clouds & Rain Water over Ocean
50 to 60 GHz	V	Temperature Soundings over Land & Ocean
85 GHz	V	Snow cover & Rain Rate over Land & Ocean
150 GHz	V	Rain & Cloud Ice over Land & Ocean
170 to 183 GHz	V	Water Vapor Soundings over Land & Ocean

Scan pattern on earth for a cross-track and conical scanner

Cross Track Scanner

(+) Provides *greatest* coverage

(-) FOV & Polarization varies with scan angle

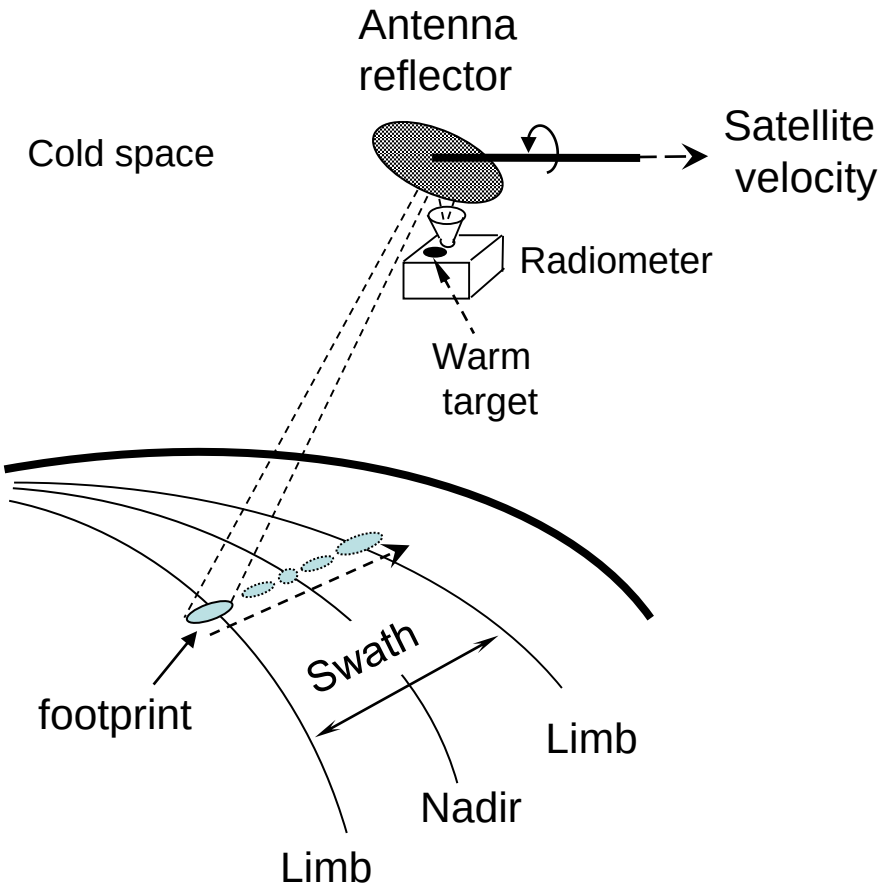

Conical Scanner

(-) Produces less coverage

(+) FOV & Polarization *constant* with scan angle

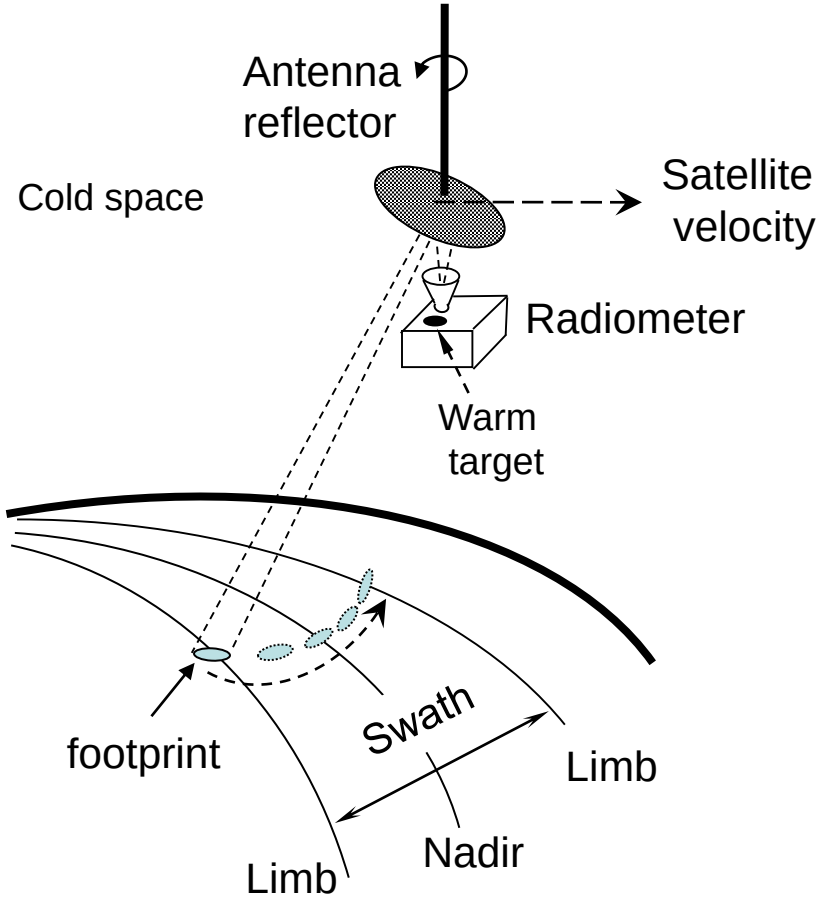

Satellite Microwave Radiometery

1. **Imagers use window channels outside oxygen and strong water vapor bands to view the surface. They use conical scanning antennas to obtain fixed polarization with a constant FOV.**

2. **Sounders use opaque channels in oxygen and strong water vapor bands to probe the atmosphere. They use cross track scanning antennas to obtain the largest swath width. However, the polarization, FOV, and slant path varies with scan angle.**

AMSU A & B Channels

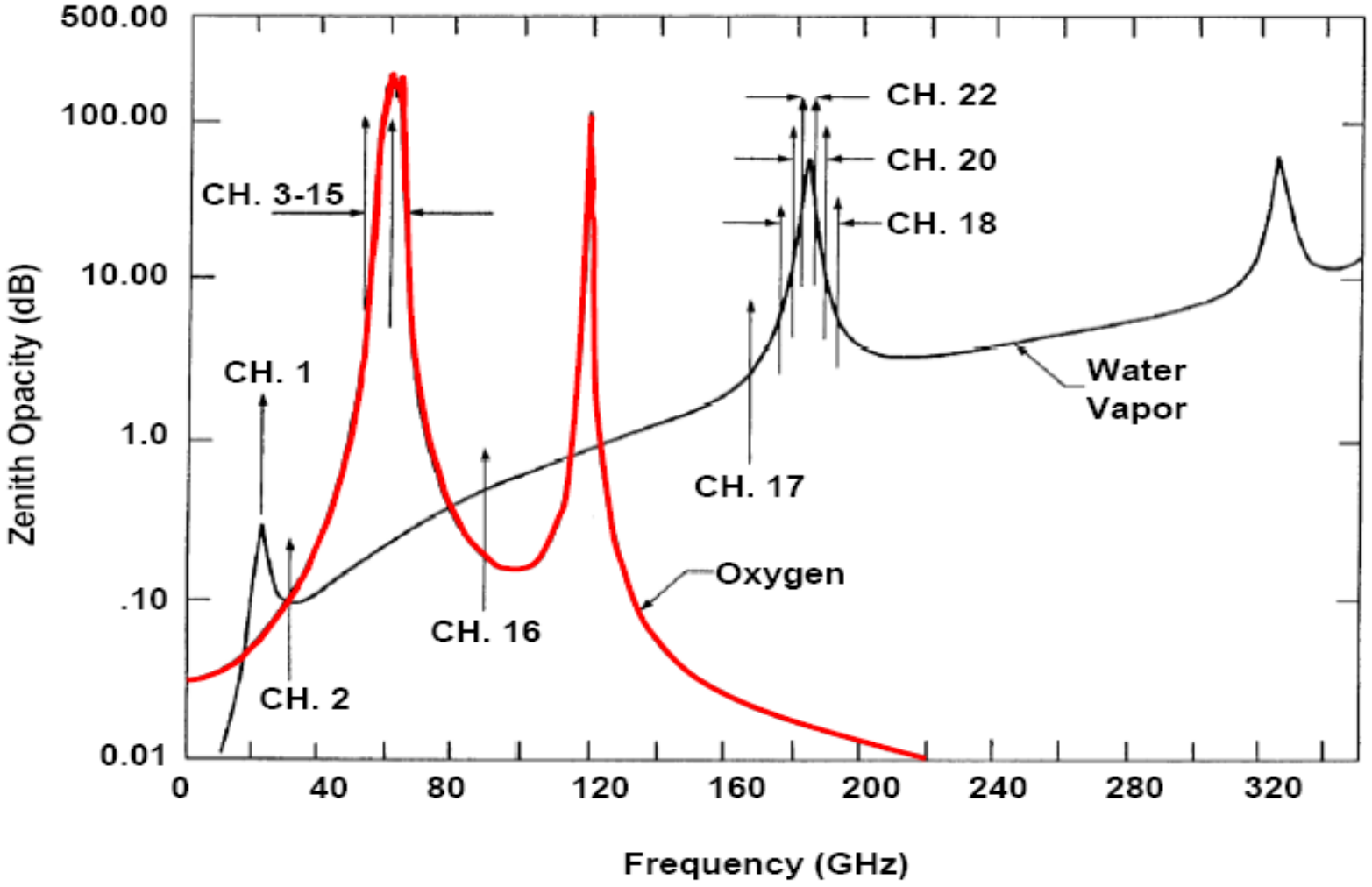

Goodrum, G. *et al.*, *NOAA KLM Users Guide*, section 3.4, p. 2, NOAA, 2000

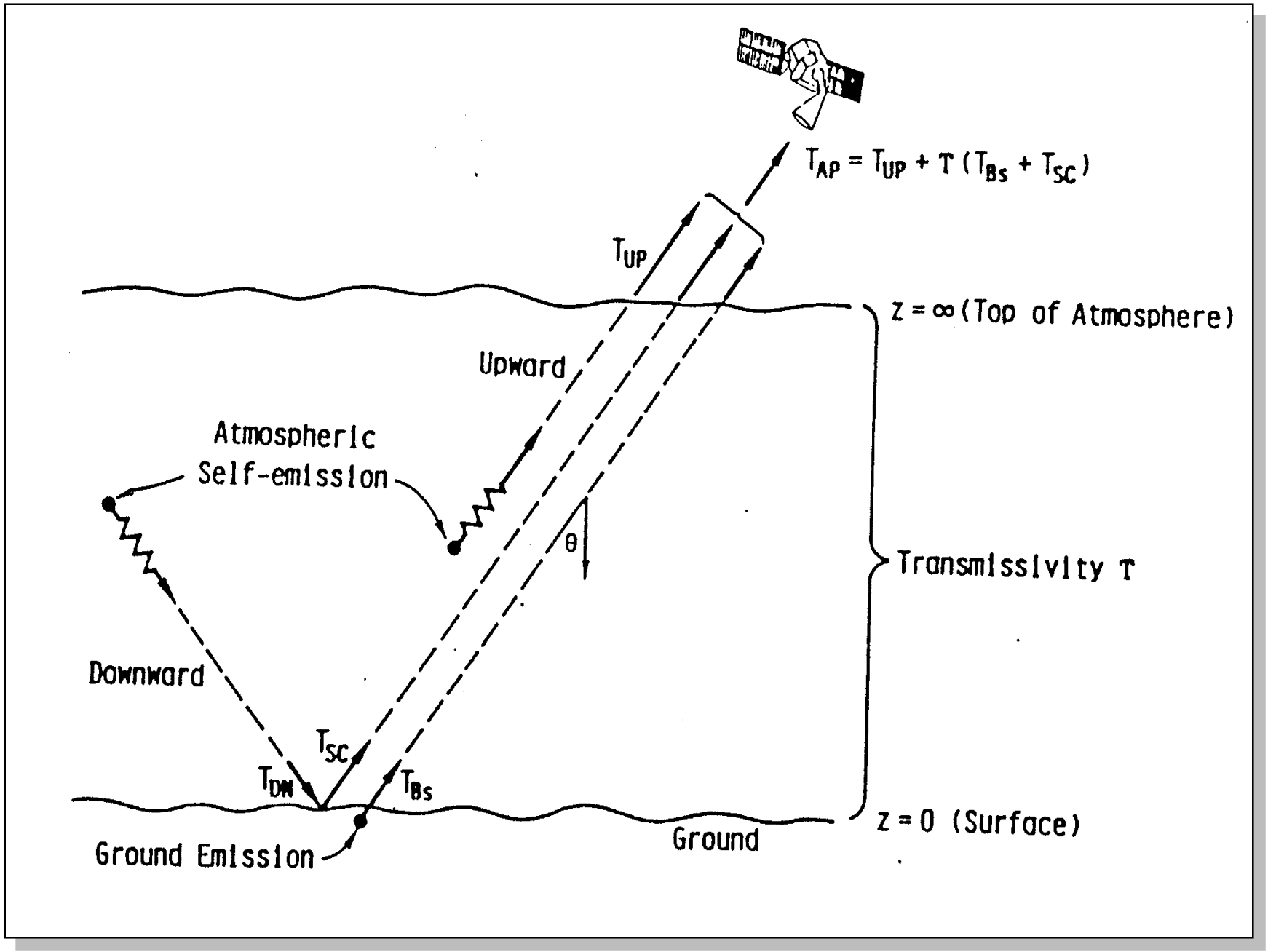
$T_{AP} = T_{UP} + T(T_{Bs} + T_{SC})$
T_{UP}
$z = \infty$ (Top of Atmosphere)
Upward
Atmospheric
Self-emission
θ
Transmissivity T
Downward
T_{SC}
T_{DN}
T_{Bs}
Ground Emission
Ground
$z = 0$ (Surface)

Brightness Temperature T_b Measured by Satellite Radiometers

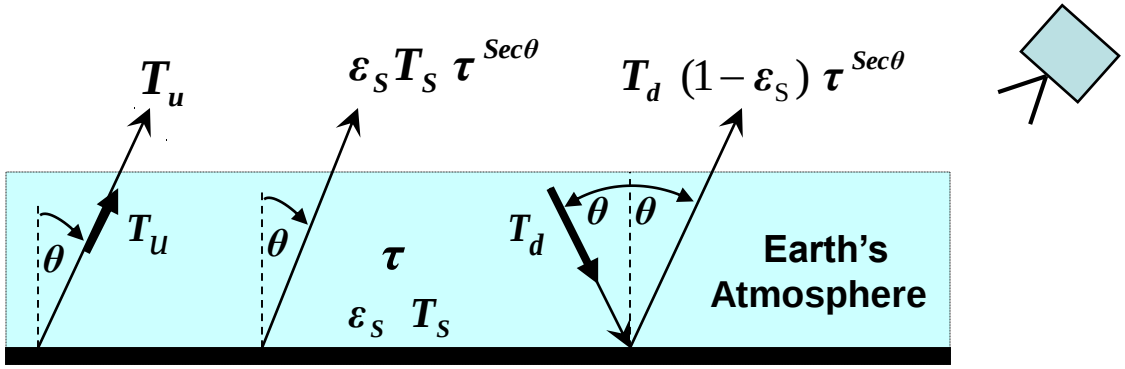

$$T_b = T_u + \underbrace{\varepsilon_S}\ T_S\ \tau^{Sec\theta} + T_d\ (1-\varepsilon_S)\ \underbrace{\tau}^{Sec\theta} \leftarrow \text{Zenith Angle}$$

Surface Emissivity

Atmospheric Transmittance

$$T_u \approx T_d = \underbrace{(1-\tau^{Sec\theta})}\ * \underbrace{T_M}$$

Atmospheric emission

Mean Temperature

$$T_b \cong [\,1-(1-\varepsilon_S)\,\tau^{2\,Sec\theta}\,]\,T_M + \tau^{Sec\theta}[\,T_S - T_M\,]$$

Average Nadir Viewing Surface Emissivity over Land

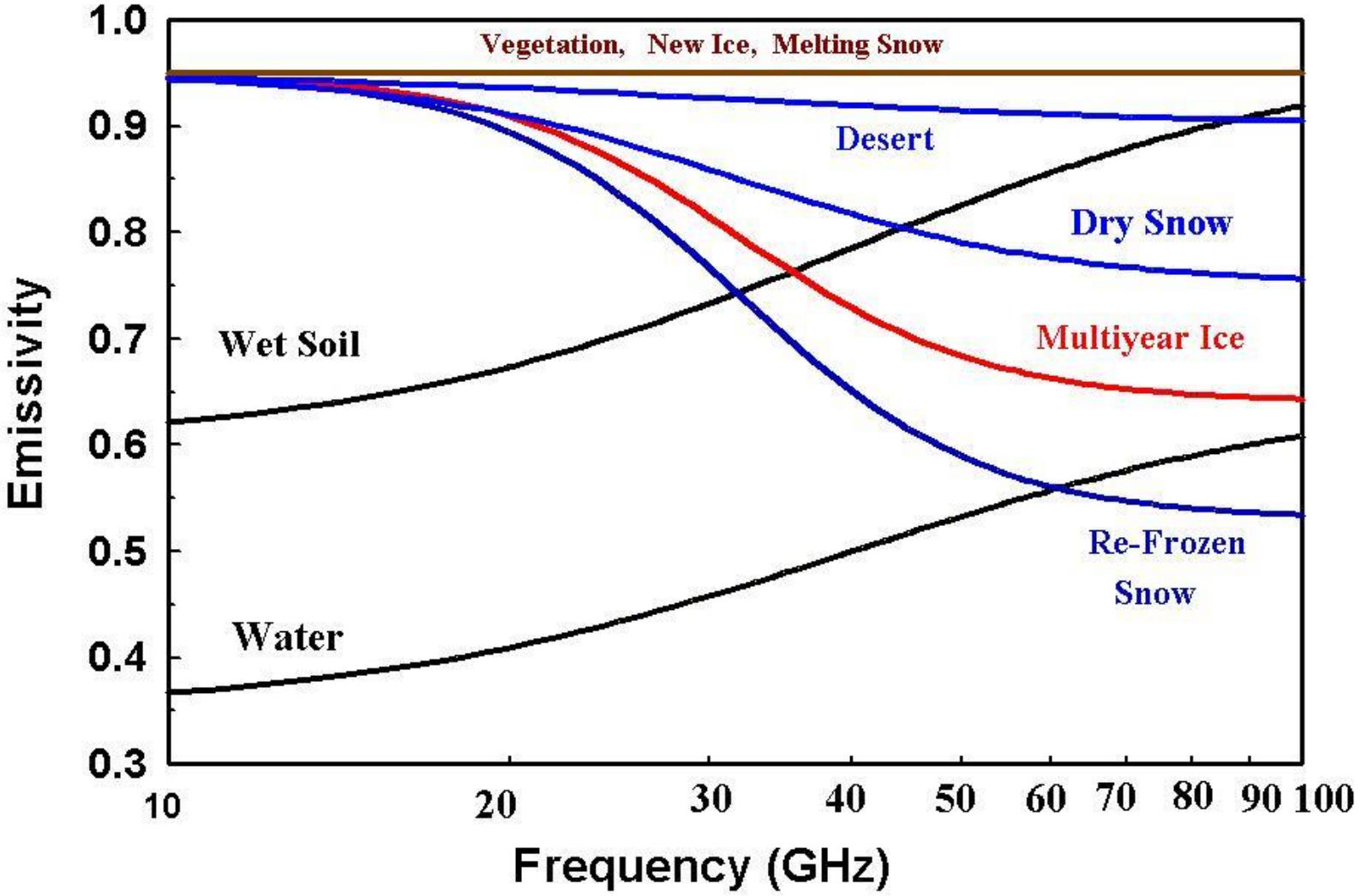

$$T_b \cong [\,1-(1-\varepsilon_S)\,\tau^{2\,Sec\theta}\,]\,T_M + \tau^{Sec\theta}[\,T_S - T_M\,]$$

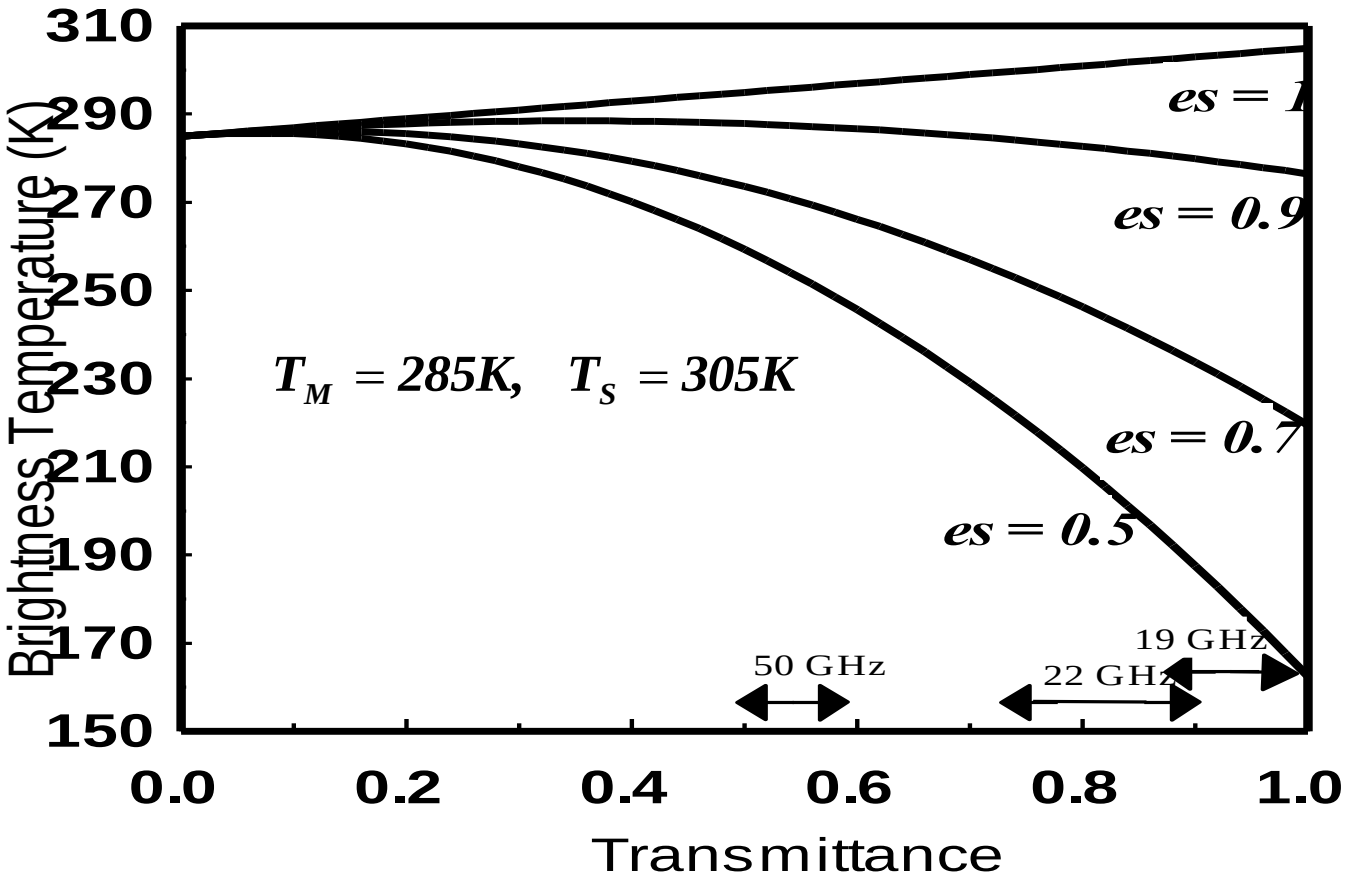

Simulated satellite observed brightness temperature as a function of transmittance. Shown is the transmittance at different frequencies due to water vapor and clouds.

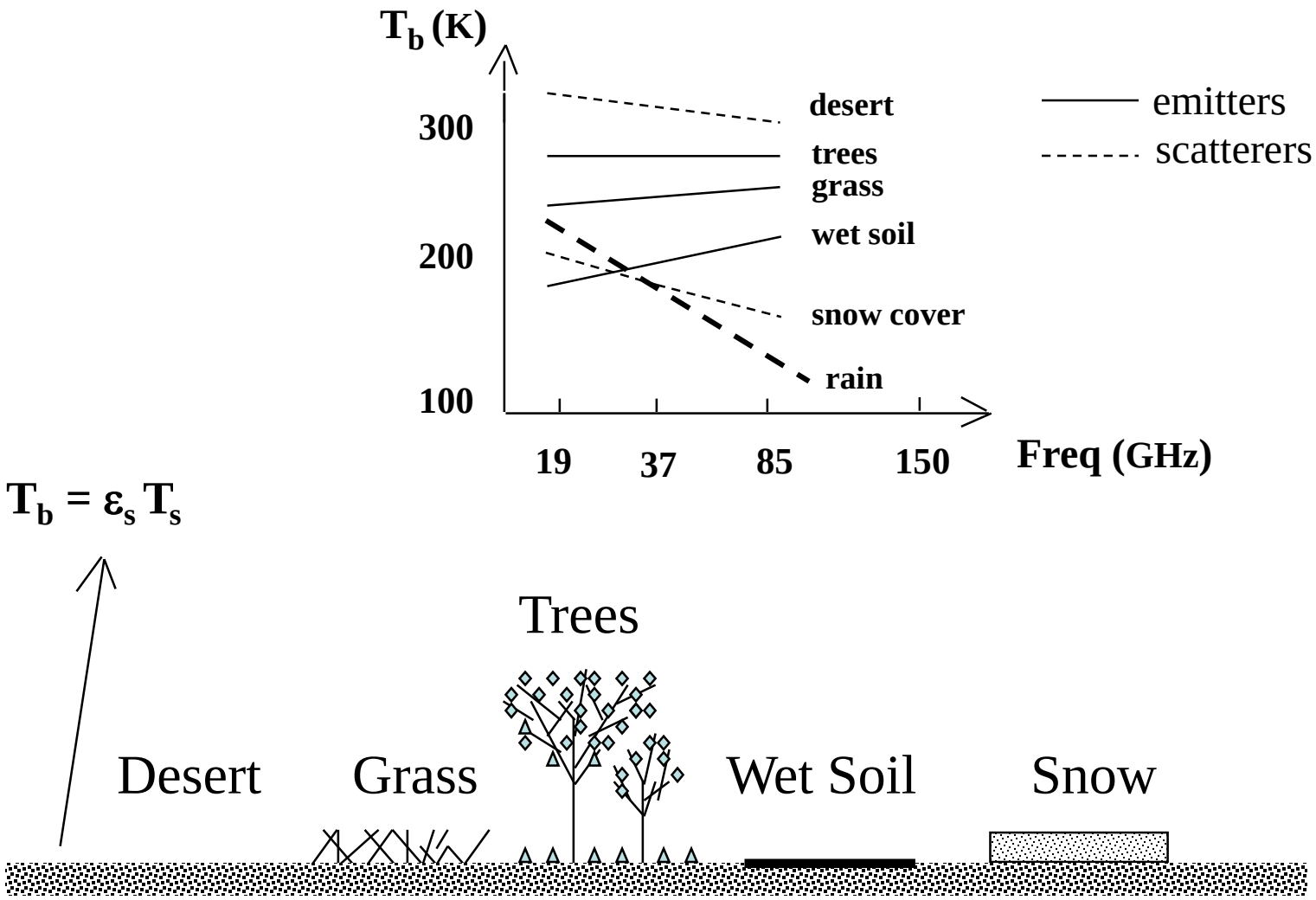

Surface types having distinct microwave signatures

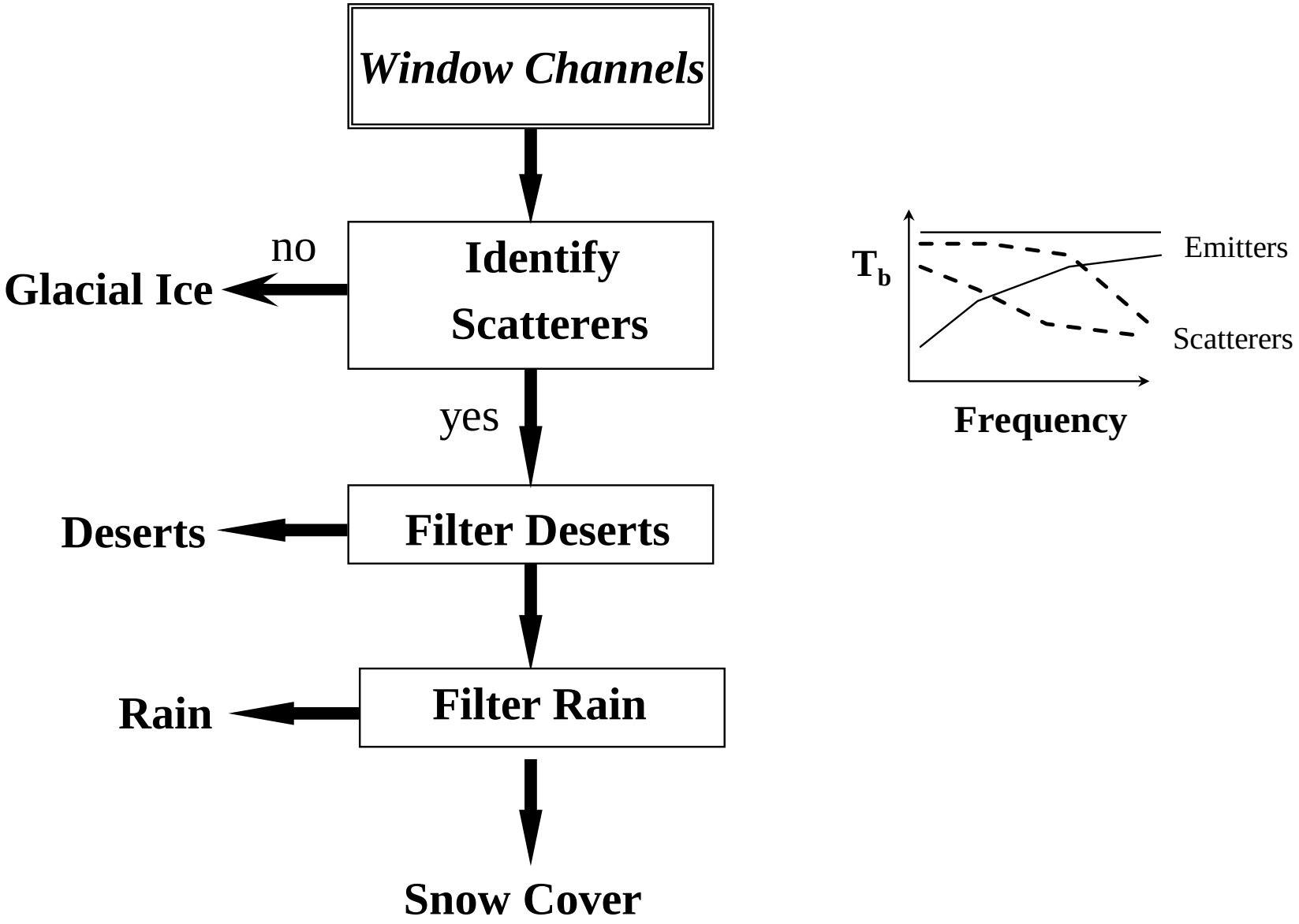

Decision Tree to Identify Rain and Snow Cover

Special Sensor Microwave Imager SSM/I

19 GHz V H, 22 GHz V
37 GHz V,H, 85 GHz V,H

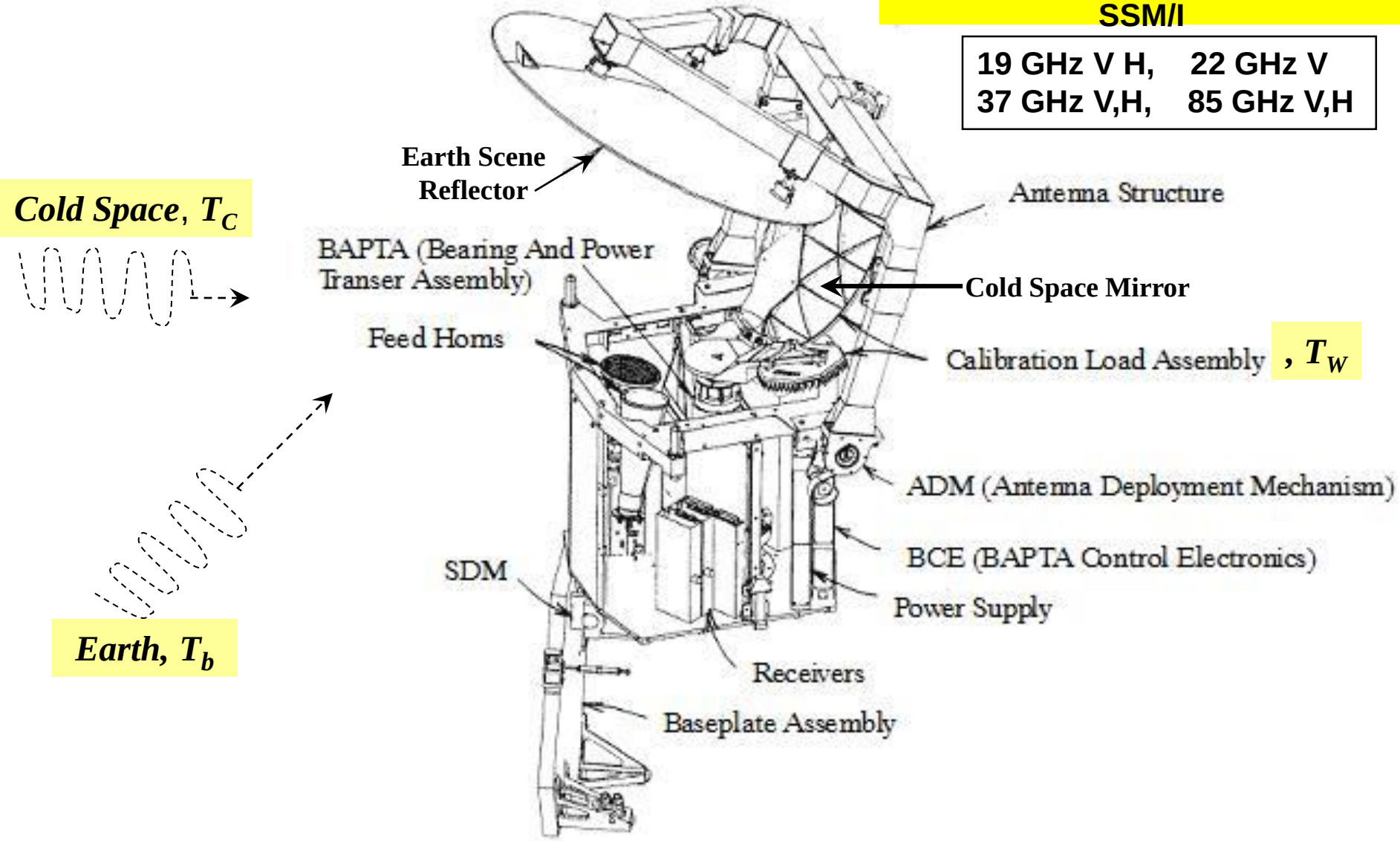

The SSM/I was built by Hughes Aircraft Company and flown on a sequence of polar orbiting satellites beginning in 1987. It is a 7-channel, 4 - frequency microwave radiometer that is dual polarized (V, H) at 19, 37 and 85 GHz and single polarized (V) at 22 GHz. It's measured brightness temperatures are converted into environmental parameters such as sea surface winds, temperature, rain rates, cloud liquid water, water vapor, precipitation, soil moisture, sea ice edge and ice age.

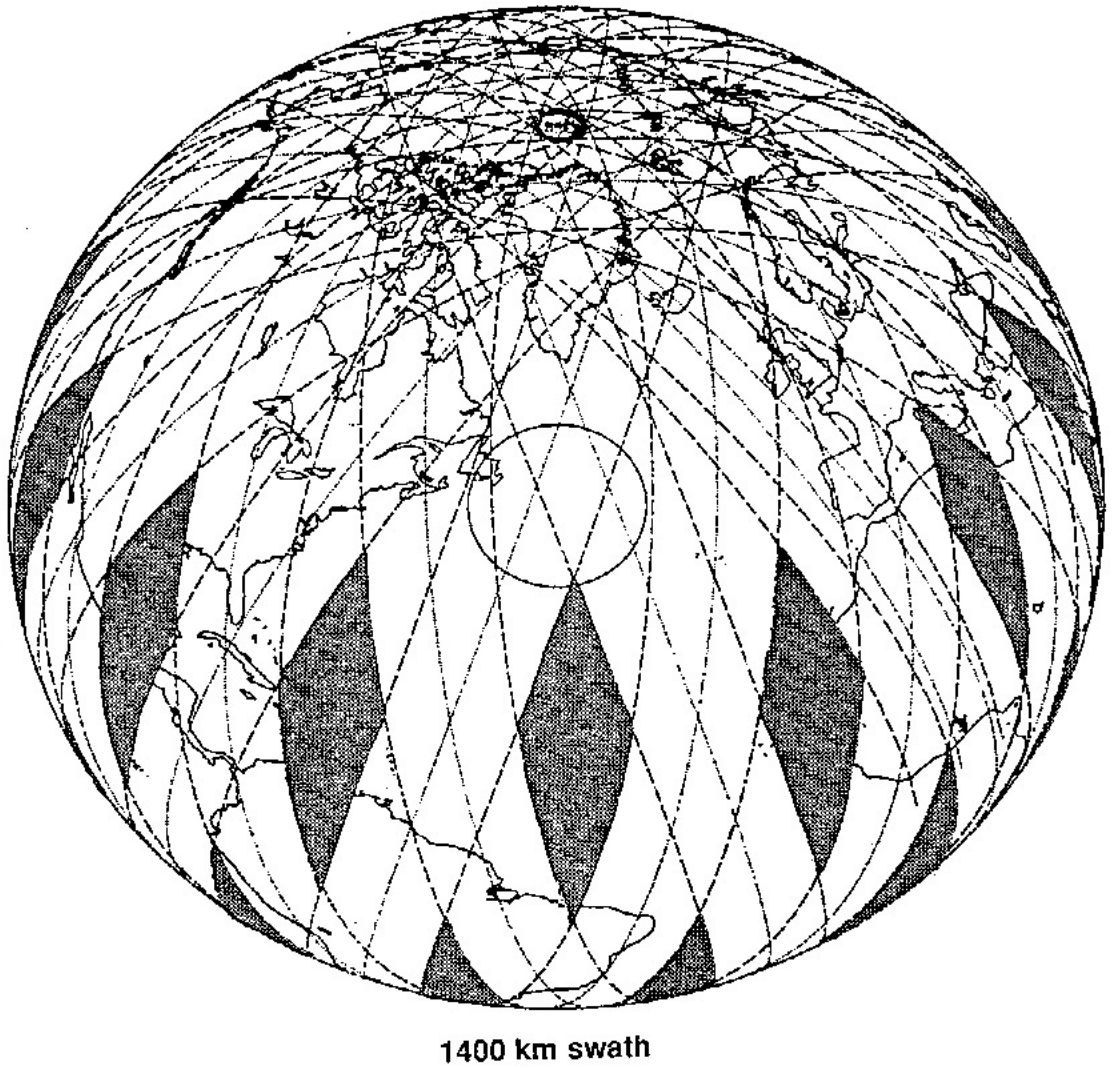

Global coverage of SSM/I instrument over a 24-hr period.

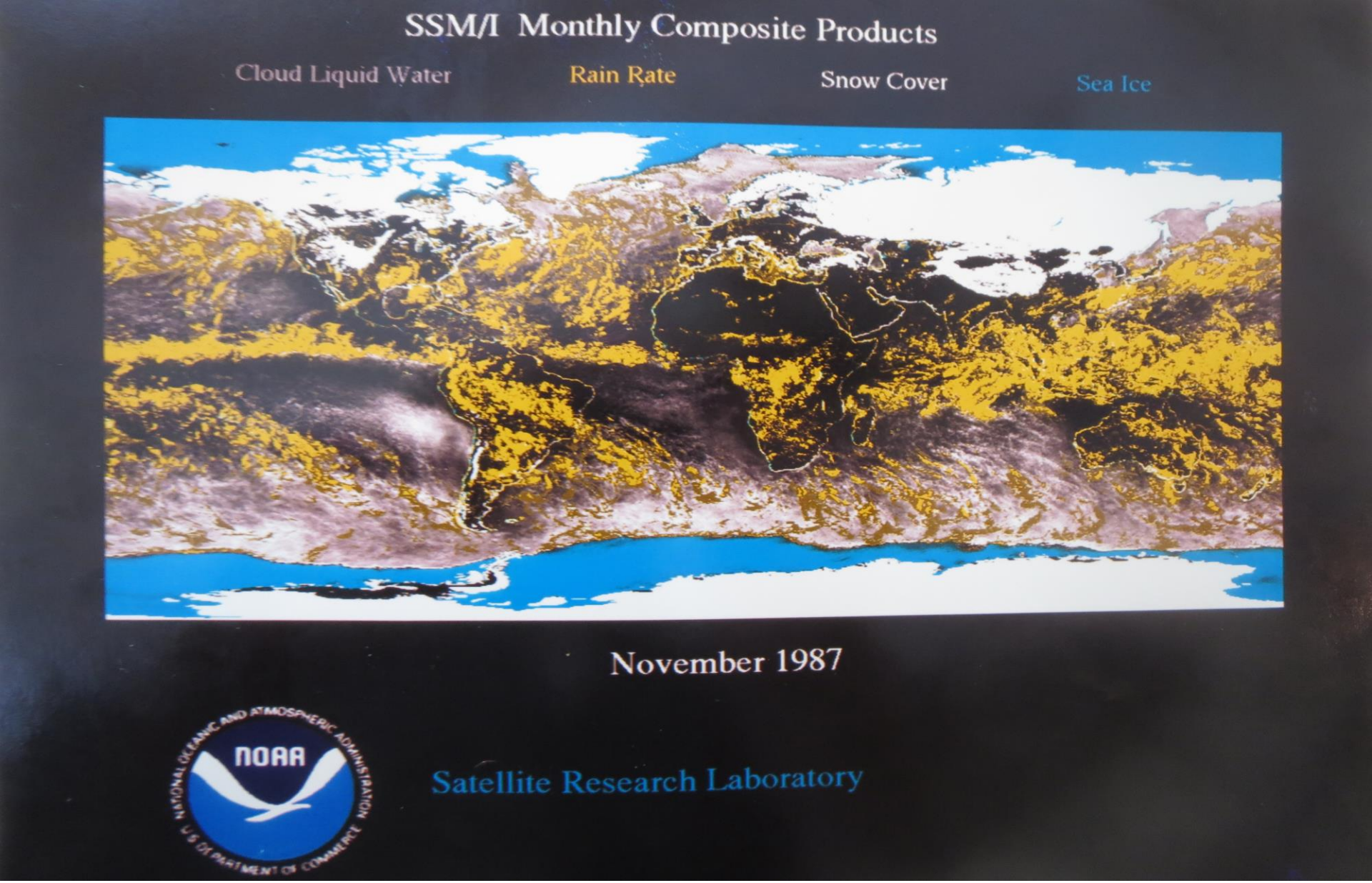

Products such as shown above are obtained daily using the Special Sensor Microwave Imager (SSM/I). Daily products are monthly averaged to obtain this composite image. Measurements (19, 22, 37, 85 GHz) are combined using a decision tree to generate each product globally. Particularly important is the 85 GHz, which detects scattering by millimeter size Ice particles in rain clouds and snow cover.

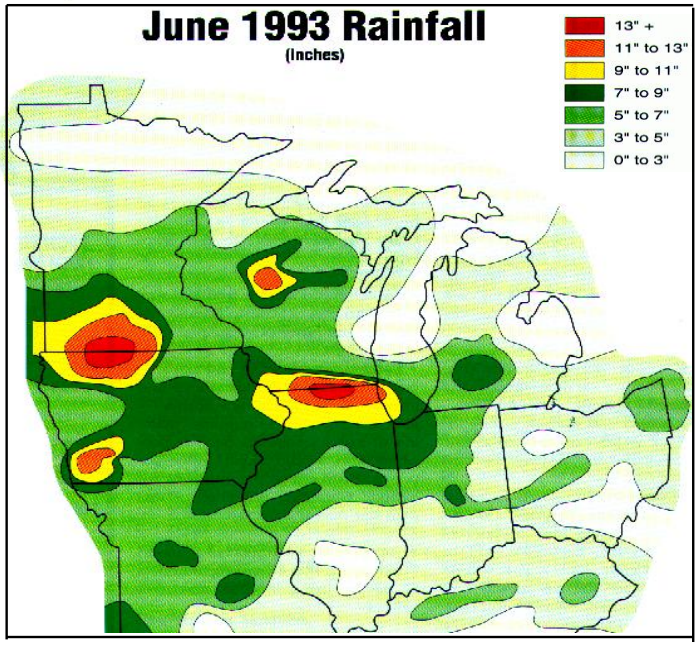

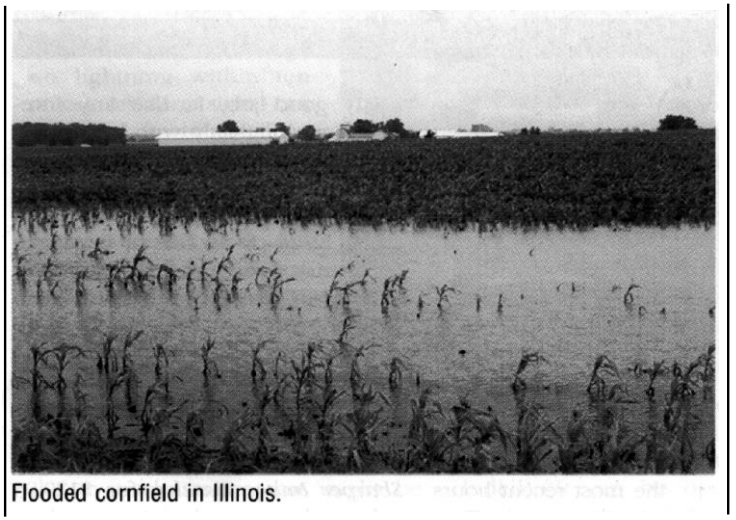

Flooded cornfield in Illinois.

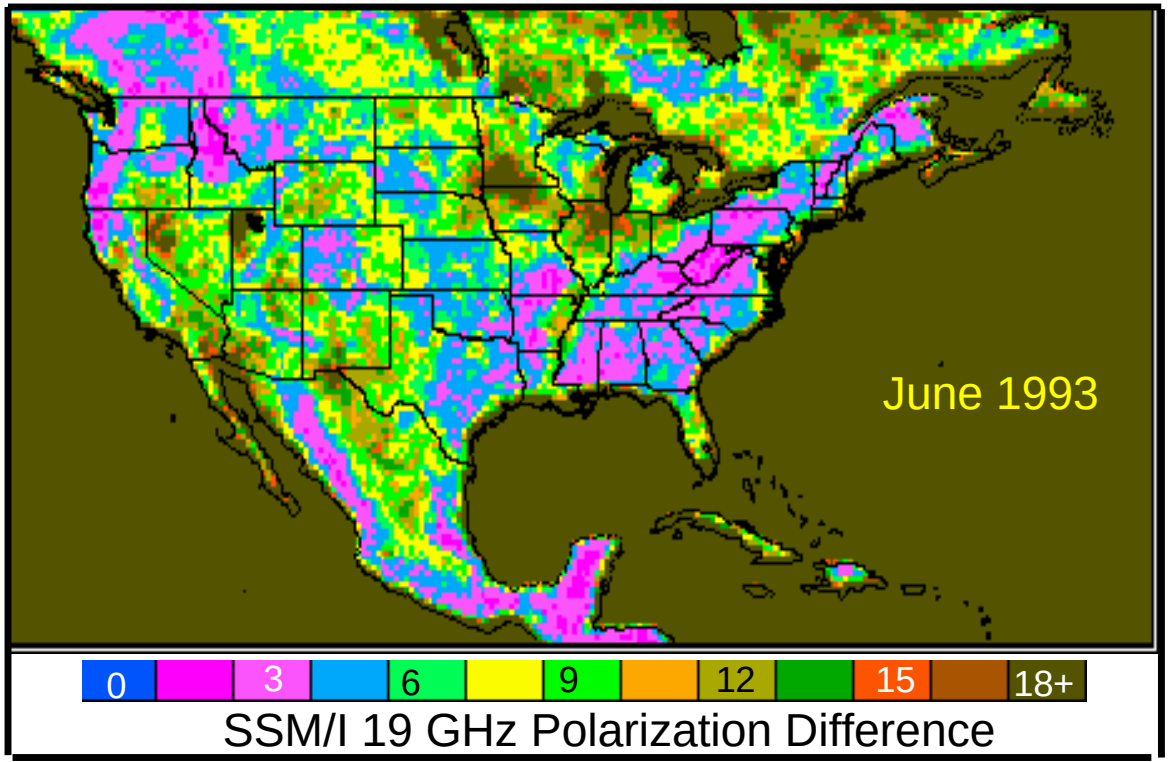

July 1996 (F-13 Asc)

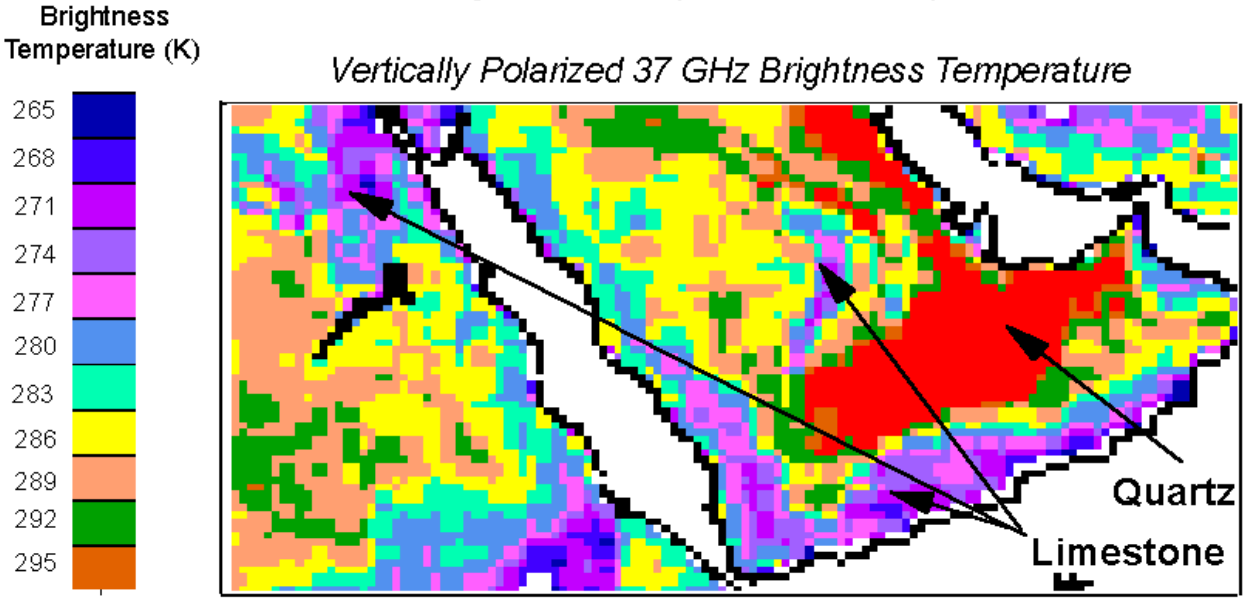

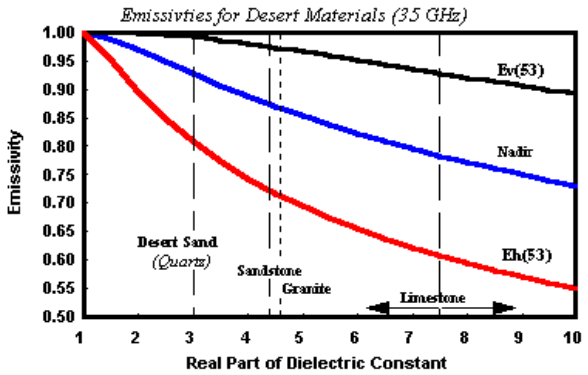

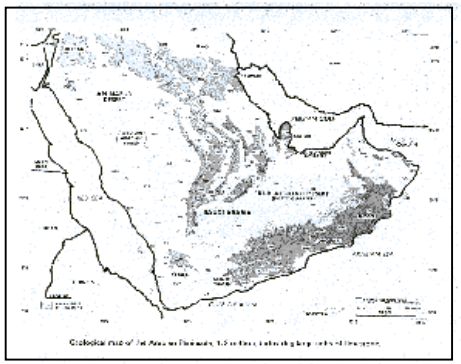

Top: SSM/I brightness temperatures at 37 GHz - vertical polarization.
Bottom-left: Emissivity calculated as a function of dielectric constant.
Bottom-right: Map of limestone deposits over Saudi Arabia .

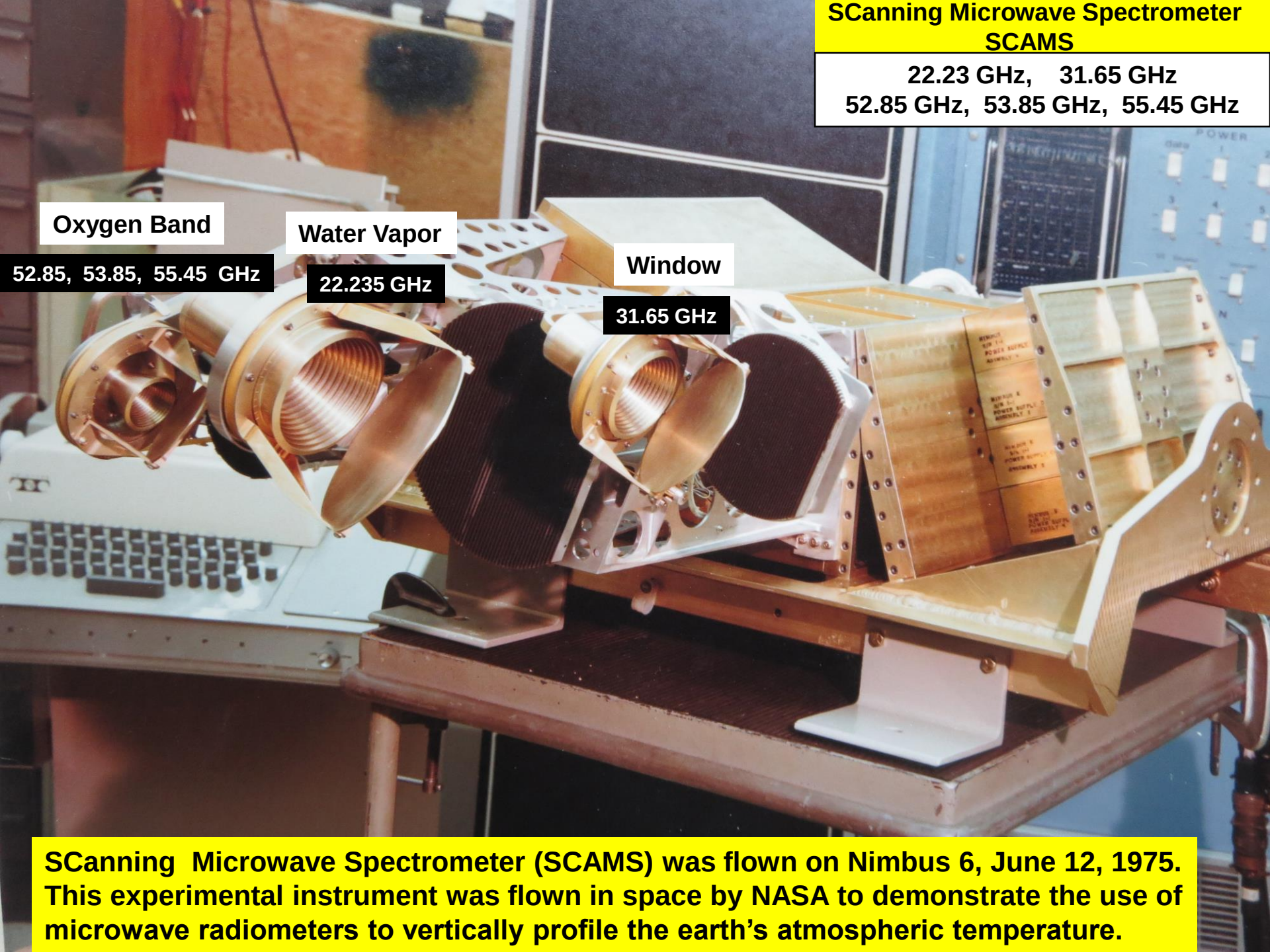

SCanning Microwave Spectrometer (SCAMS) was flown on Nimbus 6, June 12, 1975. This experimental instrument was flown in space by NASA to demonstrate the use of microwave radiometers to vertically profile the earth's atmospheric temperature.

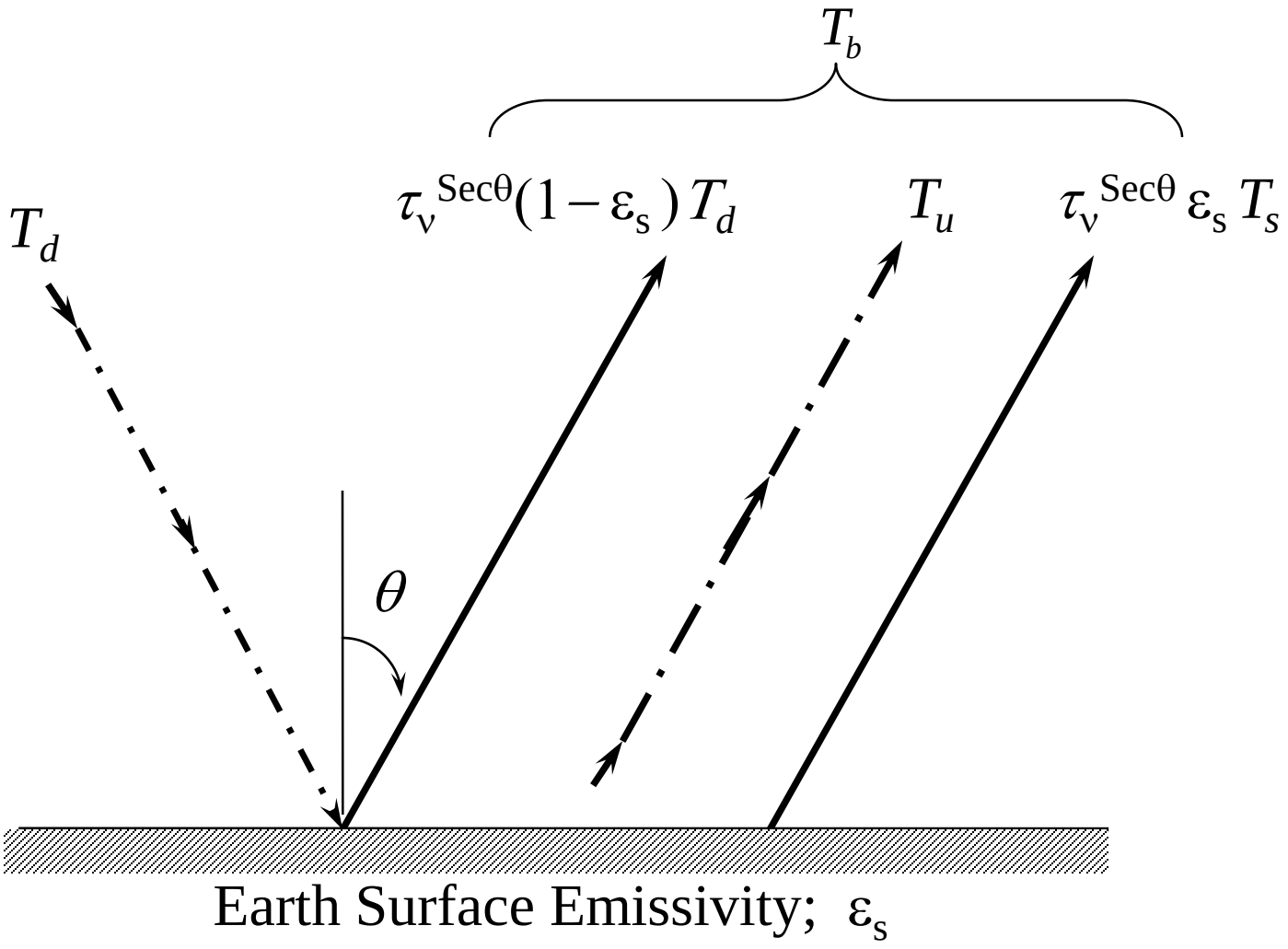

Within the opaque 53 – 60 GHz oxygen band, $T_b \cong T_u = \int_{-\infty}^{lnP_S} T(p)W(p\,;\nu,\theta)\,dlnp$

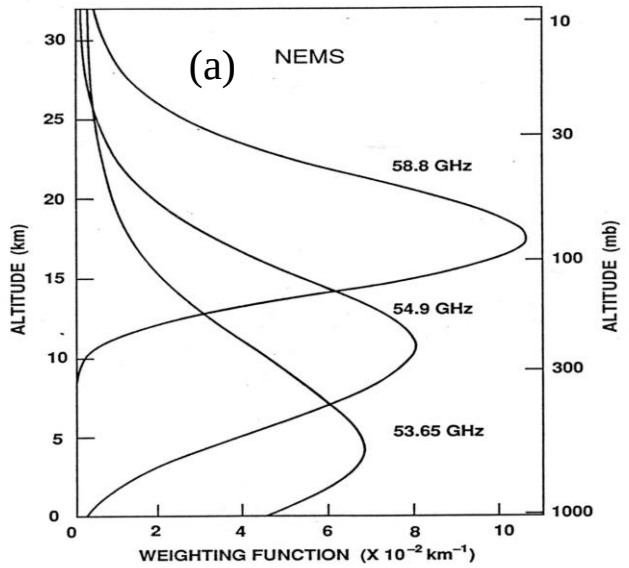

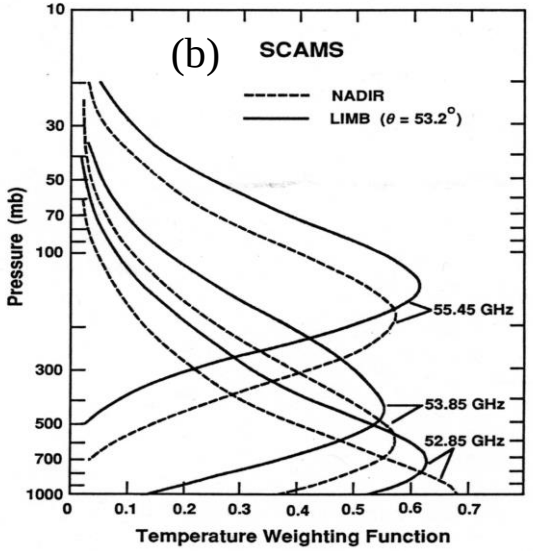

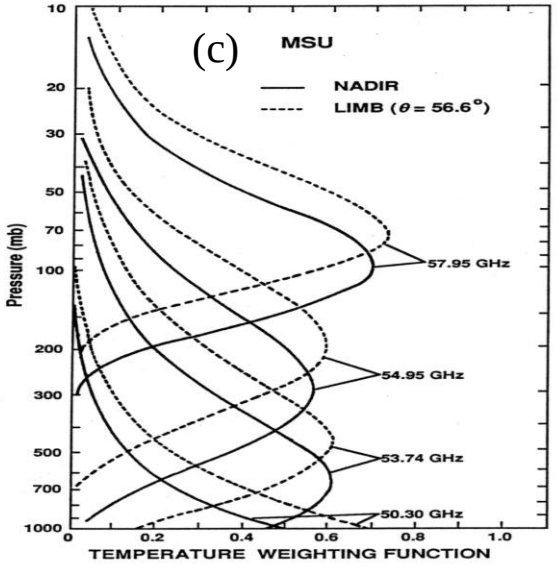

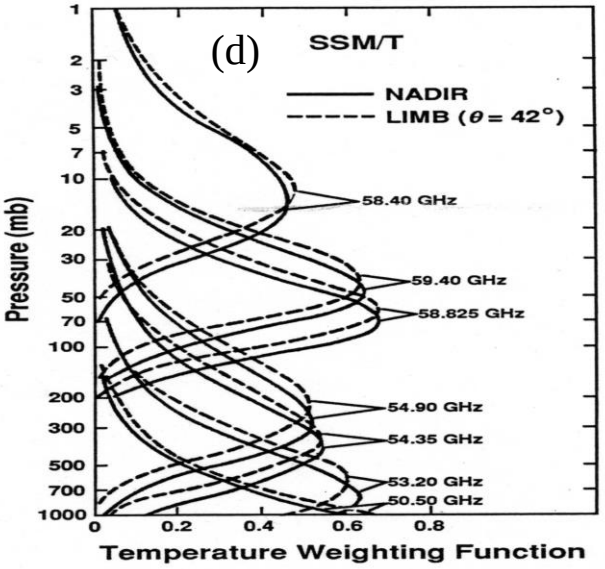

Temperature weighting functions for the (a) NEMS, (b) SCAMS, (c) MSU and (d) SSM/T sensors.

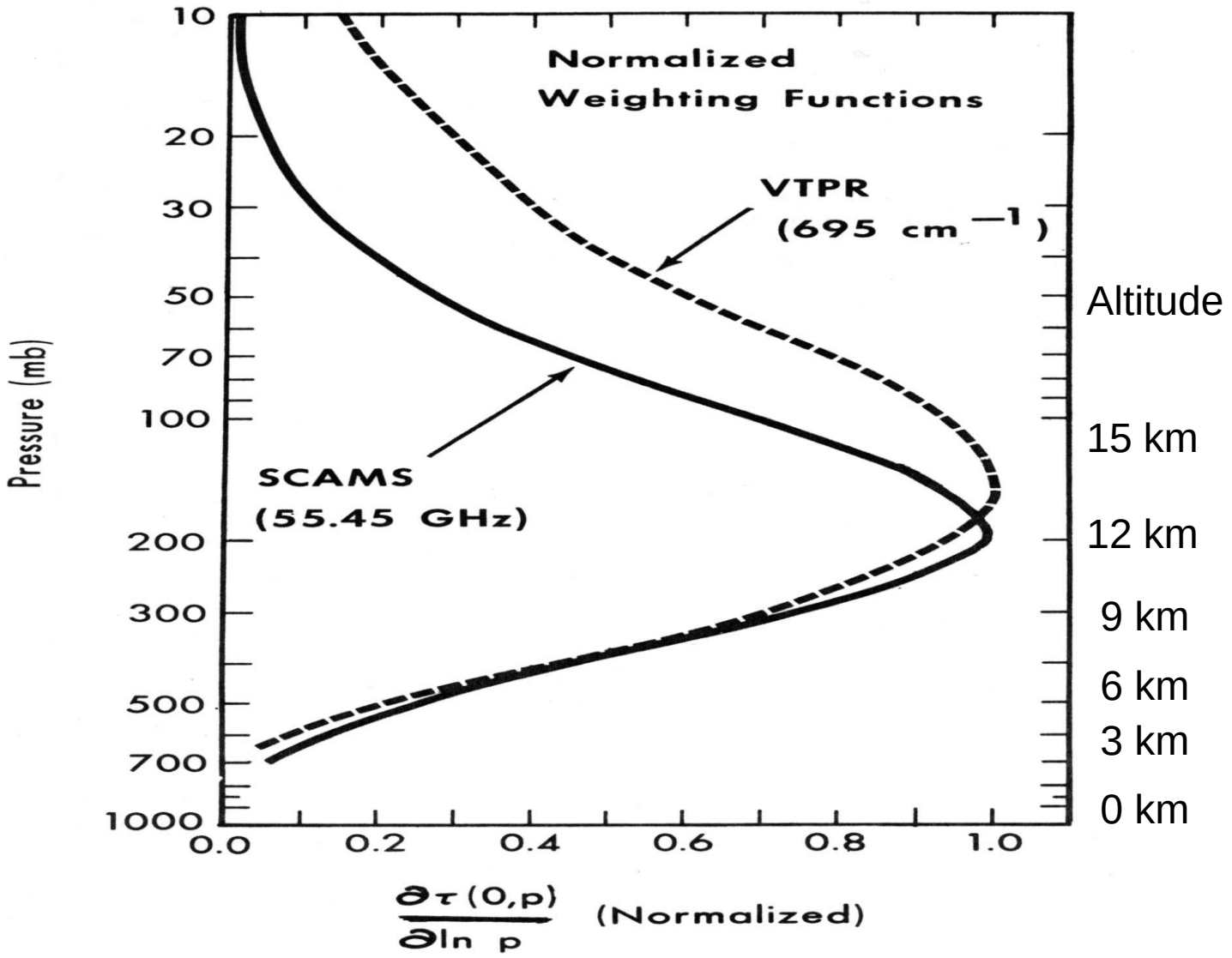

Weighting functions at 55.45 GHz (O_2 band) and 695 cm^{-1} (CO_2 band). The 55.45 GHz channel is one of five frequencies measured by the Scanning Microwave Spectrometer (SCAMS) on Nimbus-6, and the infrared channel at 695 cm^{-1} (14.29μm) is one of six channels measured by the Vertical Temperature Profile Radiometer (VTPR) on NOAA-4.

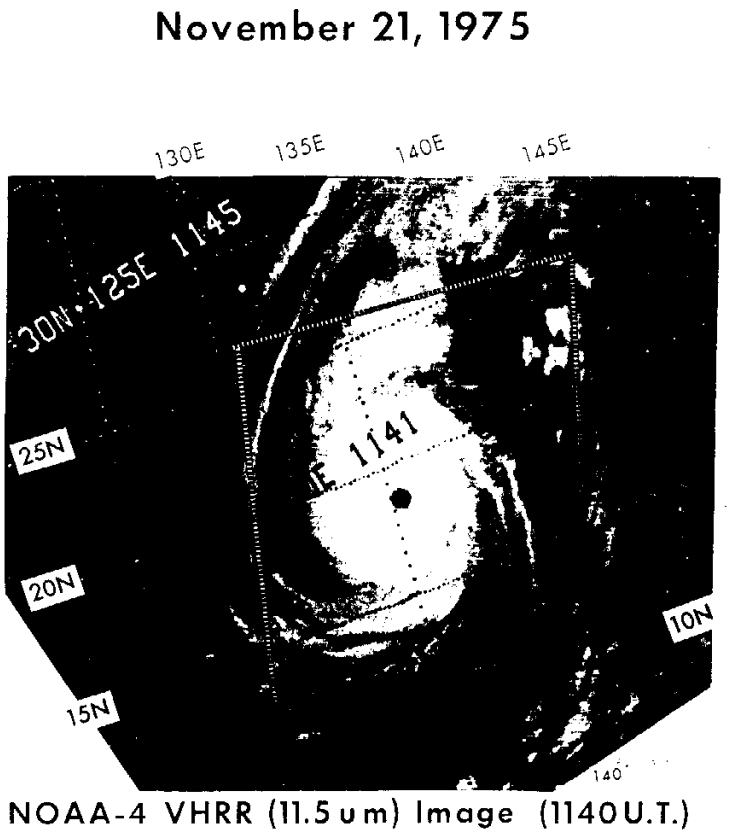

Figure 6: Image of Typhoon June on November 21, 1975 at 1140 GMT using 11.5 μm measurements from the Vertical High Resolution Radiometer (VHRR) on NOAA-4.

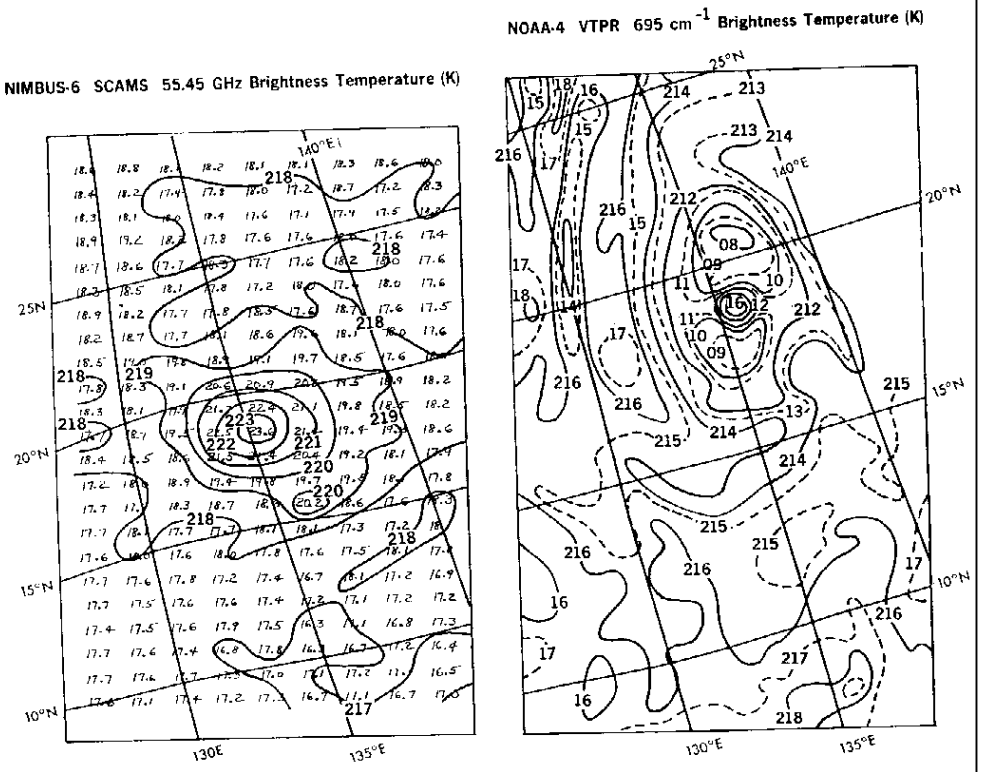

Figure 8: Brightness temperatures (K) for Typhoon June from SCAMS 55.45 GHz measurements (left) and VTPR 695 cm-1 measurements (right).

First dramatic demonstration in 1975 of the cloud penetration property of microwaves using SCAMS, an experimental sounder. Compared to the infrared sounder (VTPR), the SCAMS probes through cloud cover to measure the warm core temperature distribution around 200 mb (12 km) for a Pacific Typhoon named Typhoon June

Microwave Sounding Unit (MSU)

MSU was the first operational microwave sounder flown aboard satellites by NOAA in 1978. Prior to this time only Visible and Infrared sensors were used to monitor the atmosphere. MSU has four channels within the 50-60 GHz oxygen region to profile temperature from the surface to lower stratosphere.

Important Characteristics of MSU Instruments

Besides its *cloud penetrating property*, which lead to a more advanced sounder, of critical importance for climate applications is its *long-term stability* and *precise spectral resolution* which has been duplicated by each MSU flown in space.

Application of MSU Instruments

NOAA and the ECMWF have used MSU temperature soundings to help forecast weather and analyze climate changes globally. It provided the first measurements of global temperature warming from satellites. It's success lead to a more advanced twenty channel instrument in 1998 called AMSU.

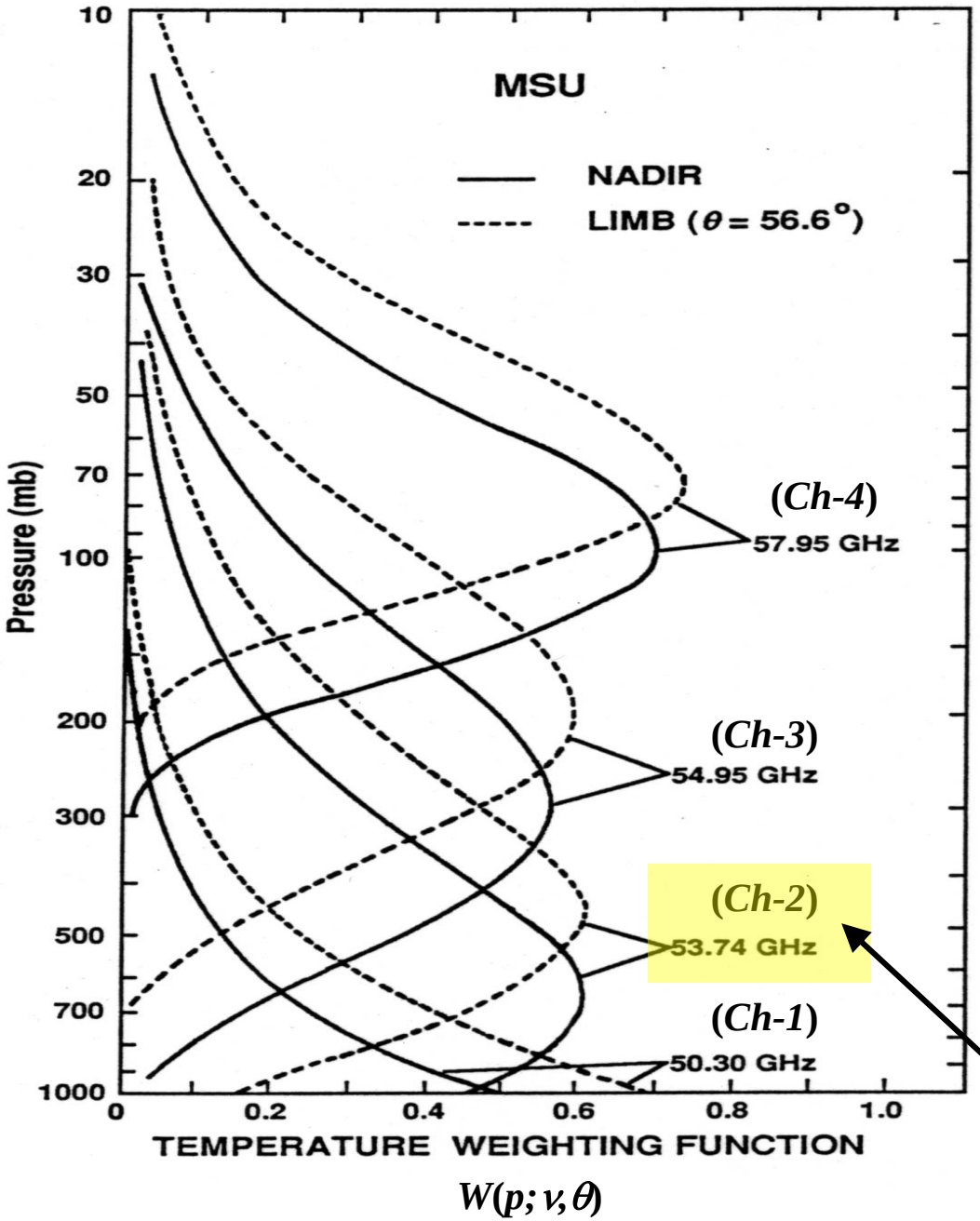

Microwave Sounding Unit MSU

MSU – channels, frequencies and nadir - transmittance

Channel #	Freq. (GHz)	τ
4	57.95	0.000
3	54.95	0.001
2	53.74	0.100
1	50.30	0.700

For MSU channels – 2, 3, 4

$$T_b \cong \int_{-\infty}^{\ln P_S} T(p)\, W(p;\nu,\theta)\, d\ln p$$

Channel Used to Monitor Global Warming

Microwave Sounding Unit (MSU)

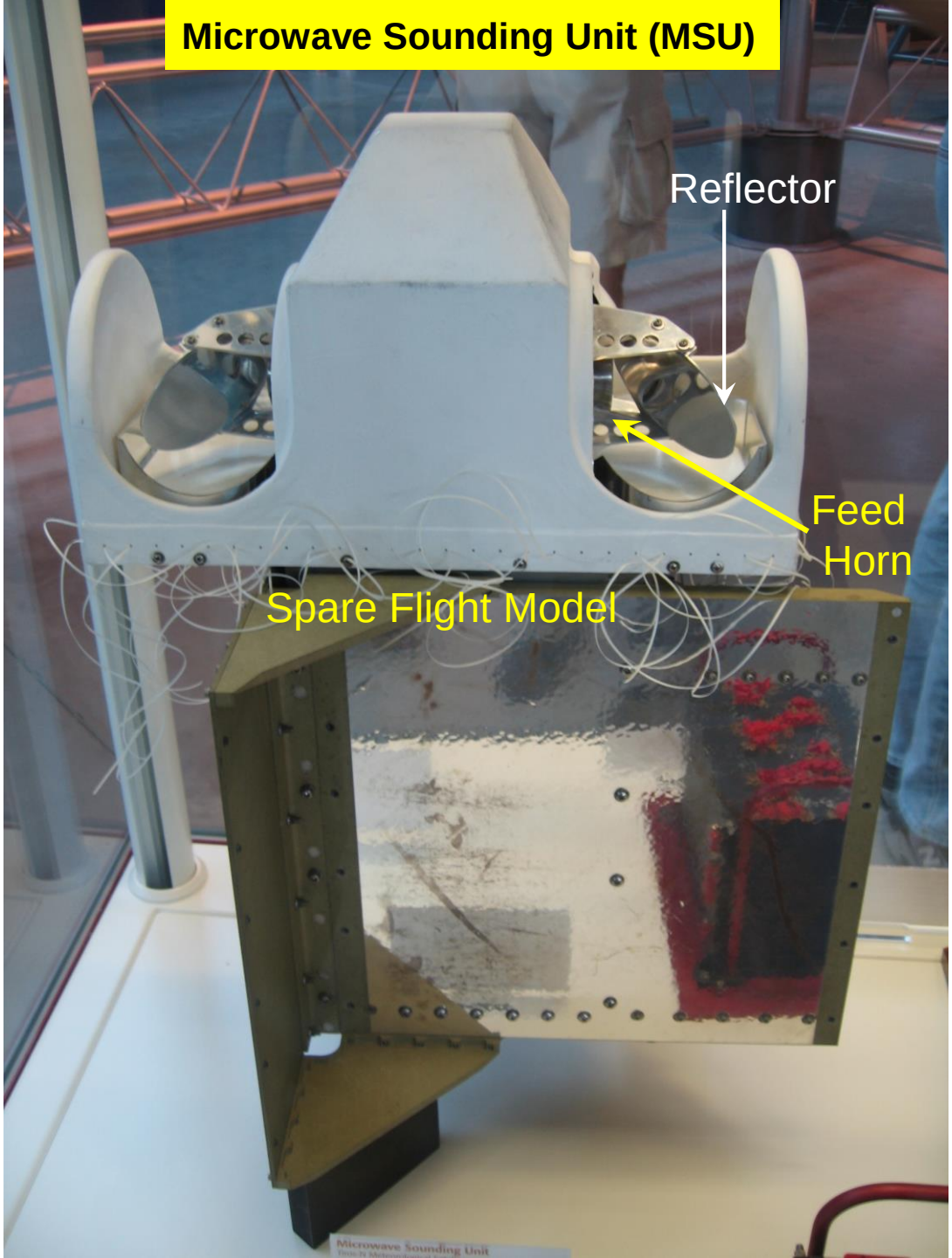

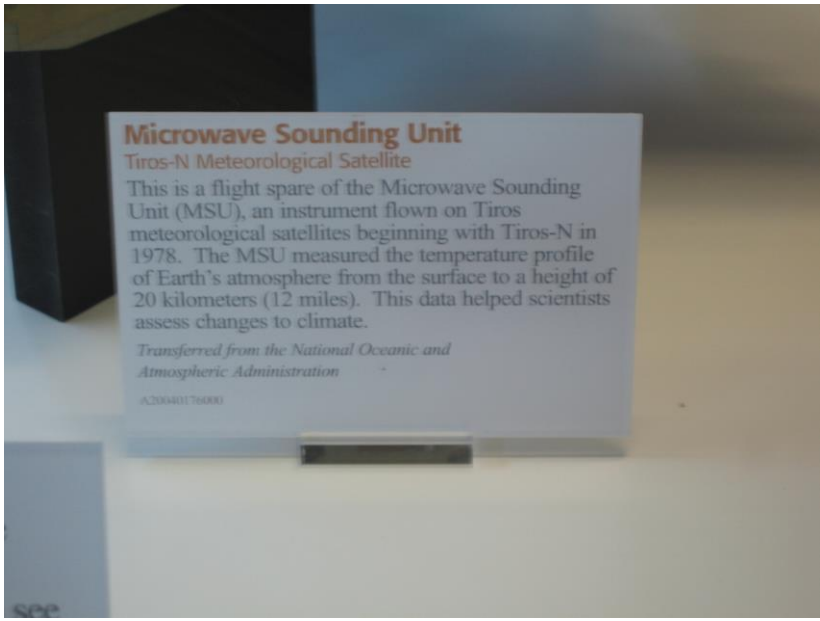

Smithsonian Institution
National Air & Space Museum

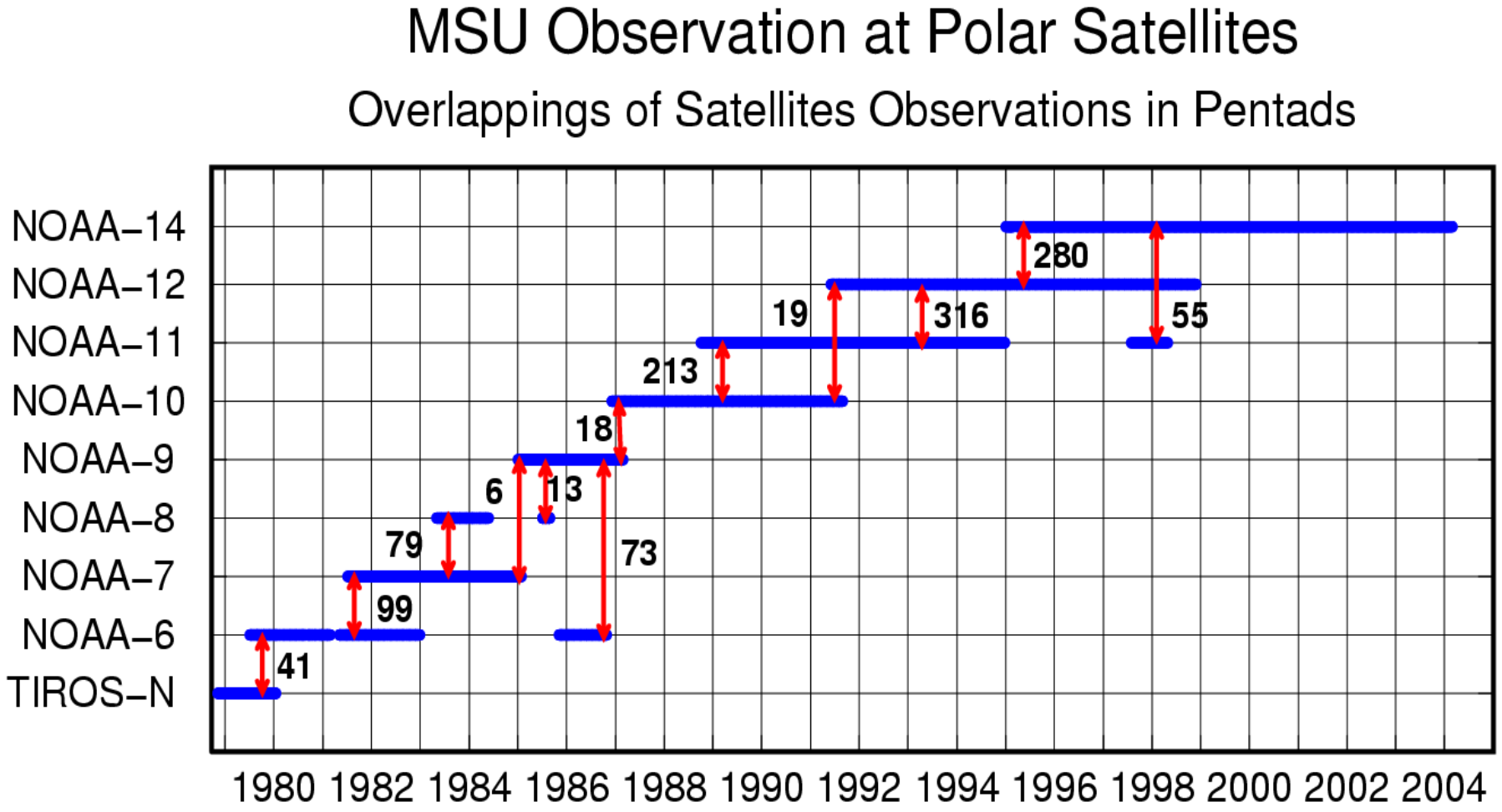

This figure shows all **12** overlaps for the **9- MSU** satellites. Note that **NOAA-9** is a critical satellite since it interconnects the later MSU's through **NOAA-10**.

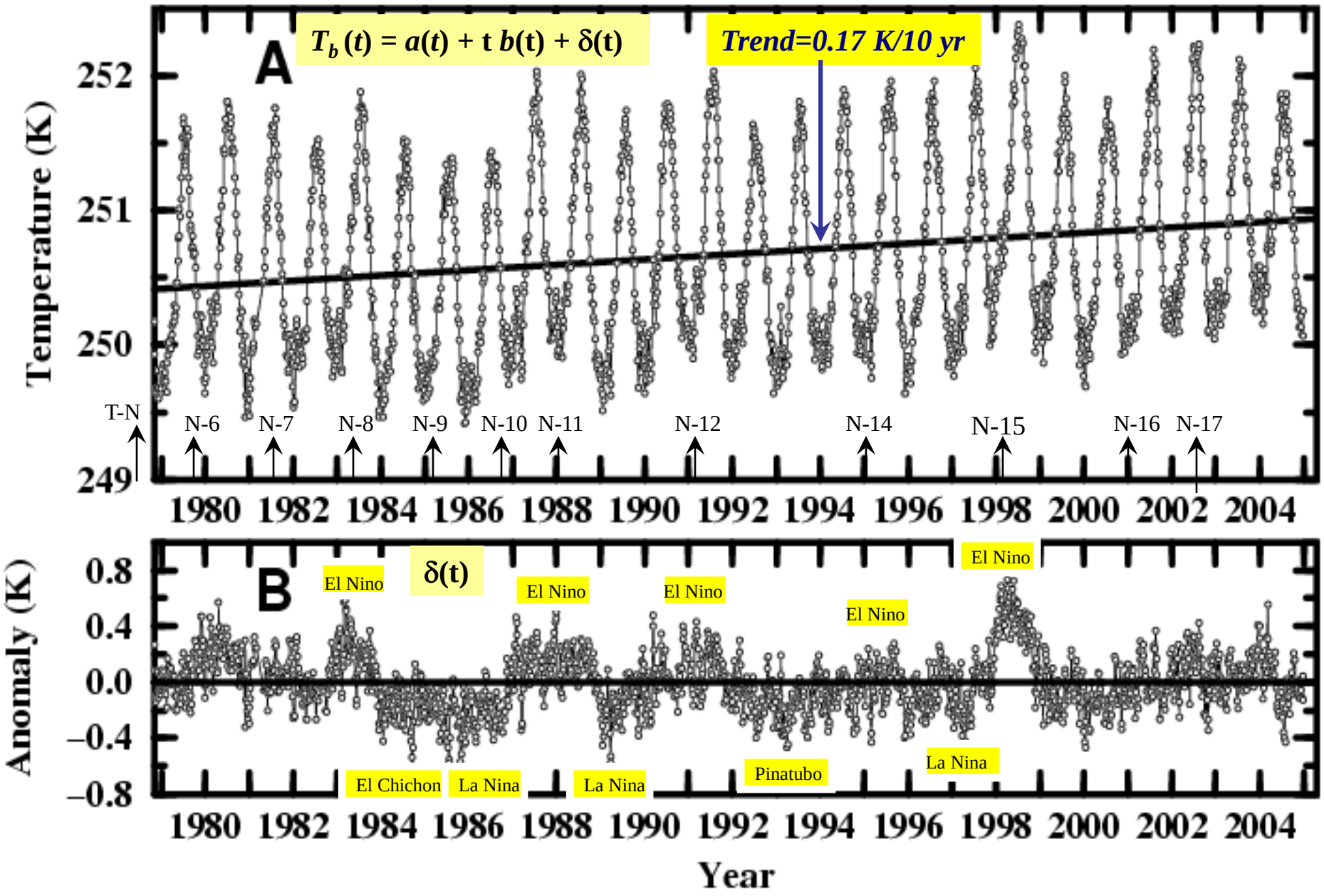

Global & pentad averaged MSU Channel 2 T_b and linear trend in global averages (A) and detrended anomalies (B), Δ(t). $T_b(t) = a(t) + t\,b(t) + \delta(t)$ where $a(t)$ and $b(t)$ contain diurnal & seasonal variations.

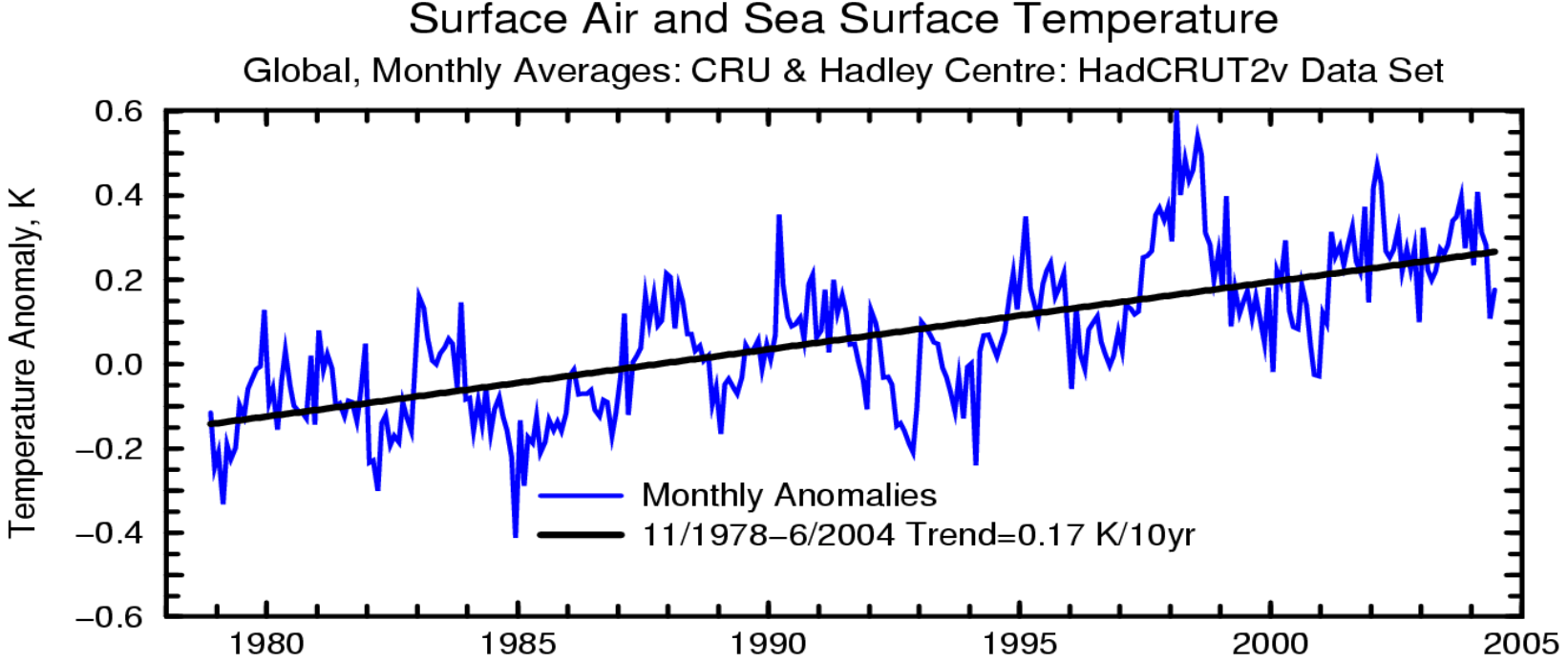
Surface Air and Sea Surface Temperature
Global, Monthly Averages: CRU & Hadley Centre: HadCRUT2v Data Set
Temperature Anomaly, K
0.6
0.4
0.2
0.0
−0.2
−0.4
−0.6
1980
1985
1990
1995
2000
2005
Monthly Anomalies
11/1978–6/2004 Trend=0.17 K/10yr

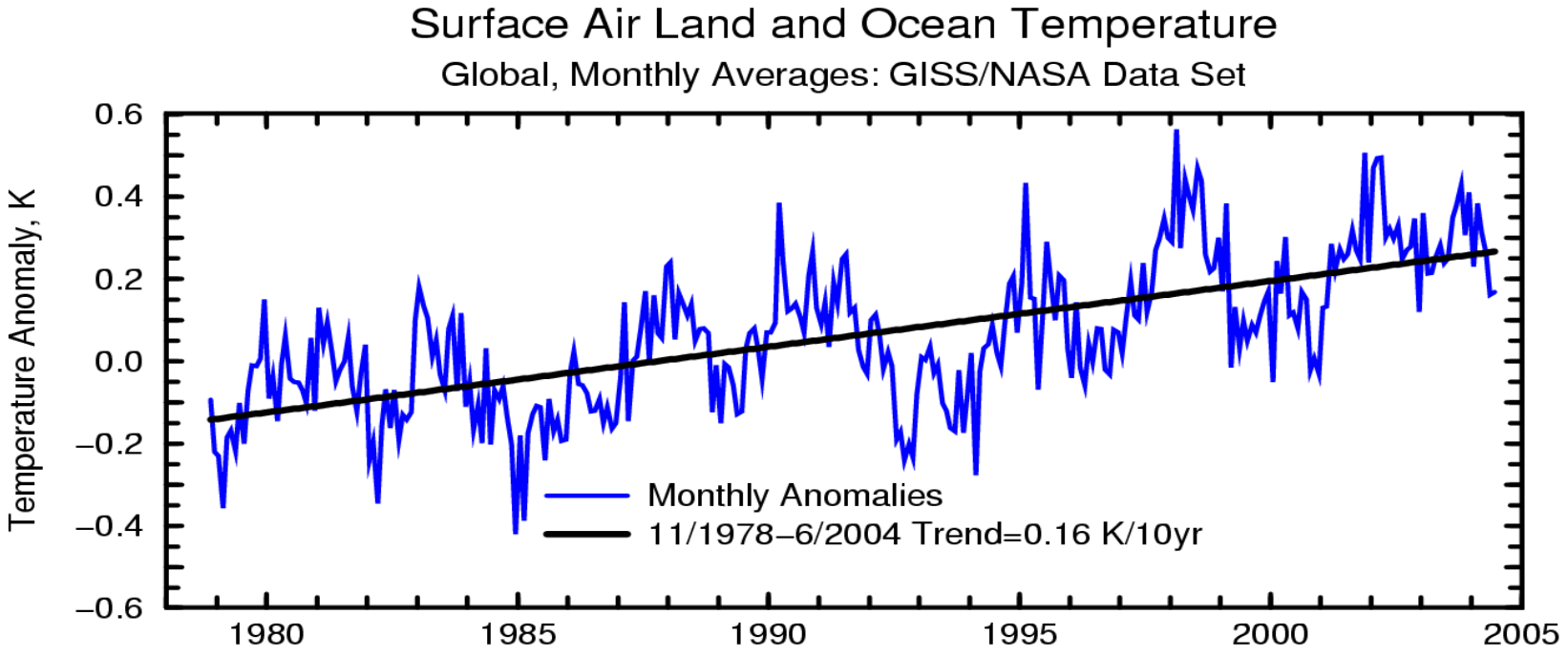
Surface Air Land and Ocean Temperature
Global, Monthly Averages: GISS/NASA Data Set
Temperature Anomaly, K
0.6
0.4
0.2
0.0
−0.2
−0.4
−0.6
1980
1985
1990
1995
2000
2005
Monthly Anomalies
11/1978–6/2004 Trend=0.16 K/10yr

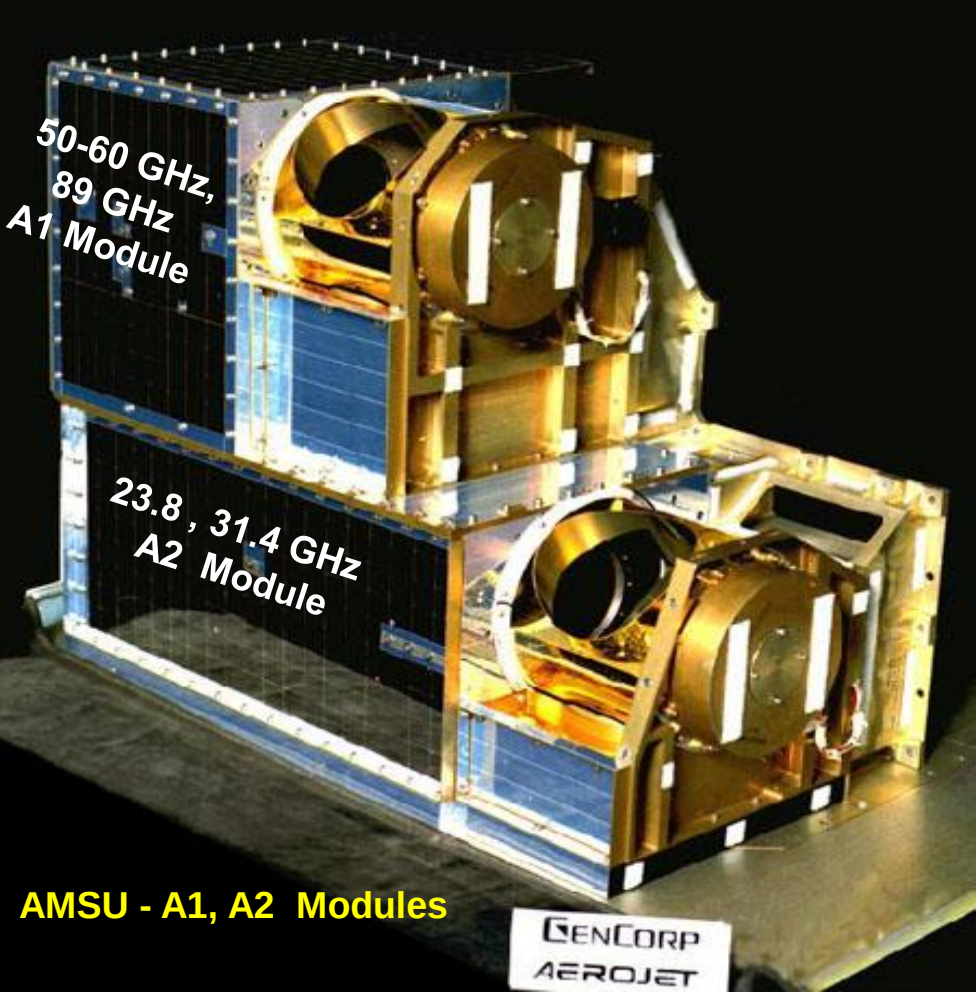

AMSU - A1, A2 Modules

Advanced Microwave Sounding Unit (AMSU) is a 20-channel cross-track total power radiometer. The above shows the AMSU-A module which contains 12 temperature sounding channels within the 50-60 GHz oxygen absorption band. It's weighting functions are shown on the right-side.

This instrument has an instantaneous field-of-view of 3.3° at the half-power points providing a spatial resolution at nadir of 48 km. The antenna provides a cross-track scan, scanning ±48.3° from nadir with a total of 30 Earth fields-of-view per scan line. It completes one scan every 8 seconds

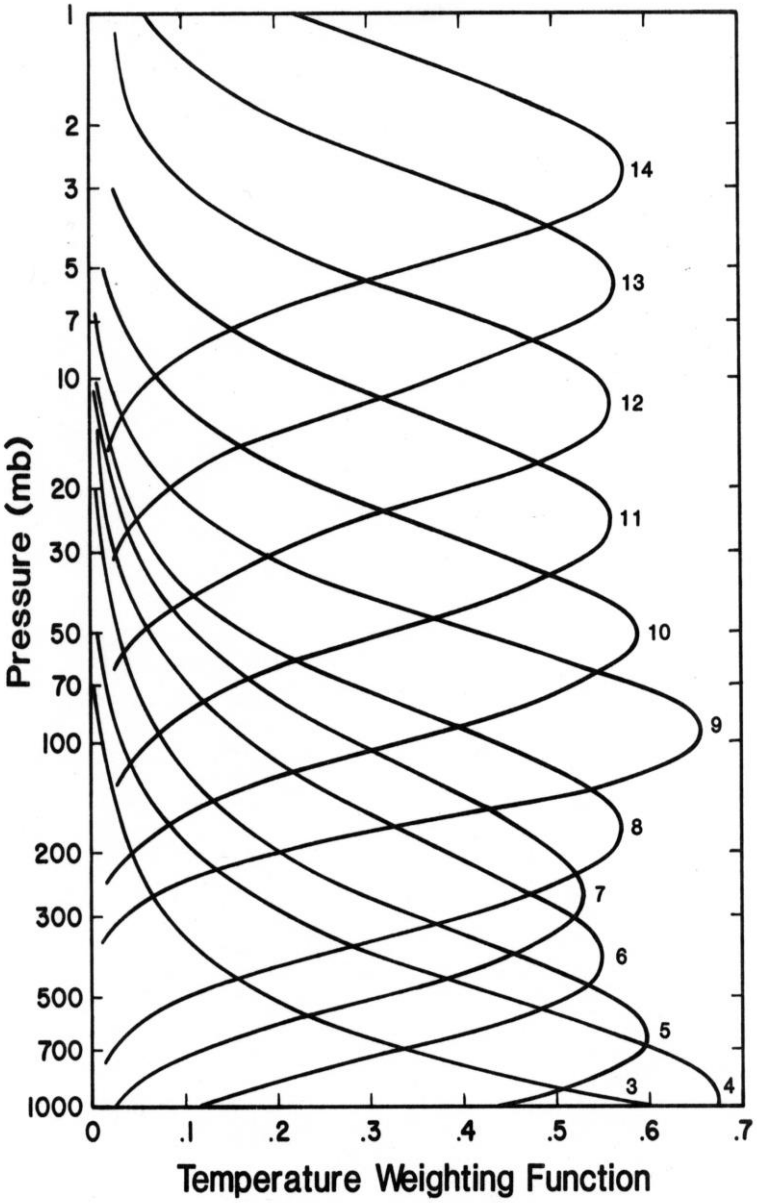

AMSU Temperature Weighting Functions at Nadir Viewing

AMSU COMPONENT MODULES

AMSU A1

O_2 Channels

A1-1

89.0 GHz
54.4 GHz
54.9 GHz
57.3 GHz
- - - GHz

A1-2

50.3 GHz
52.8 GHz
53.6 GHz
55.5 GHz

48 km IFOV at Nadir

AMSU A2

Window Channels

23.8 GHz
31.4 GHz

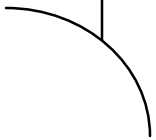

48 km IFOV at Nadir

AMSU B

H_2O Channels

89 GHz
150 GHz
183 +/- 7 GHz
183 +/- 3 GHz
183 +/- 1 GHz

16 km IFOV at Nadir

AMSU A & B Channels

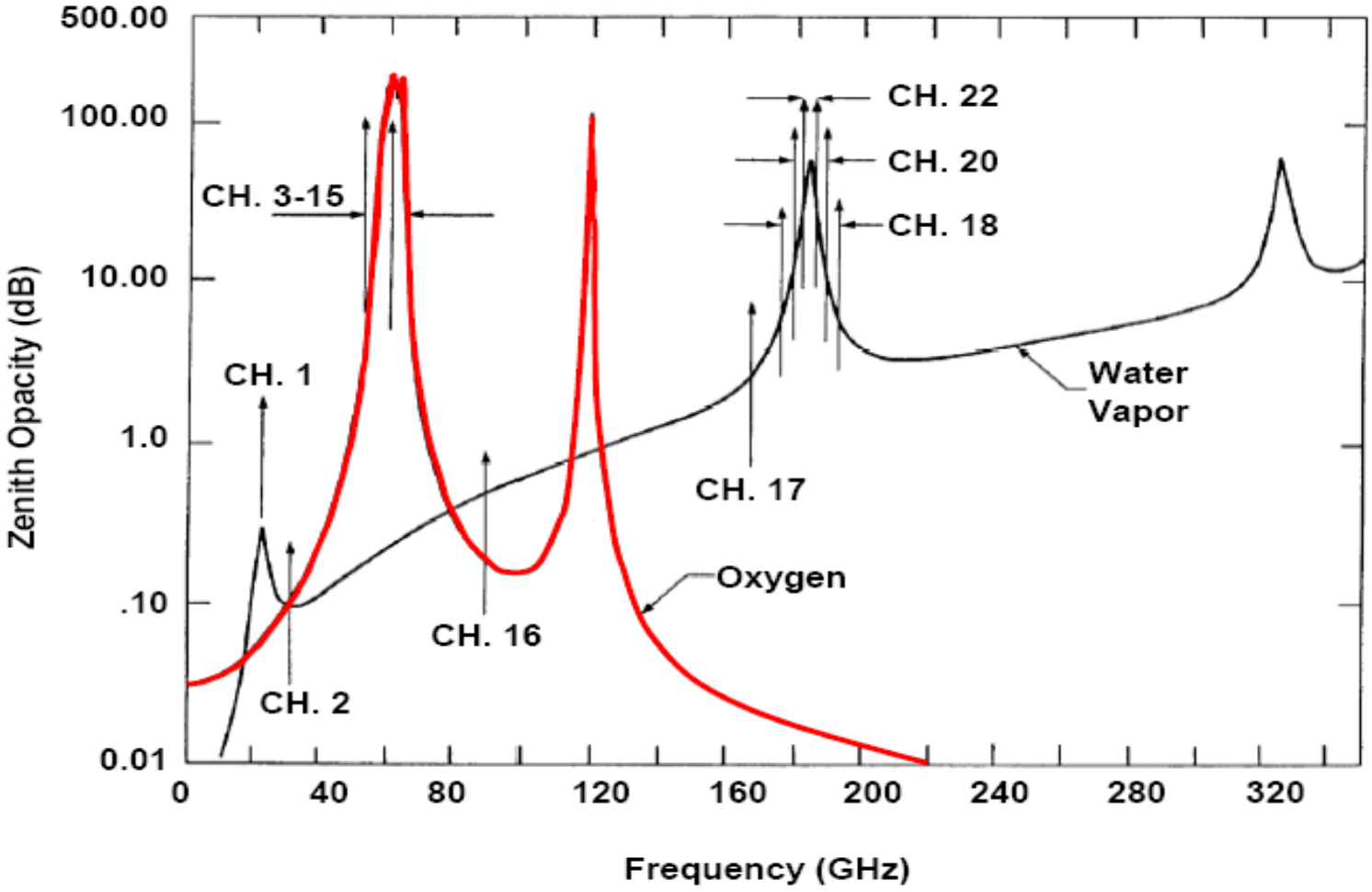

Goodrum, G. *et al.*, *NOAA KLM Users Guide*, section 3.4, p. 2, NOAA, 2000

Hurricane Isabel Temperature Anomaly Derived from AMSU Measurements

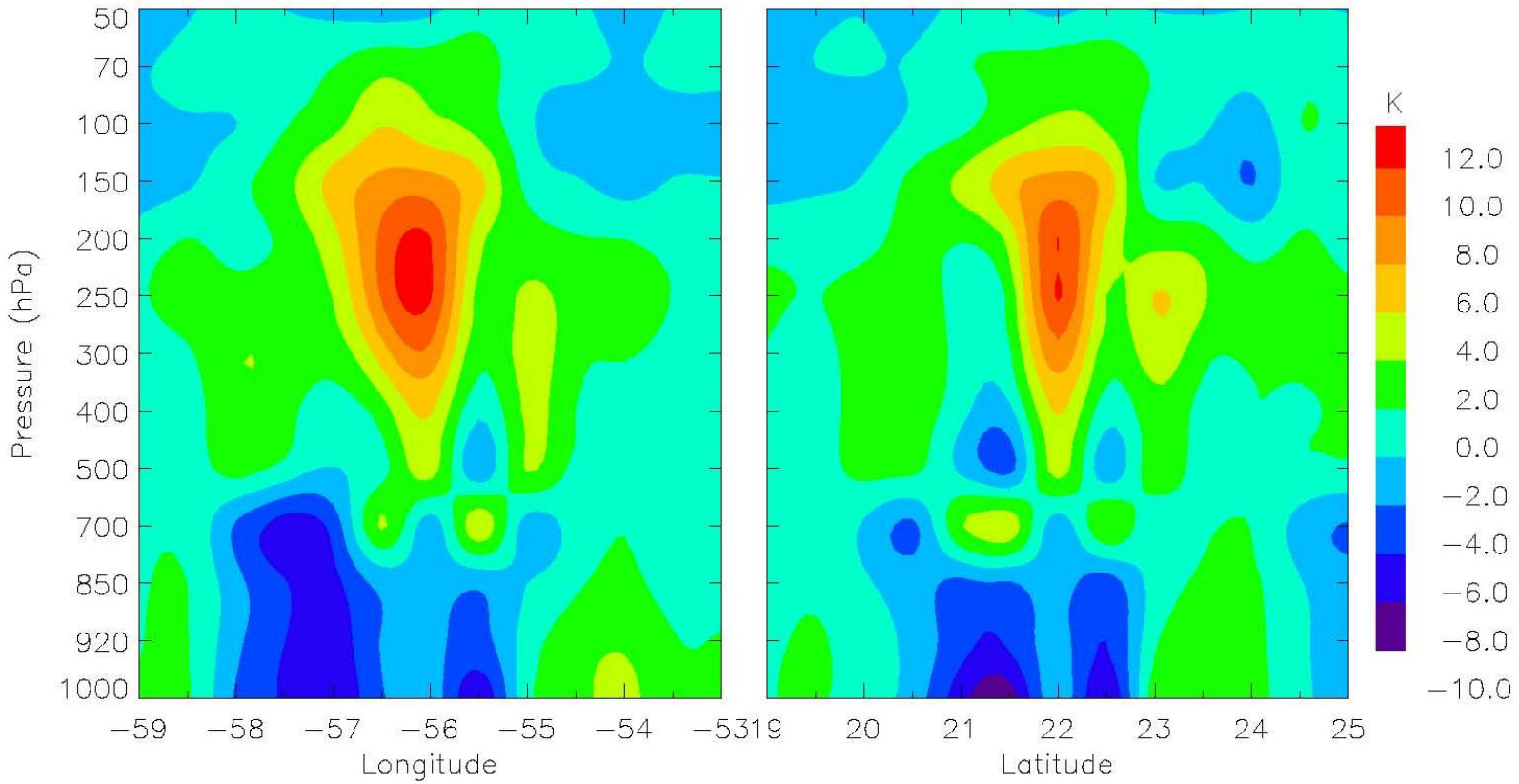

Vertical cross section of temperature anomalies at 06:00 on Sept. 12. 2003.

Left panel: west-east cross section. Right panel: south-north cross section.

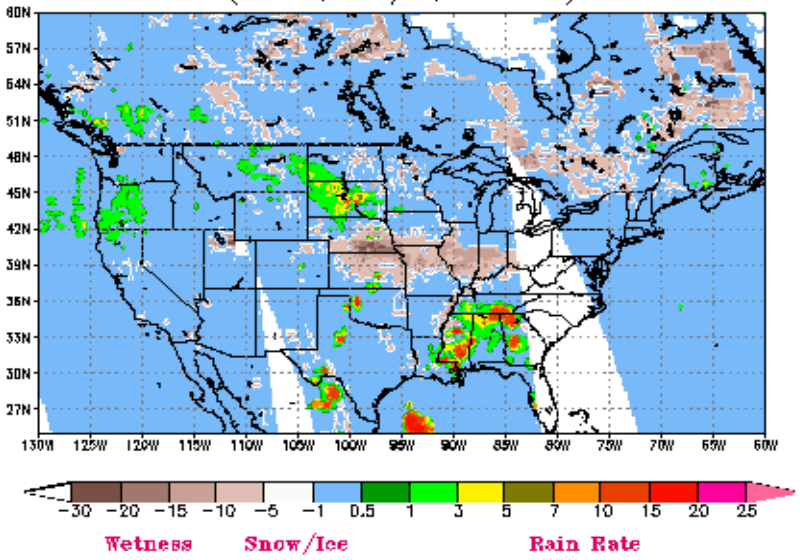
NOAA-15 AMSU Hydrology Product Composite at 2001-06-04 LST 19:30
(Wetness, Snow/Ice, Rain Rate)
Wetness
Snow/Ice
Rain Rate

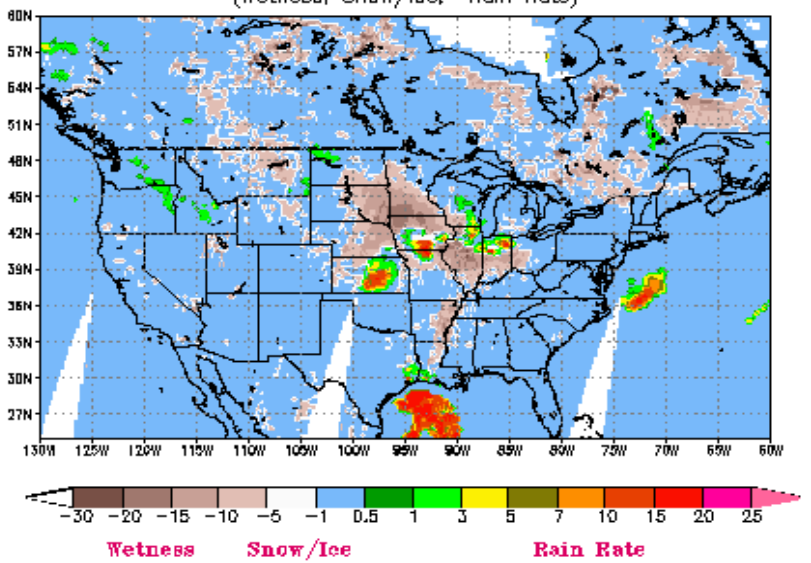
NOAA-15 AMSU Hydrology Product Composite at 2001-06-05 LST 7:30
(Wetness, Snow/Ice, Rain Rate)
Wetness
Snow/Ice
Rain Rate

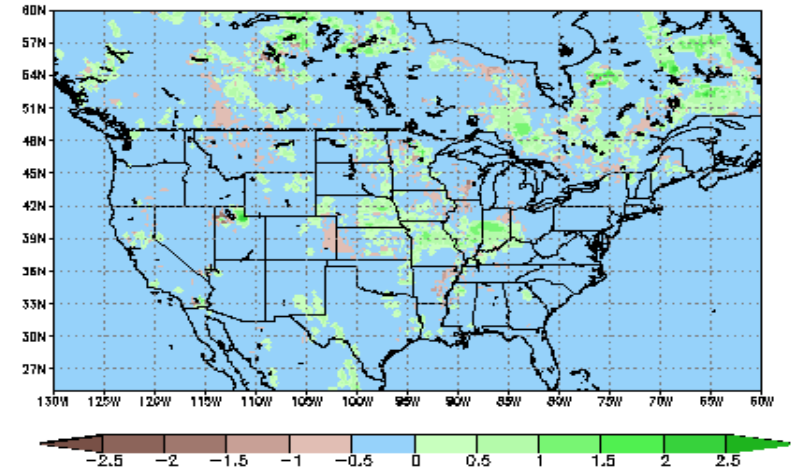
The Time Variation of Wetness at 2001-06-04 LST 19:30

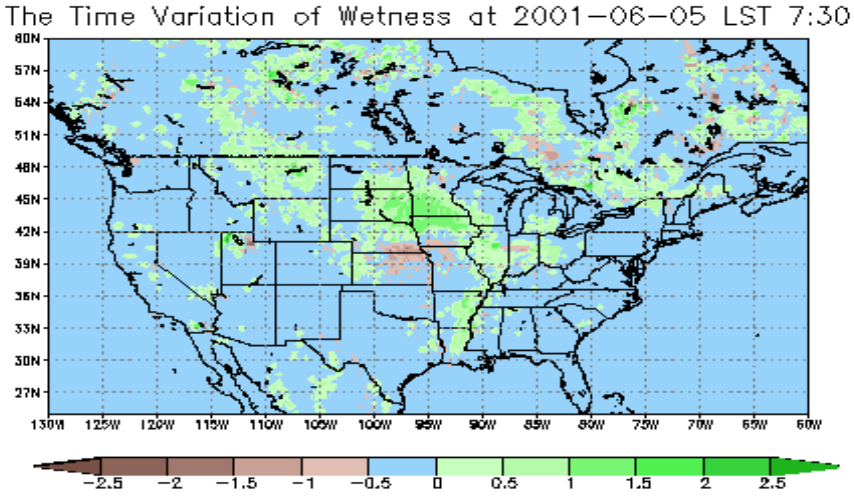
The Time Variation of Wetness at 2001-06-05 LST 7:30

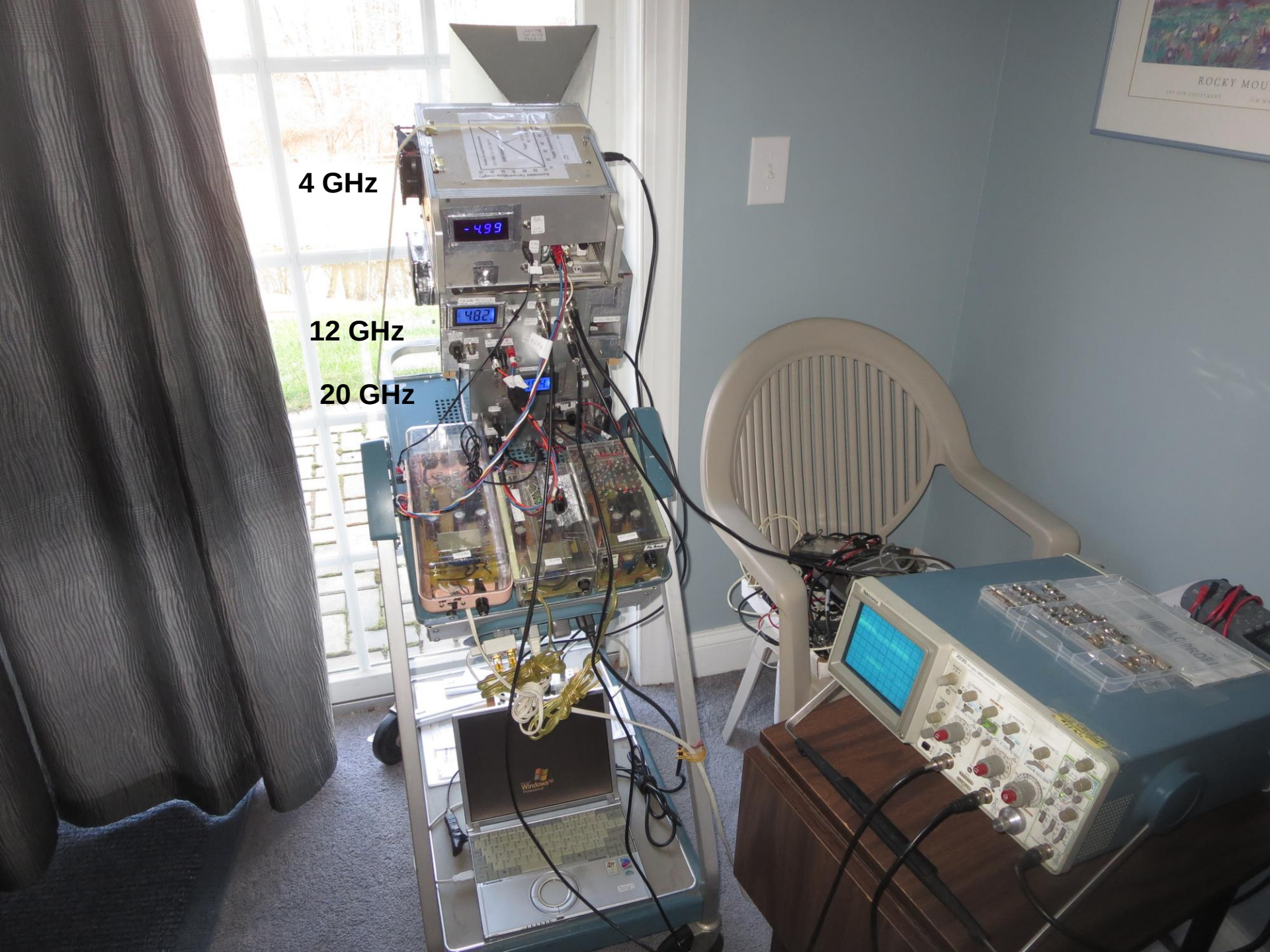
4 GHz
12 GHz
20 GHz

20 Gz
4 Gz
12 Gz

Brightness Temperature T_b received by Ground - Based Radiometers

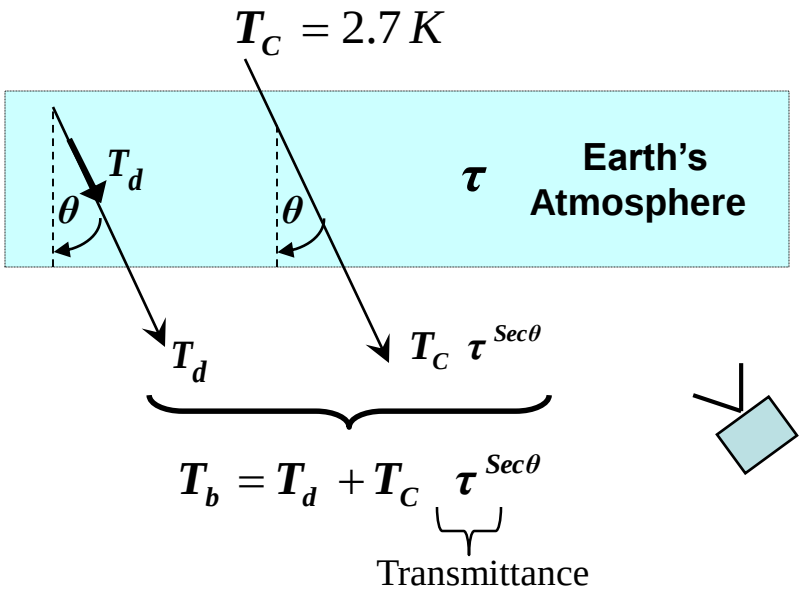

$$T_d = \underbrace{(1-\tau^{Sec\theta})}_{\text{Atmospheric emission}} * \underbrace{T_M}_{\text{Mean Temperature}}$$

$$T_b = [1-\tau^{Sec\theta}]\,T_M + \tau^{Sec\theta}\,T_C$$

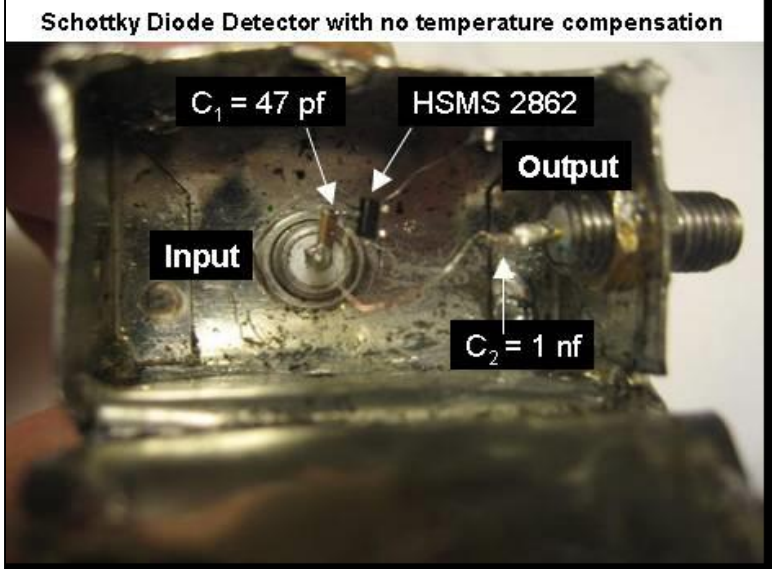

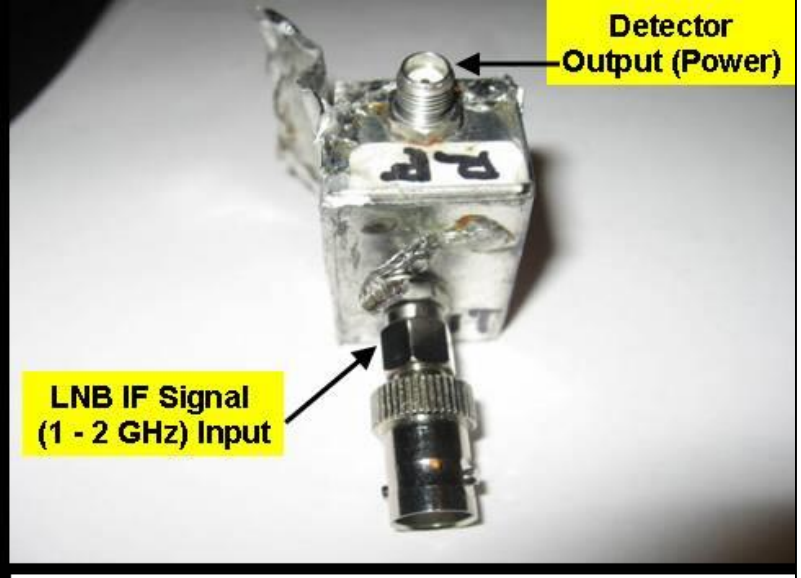

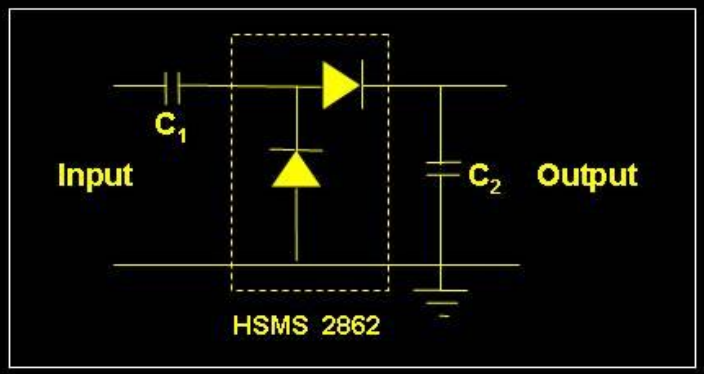

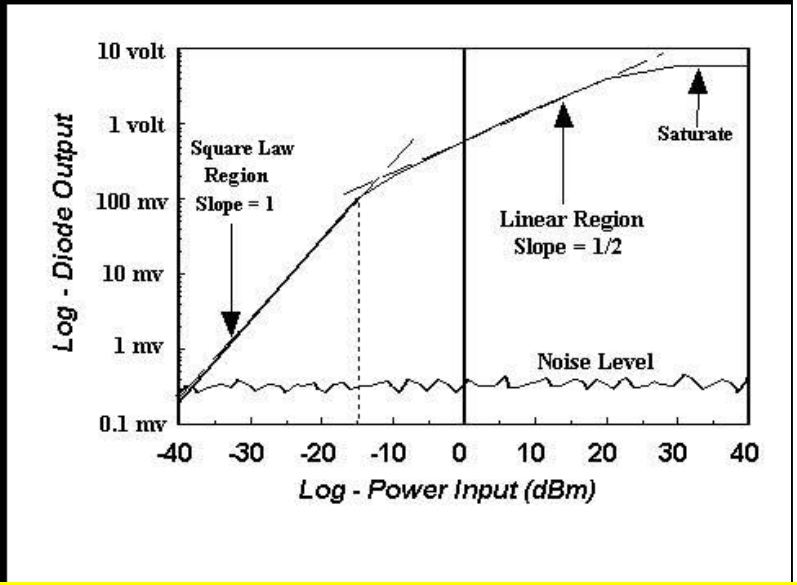

The HSMS 2862 Schottky diode contains two elements connected together to double the sensitivity. The circuit is shown in bottom-left, while the open unit (top left) shows the components wire connected.

The bottom-right shows the generic detector response on a Log-Log plot. It shows the regions for which a diode displays a square law and linear response. To assure a square law response (*i.e.*, V_{out} = k P_{in}) the input power must be below -15 dBm so that the diode's output voltage is less than 100 mv.

Detector Temperature - Uncompensated

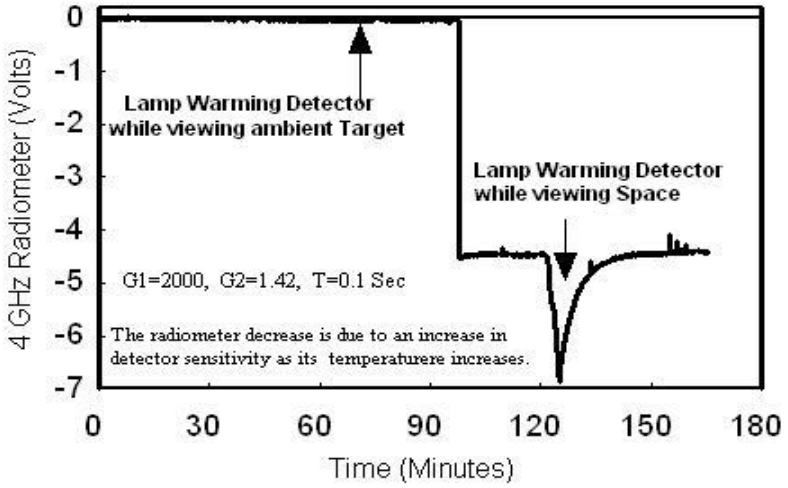

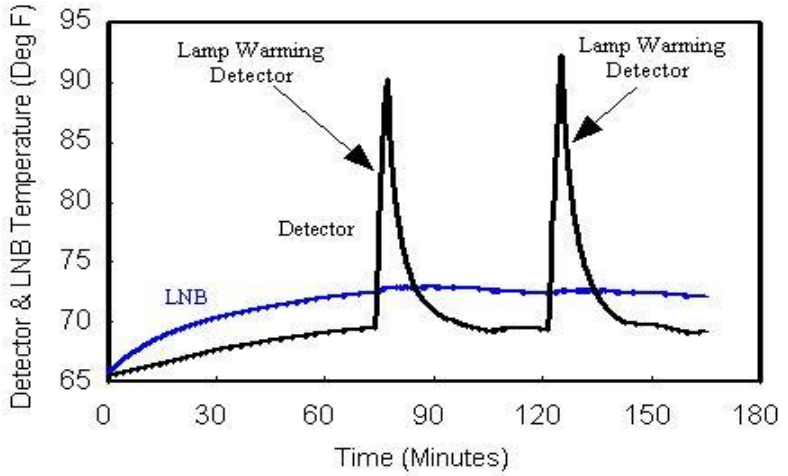

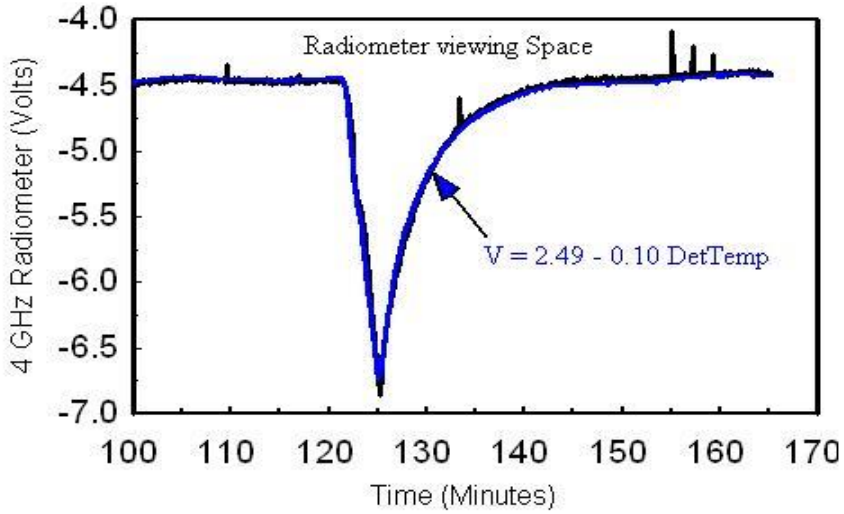

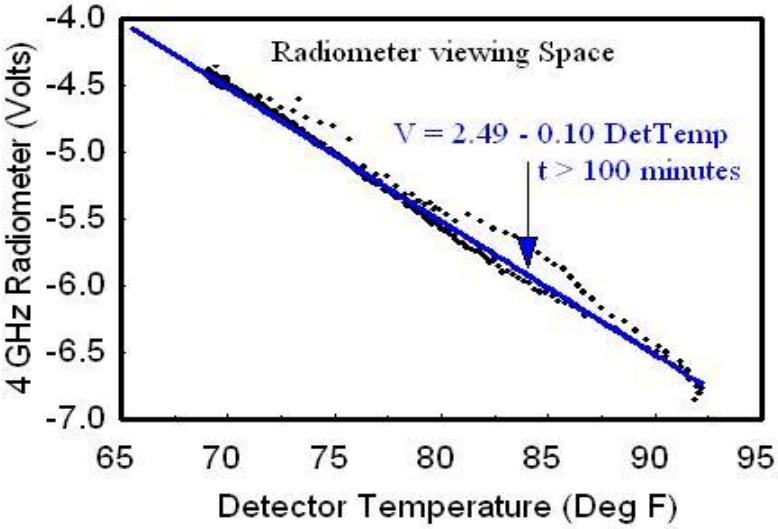

Early 4 GHz radiometer with uncompensated Schottky diode detector displays the detector temperature effect. Top-left shows the radiometer voltage when the antenna views the high emissivity target followed by the space view. Top-right shows the detector and LNB temperatures. Bottom-left shows the space viewing measurements while the bottom right plots these voltages against detector temperature.

Temperature Compensated Detector

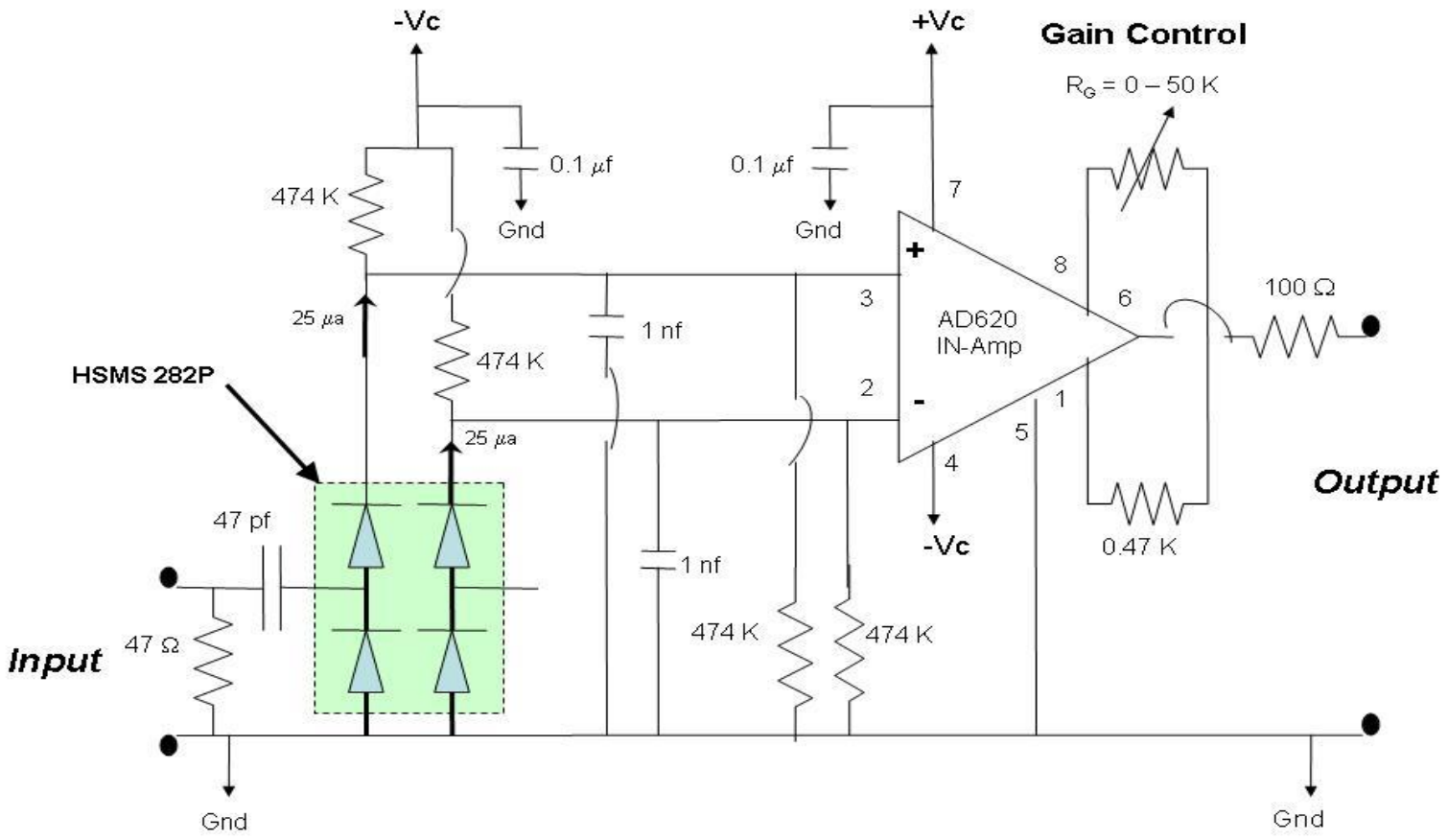

Temperature compensated square law detector for the 4 GHz radiometer uses an HSMS 282P balanced Schottky diode and an AD620 instrumentation amplifier that is powered using a supply voltage, V_C, of +/-12 volts. The amplifier gain can be varied from 2 to 100 by setting the resistor R_G according to the equation Gd =1+ 49.4/(RG+ 0.47). To optimize dynamic range, diodes are slightly forward biased (25 μa).

Detector Temperature Compensation

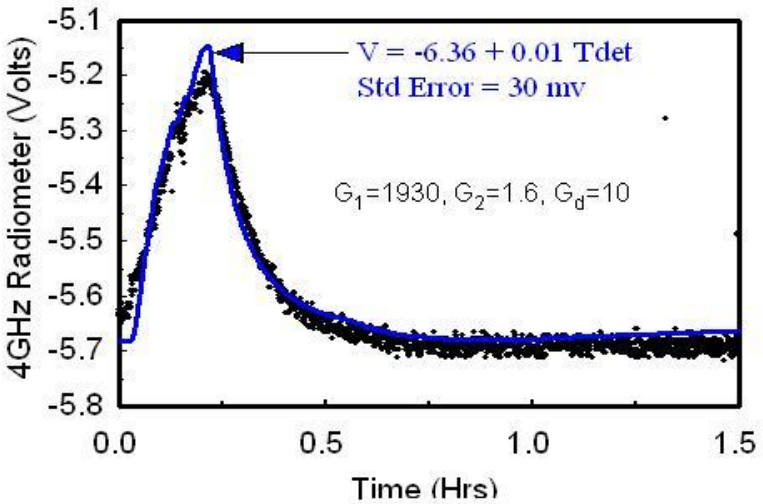

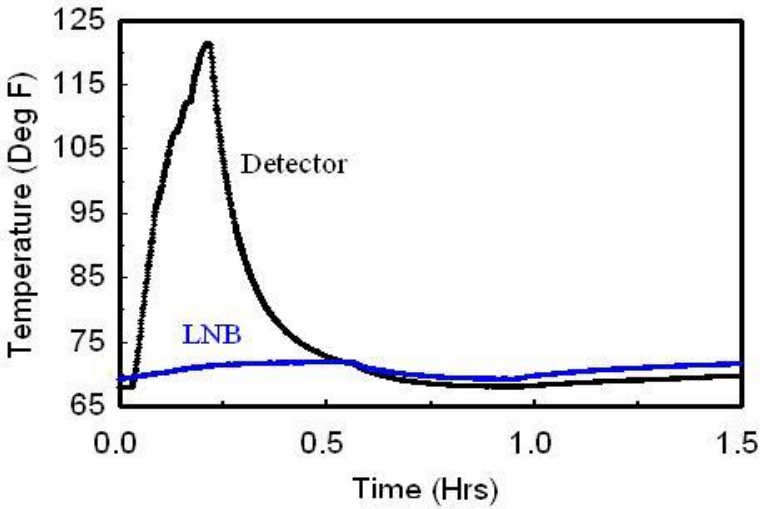

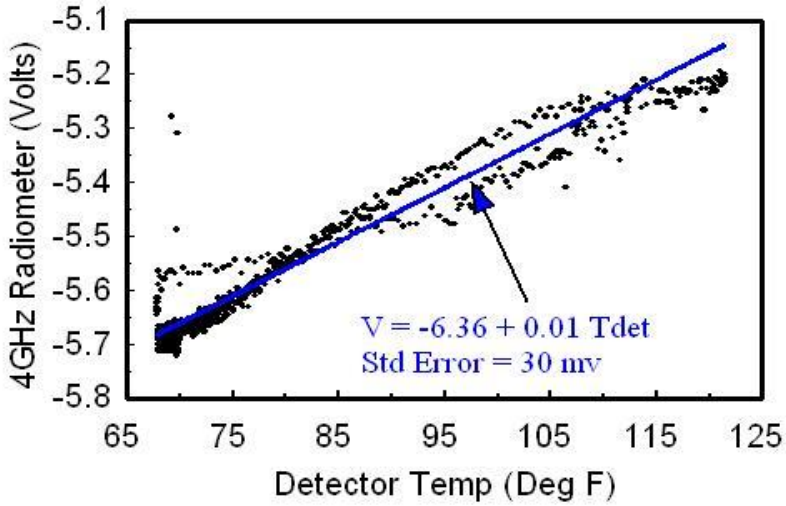

4 GHz radiometer with a temperature compensated detector displays a reduced temperature effect compared to the uncompensated detector. The radiometer views space while the detector temperature is increased by 55 ^{0}F using an incandescent lamp. The top-left shows the radiometer voltage increasing with detector temperature (top-right) with a sensitivity of +0.01 V ^{0}F (bottom). This sensitivity is 10 times less than the uncompensated detector whose temperature sensitivity is - 0.10 V ^{0}F.

Detector Square Law Response

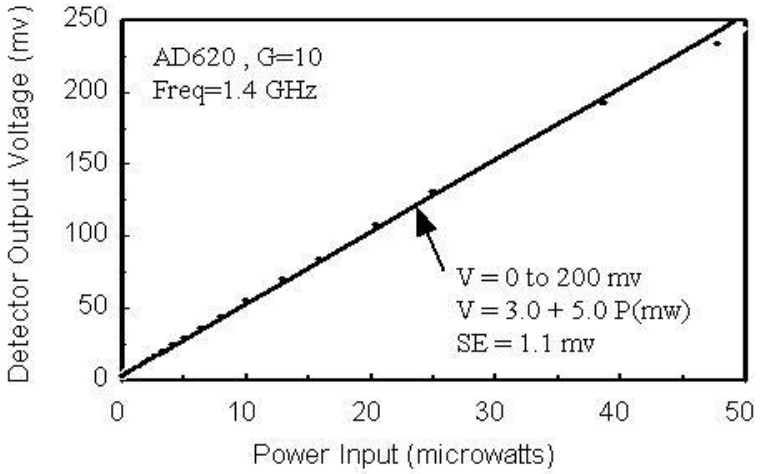

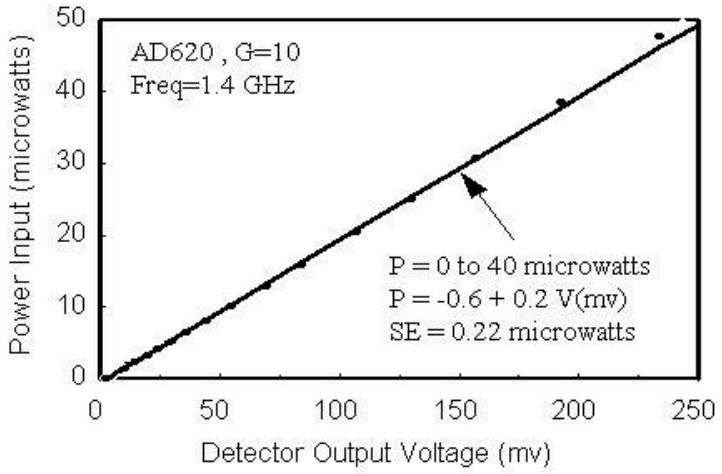

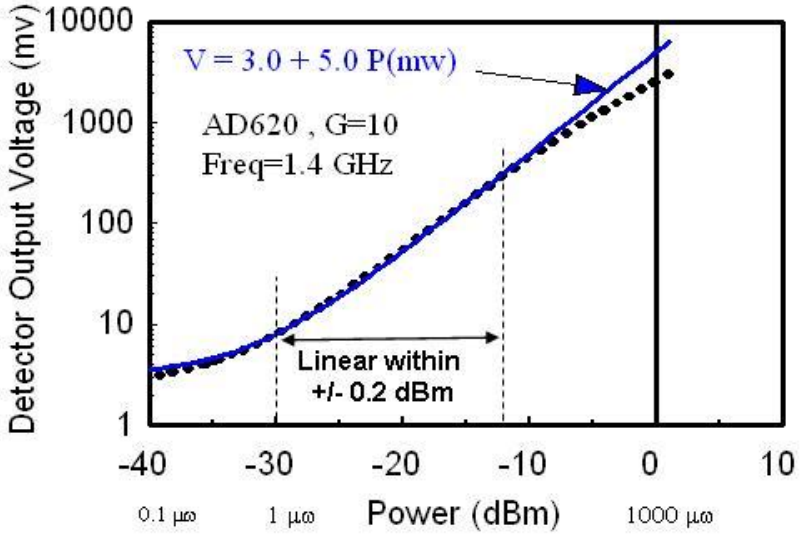

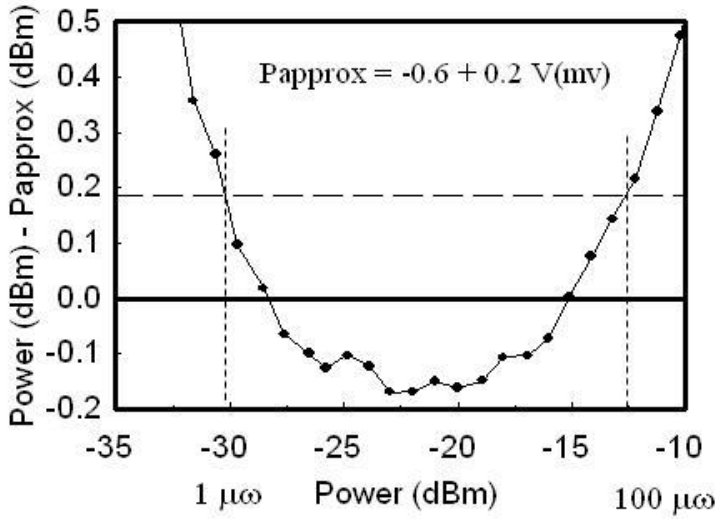

Measurements of 4 GHz radiometer detector at 1.4 GHz with the AD620 amplifier gain set to 10. The top-left shows the detector output voltage as a function of input power, while the adjacent figure shows the inverse relationship. The detector output voltage varies linearly with input power (bottom-left) over a -30 to -12 dBm range, with a +/- 0.2 dBm accuracy (bottom-right). However, the bottom figures show the detector is greater than a power law at very low levels and closer to linear at high levels.

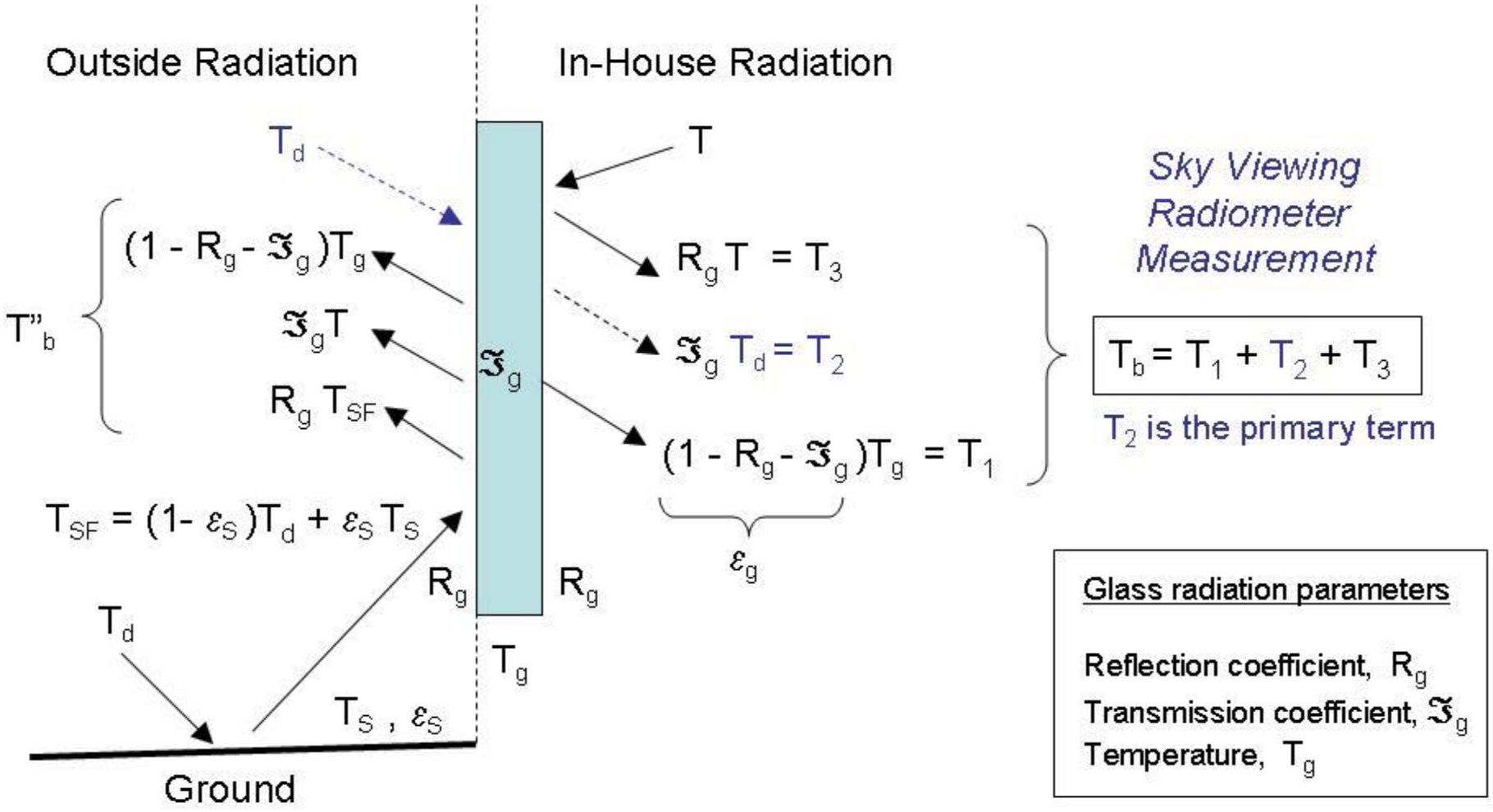

Figure 25 - Schematic of different brightness temperature, T_b, contributions seen inside my house by a radiometer viewing the sky through a glass window. Primary radiation seen outside my house is the downwelling atmospheric radiation T_d. Inside my house this term is attenuated by the glass door. It is denoted as T_2 and highlighted in blue. The other two quantities seen inside my house is the emitted, T_1, and reflected radiation T_3 by the glass.

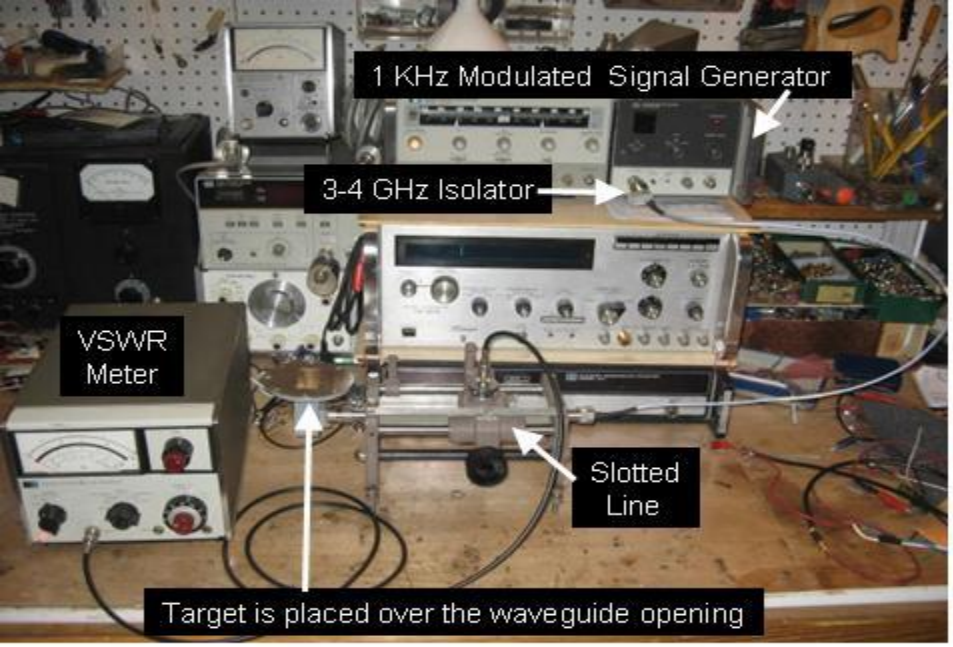

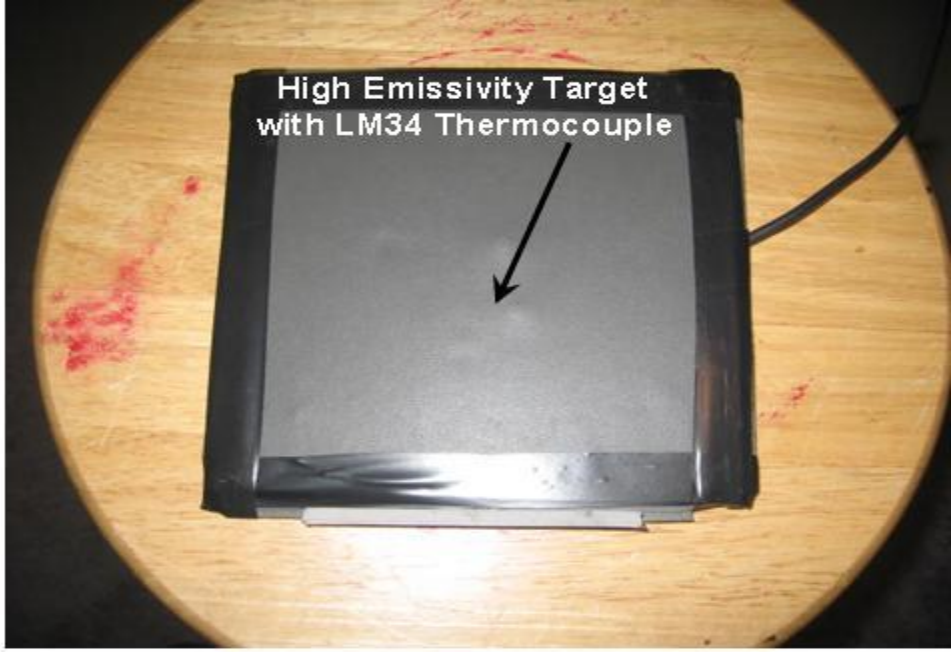

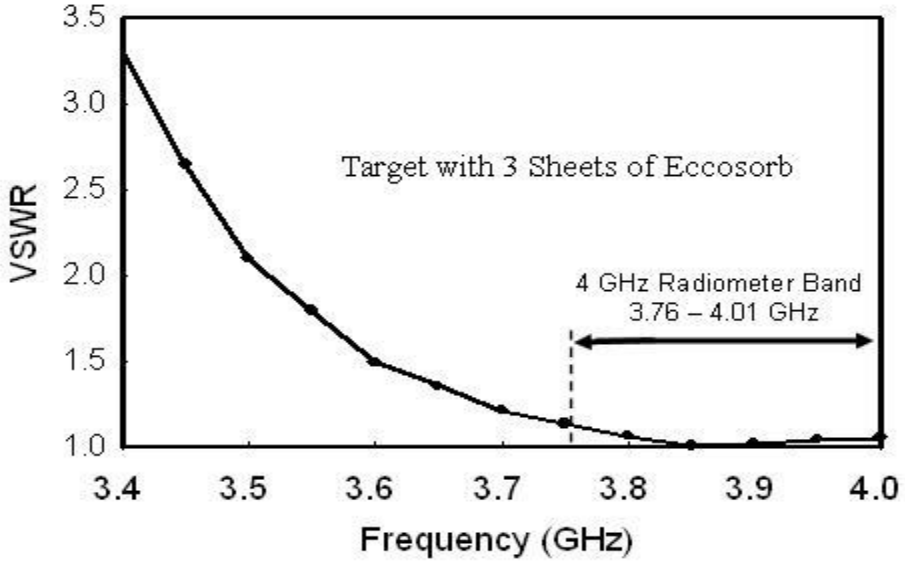

For calibrating the 4 GHz radiometer the target emissivity is determined by first measuring the VSWR using the slotted line, VSWR meter and signal generator. To minimize reflections between the slotted line and signal generator, a 3.2 – 4.2 GHz isolator is placed between the signal generator and slotted line. Shown is the setup used to measure the VSWR of the target using the slotted line and VSWR meter. Also shown is the target which uses 3 Eccosorb sheets glued together and backed with a metal plate. When calibrating the 12 GHz radiometer a similar setup is used except that a 8.2 -12.4 GHz isolator is used in place of the 3.2 – 4.2 GHz isolator.

$$|\Gamma| = \frac{VSWR - 1}{VSWR + 1} \quad where \quad \varepsilon_s = 1 - |\Gamma|^2 .$$

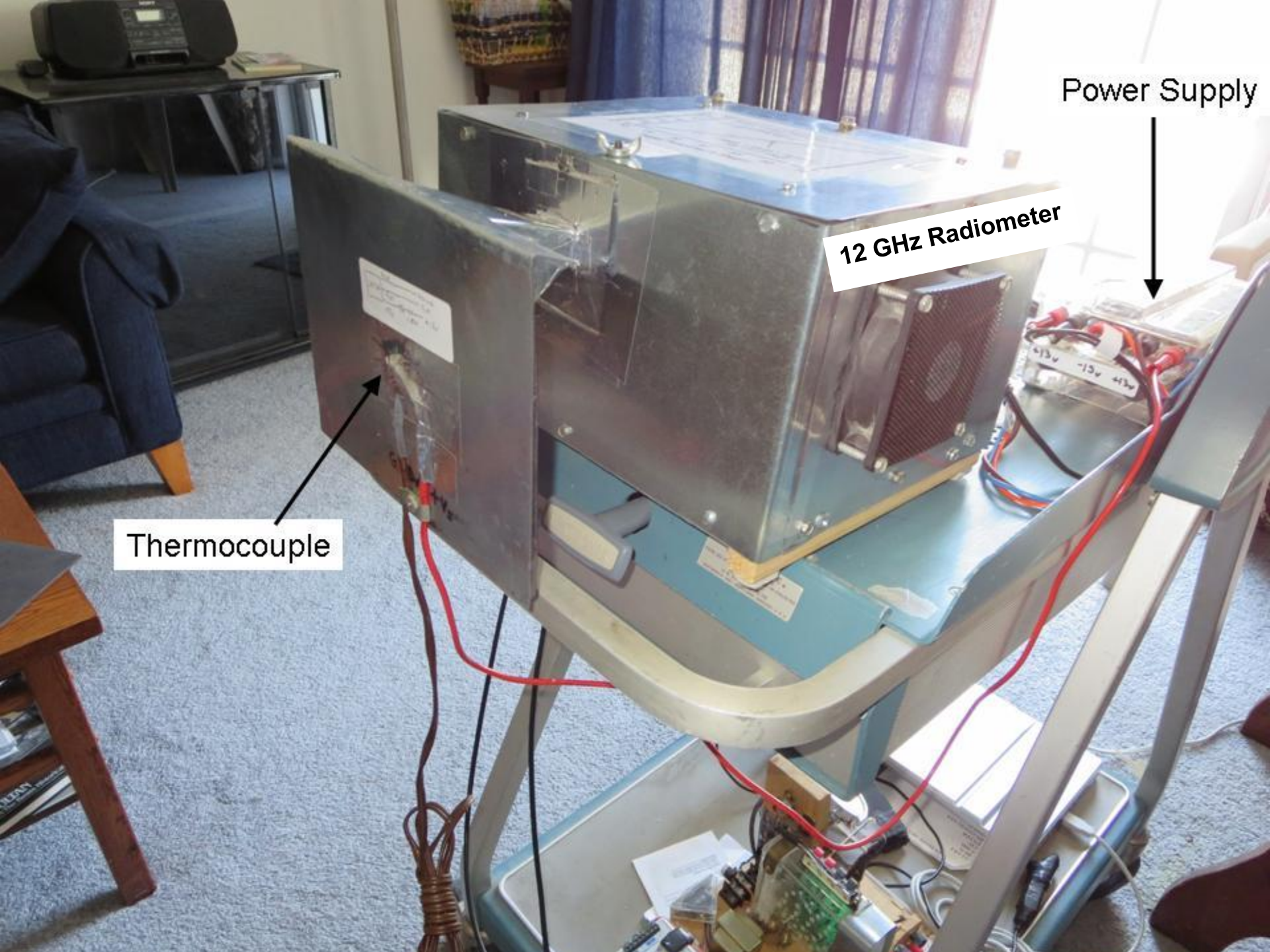
Power Supply
12 GHz Radiometer
Thermocouple

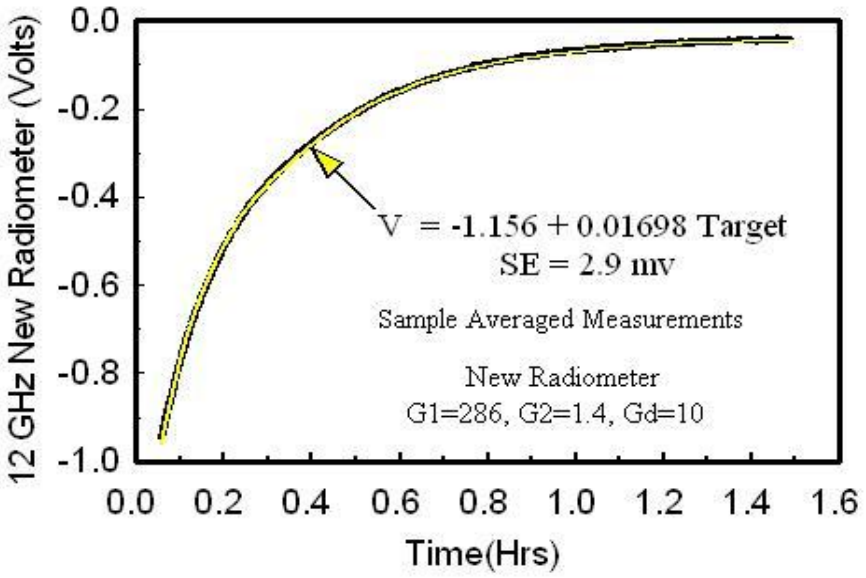

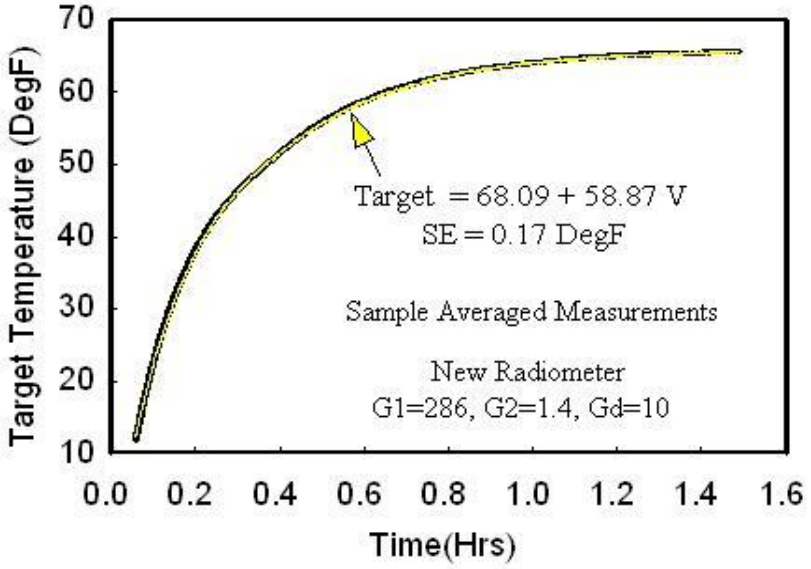

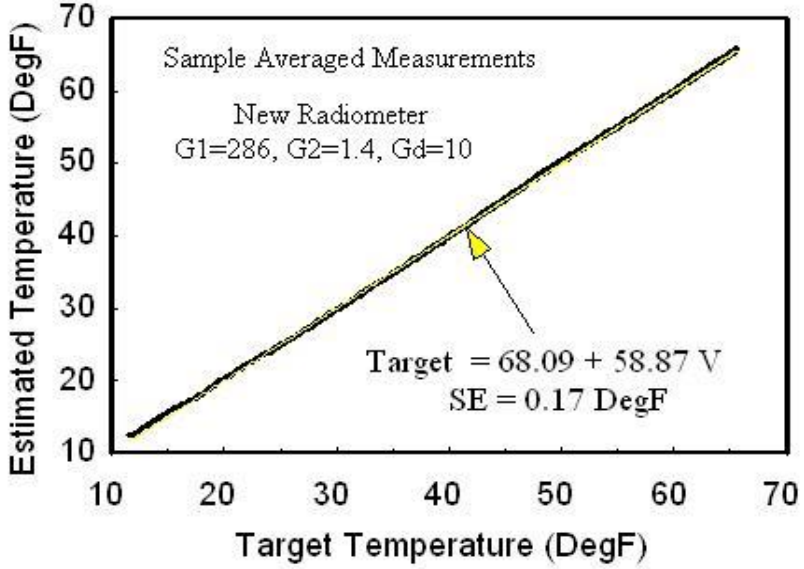

Calibration of 12 GHz radiometer using a high emissivity target.

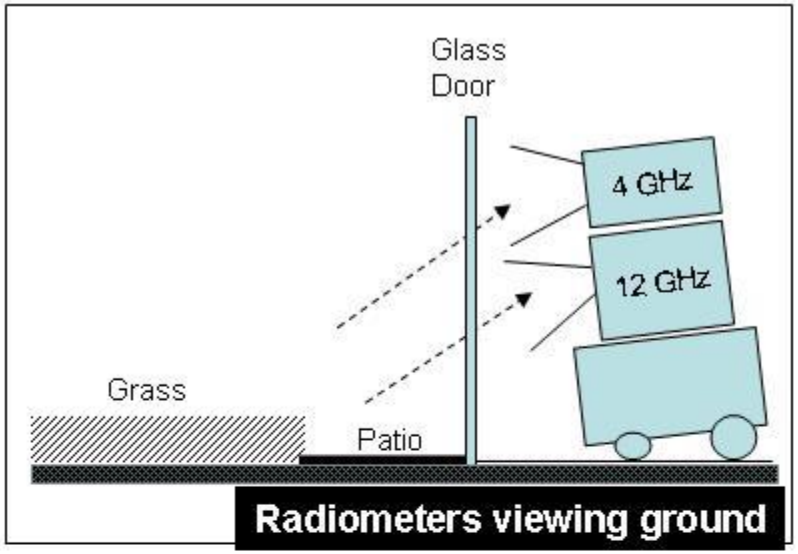

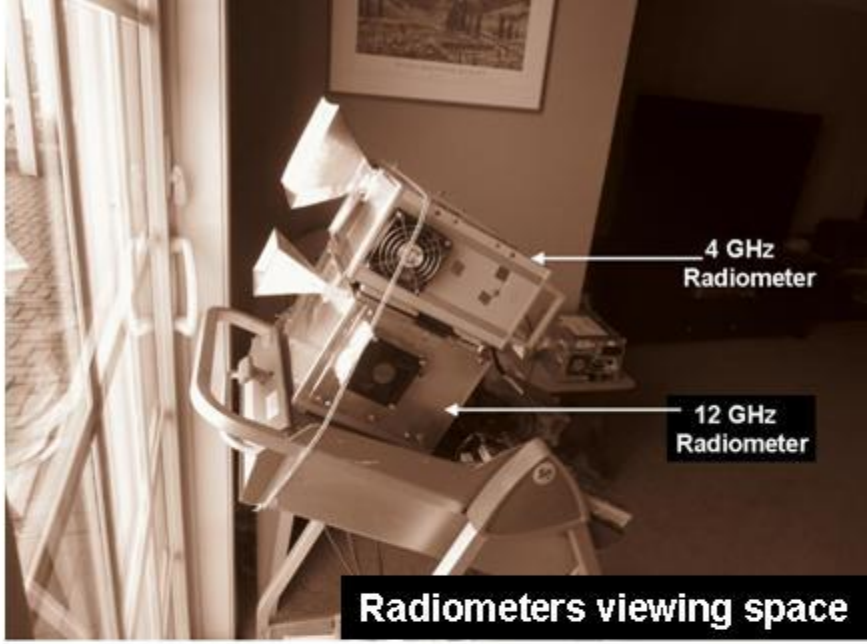

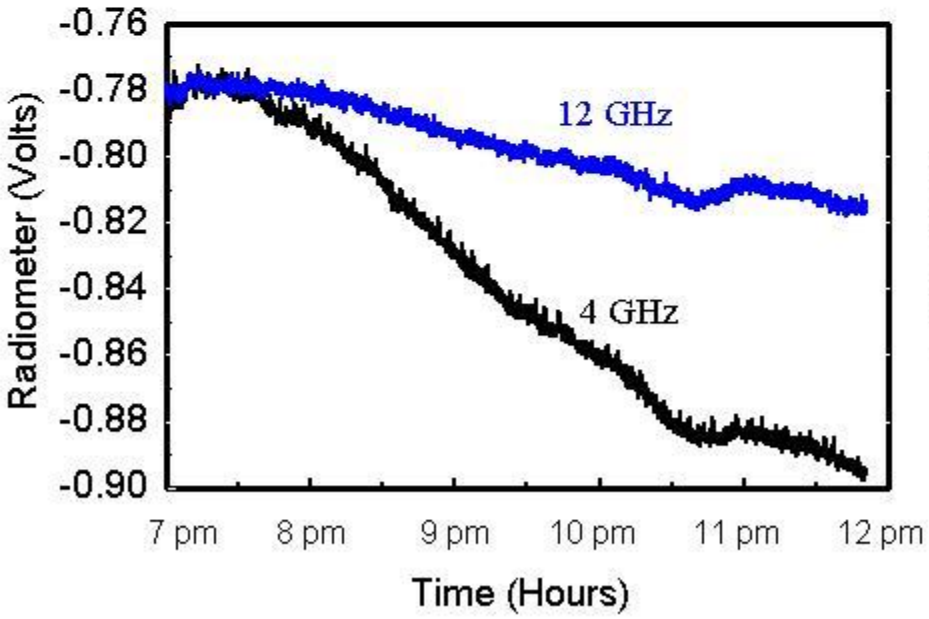

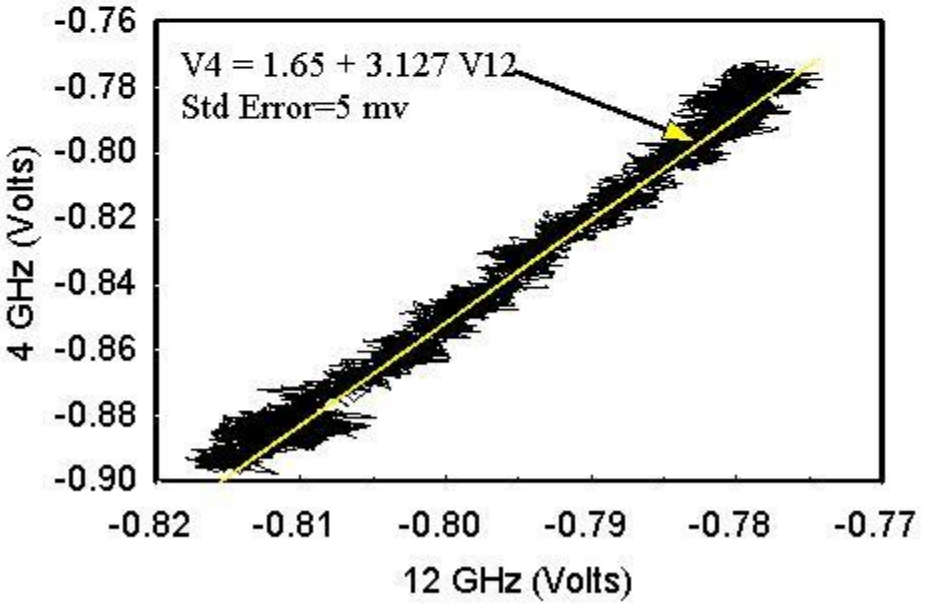

Variation of radiometer measurements (*i.e*, sfc temp) seen through glass patio door

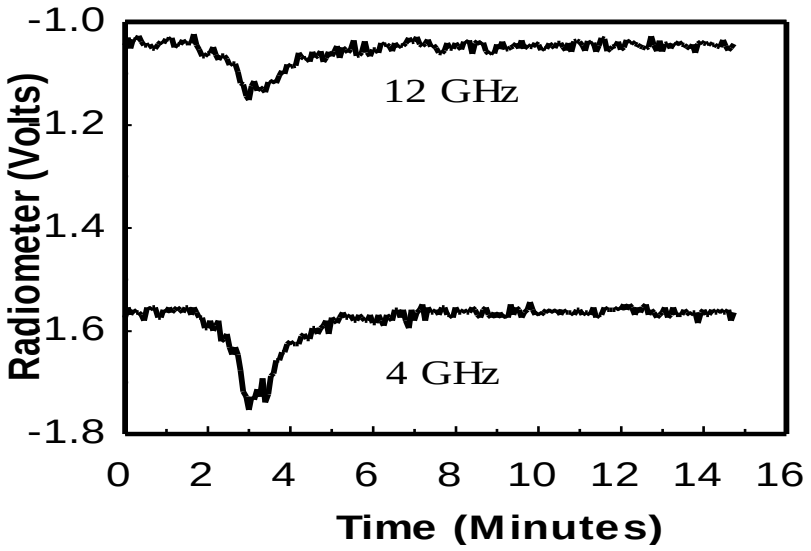

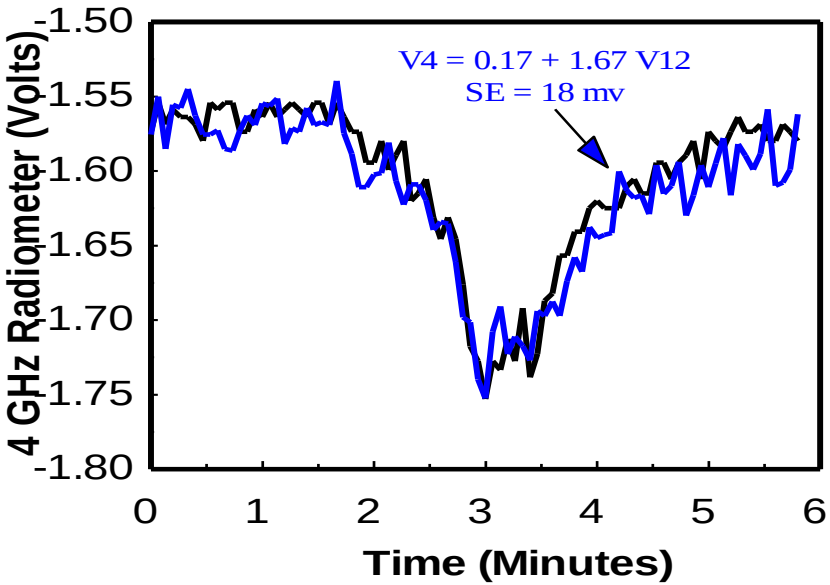

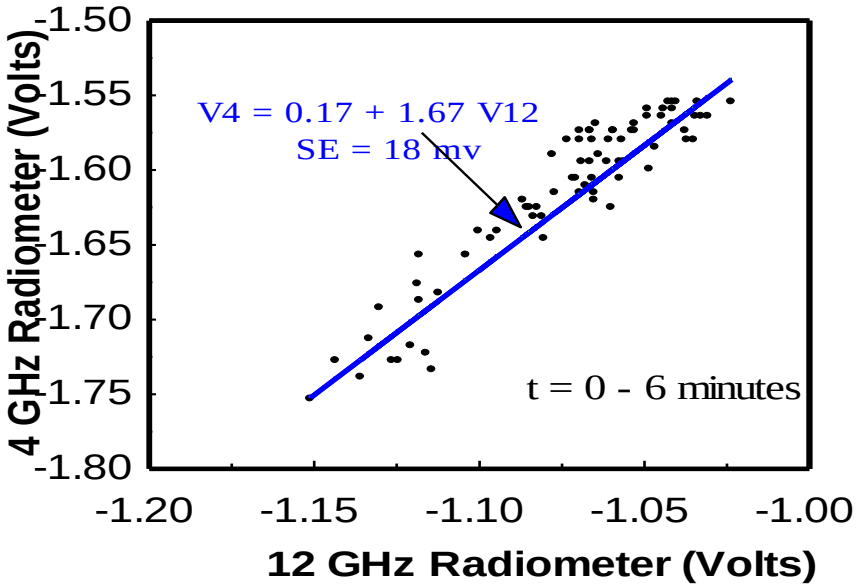

Top-right shows the patio and grass area after it was sprayed with water for about 2 minutes. Top left shows the 4 and 12 GHz radiometer measurements before and after watering. An expanded plot of 4 GHz data is shown in bottom-left. Also shown is the 4 GHz estimate using a best fit linear equation relating the 4 to 12 GHz measurements. The data along with the best fit equation is plotted in the bottom right display.

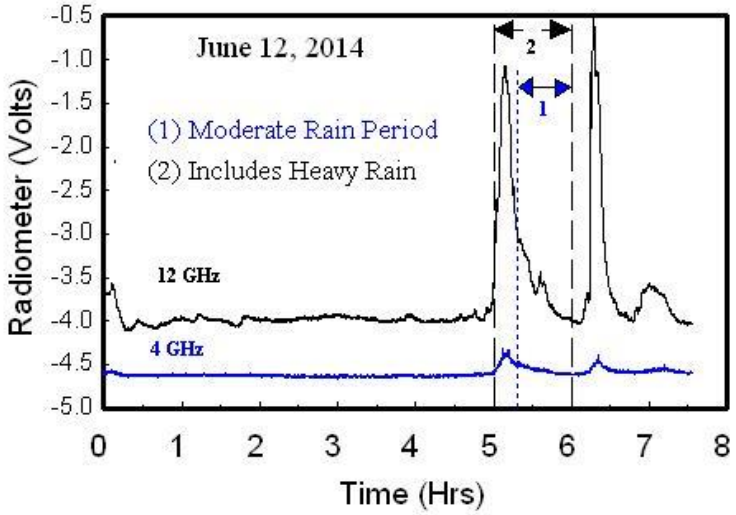

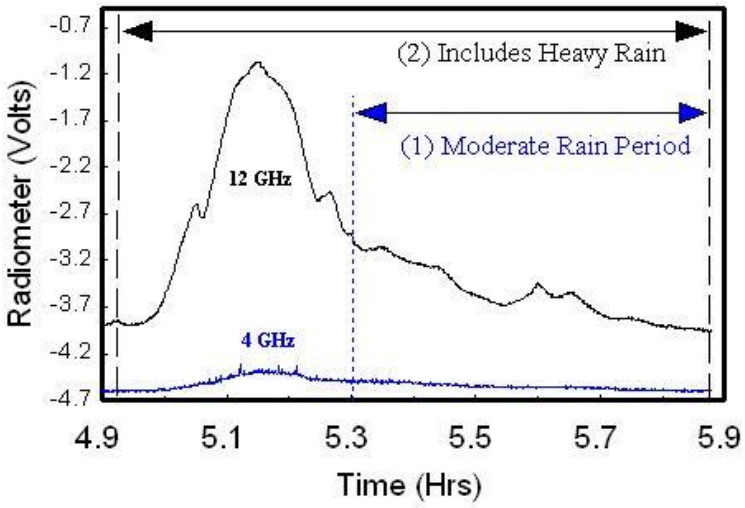

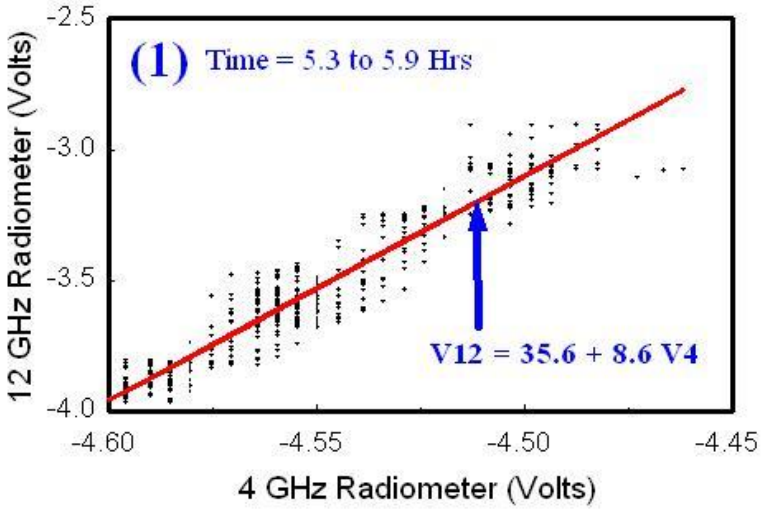

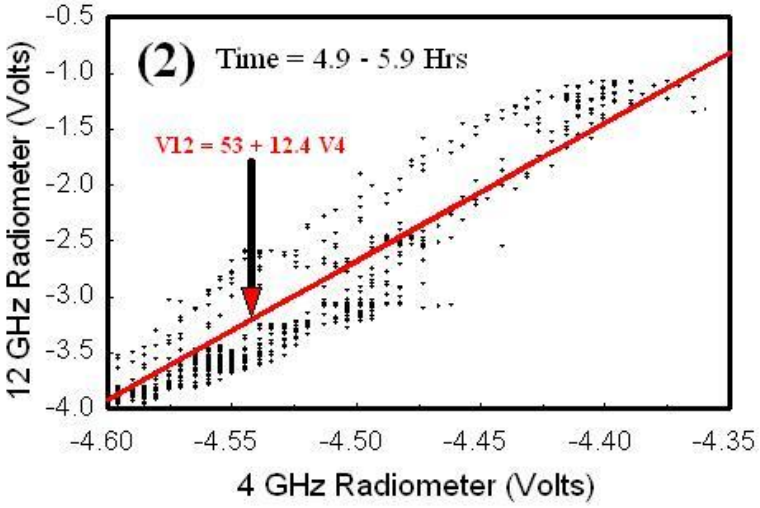

Top left plots the 4 and 12 GHz measurements over 8 hours beginning at 12pm on June 12. Two distinct rain events are seen between 5 and 7 pm, with the 12 GHz radiometer increasing from - 4 volts to less than -1 volt while the 4 GHz radiometer increases by only 0.2 volts. The top right plots the first rain event between 4.9 to 5.9 hours. During this time the bottom right shows the 12 GHz voltage increasing by a factor of 12.4 compared to 4 GHz. However, the bottom left shows the 12 GHz voltage only increases by a factor of 8.6 for the period containing widespread light rain between 5.3 and 5.9 hrs.

Rain Observed Through Glass Door

Heavy Rain at 8:15 AM

Rain Free at 10:00 AM

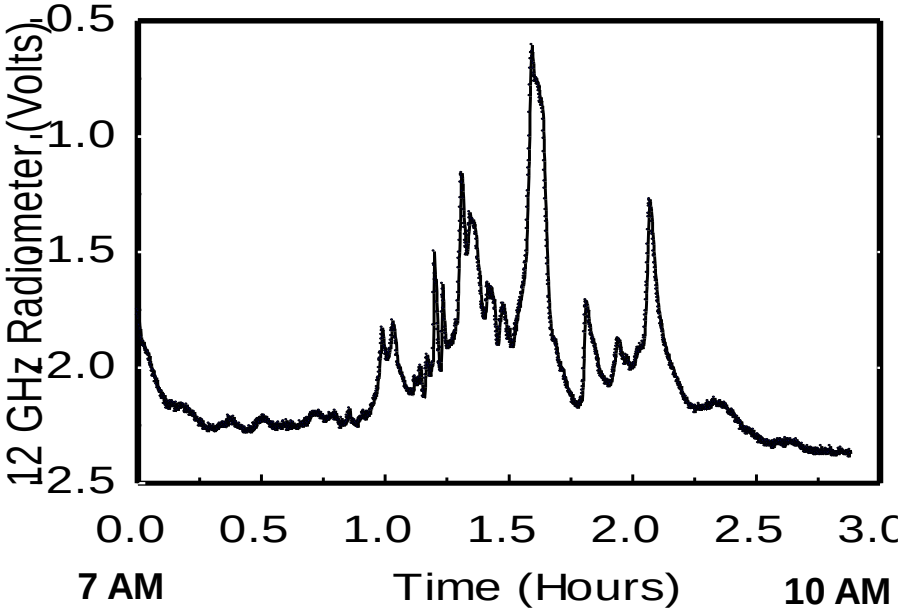

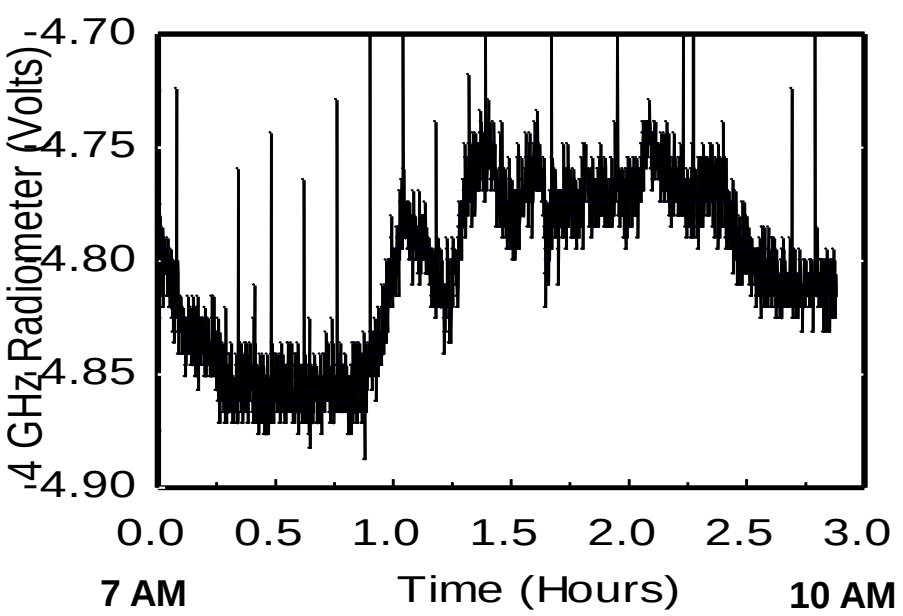

Radiometer data on Aug 1, 2013 during moderate rain at 7 AM, ending at 10 AM. The 12 GHz varies from -2.4 volts to -0.6 volts as rain increases while the 4 GHz increases from -4.87 to -4.75 volts. Spikes at 4 GHz is possibly due to radar scan.

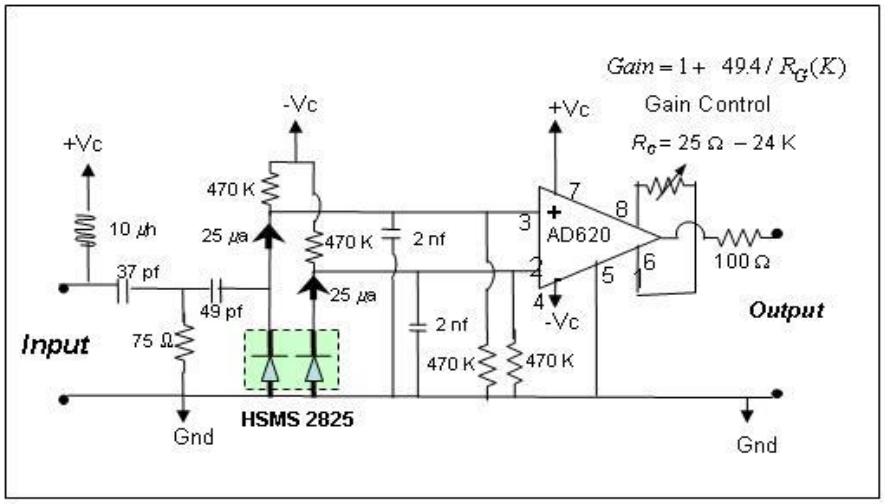

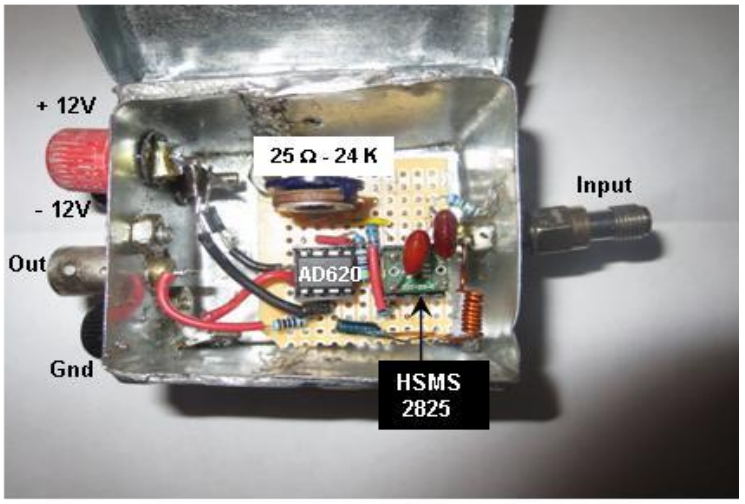

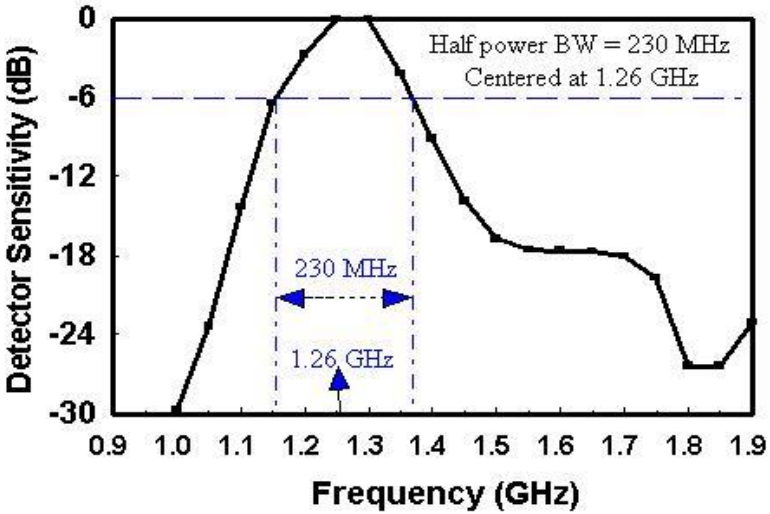

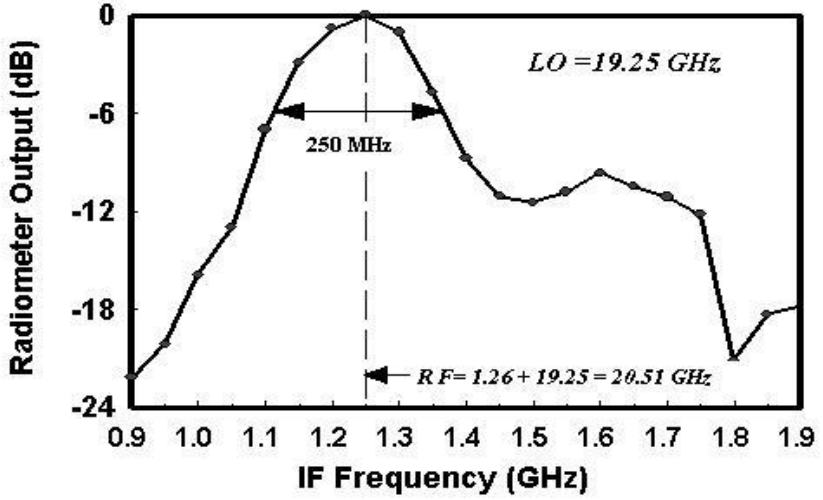

20 GHz radiometer uses a temperature compensated detector (top-right) similar to other radiometers. Its circuit (top-left) uses an AD620 difference amplifier with its gain set to 10 by setting R_G to 5.5 *K*. Its input uses a multiplexer circuit to power the LNB while passing the *IF* signal to the detector. The normalized detector sensitivity (bottom-left) peaks at 1.26 GHz with a 230 MHz bandwidth, while the normalized radiometer response (bottom-right) peaks at 19.25 GHz (*LO*) + 1.26 GHz (*IF*) = 20.51 GHz with a 250 MHz.

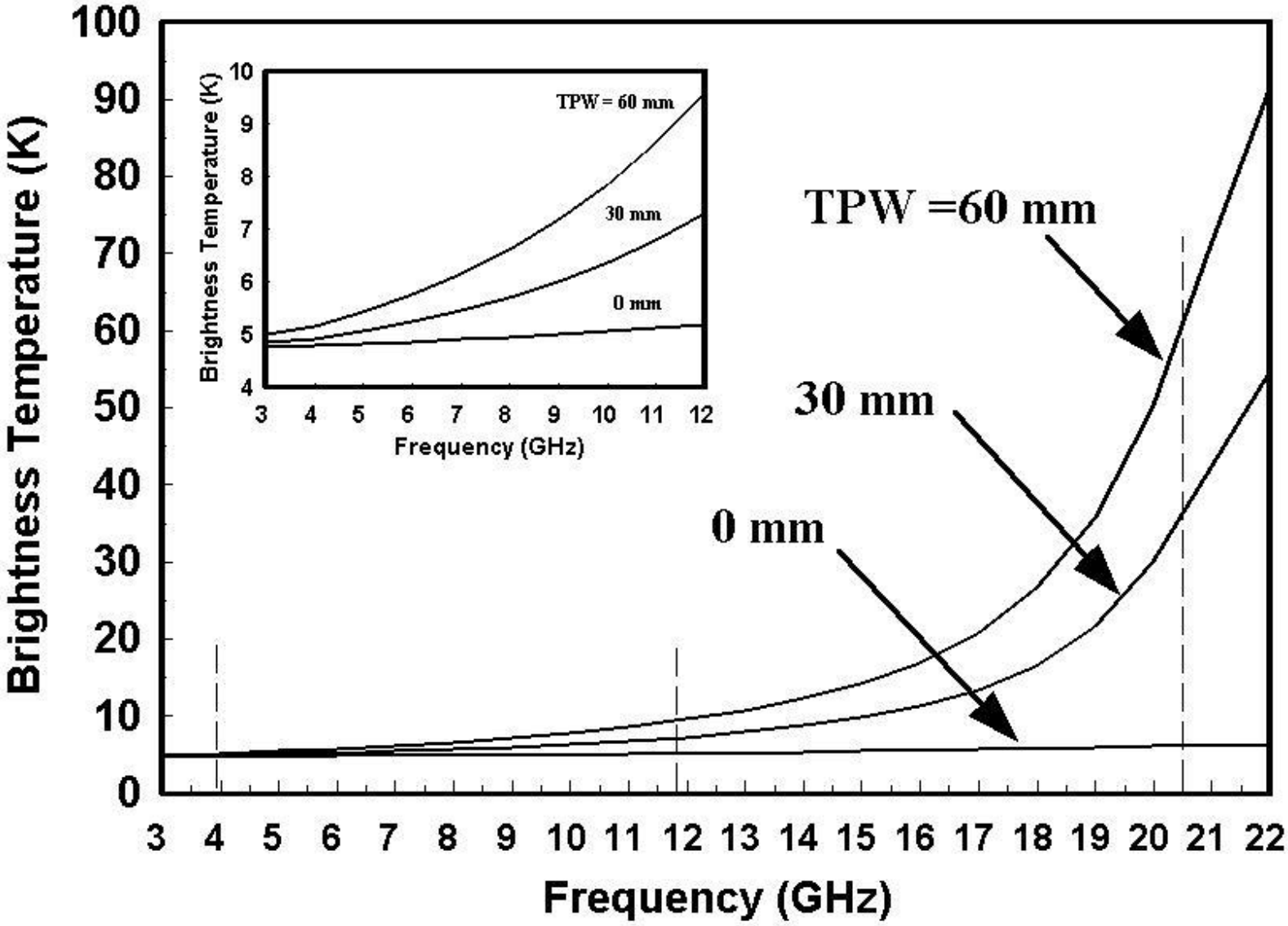

Simulated brightness temperature for cloud free atmospheres as a function of frequency for different amounts of water vapor (*TPW*). Vertical lines identify the center frequencies of the 4, 12 and 20 GHz radiometers which is at 3.9, 11.7 and 20.5 GHz, respectively.

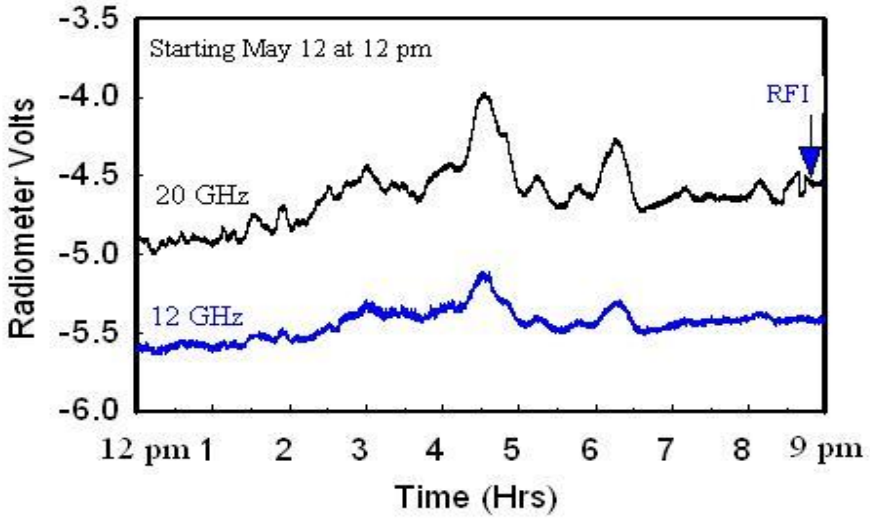

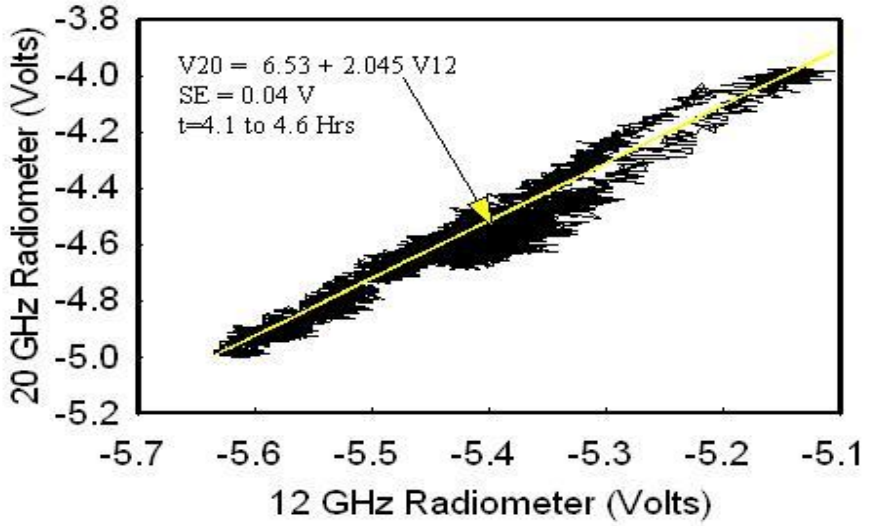

20 GHz and 12 GHz radiometers viewing clouds on May 12 between 12 pm and 9 pm (Top-Left). The best fit relationship between the 20 and 12 GHz is shown in the bottom left. Note that the 20 GHz response to clouds is about 2 times greater than at 12 GHz. Also note the onset of RFI disturbances begins at 9 pm at 20 GHz.

Clouds measured using 20 and 12 GHz radiometer on May 12, 2017 between 12 and 9 pm (Top-left). Cloud picture on top-right is at 4 pm, while bottom-left plots the 20 GHz against 12 GHz measurements between 4.1 to 4.6 hrs. Measurement ratio of 2.0 is the product of cloud transmittance and glass reflectivity factors.

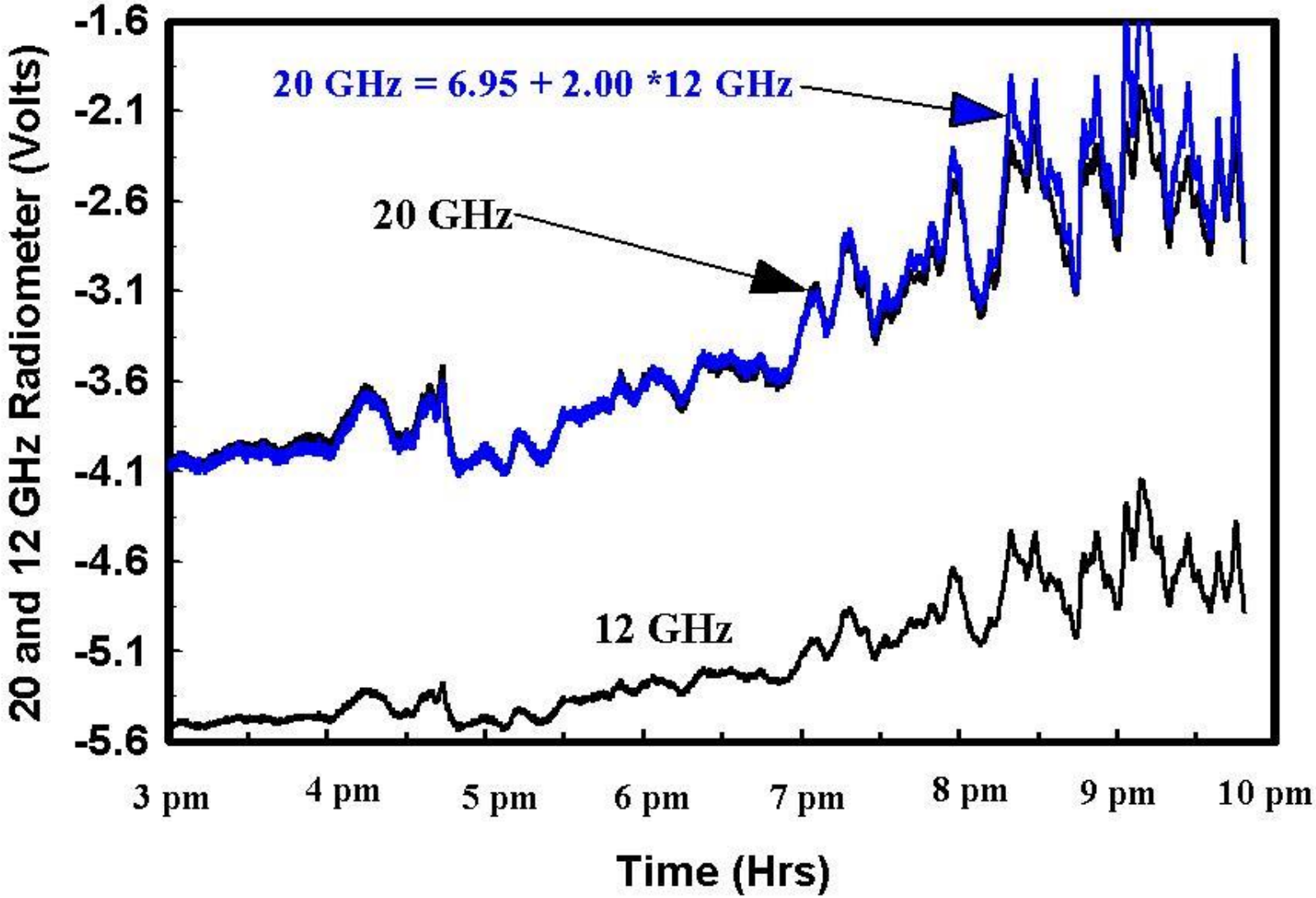

Upward viewing 20 and 12 GHz radiometer measurements on March 1, 2018 at which time there was light to moderate rain. Shown in blue is an estimate of the 20 GHz measurements using 12 GHz measurements. The 2.0 slope of the linear equation is the same ratio obtained from cloud measurements.

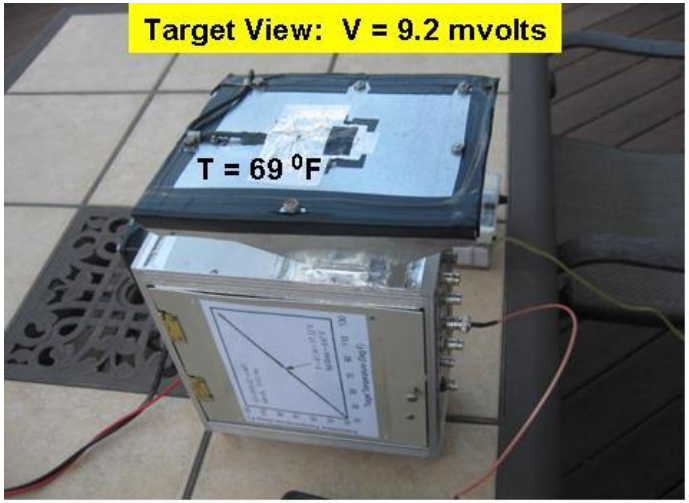

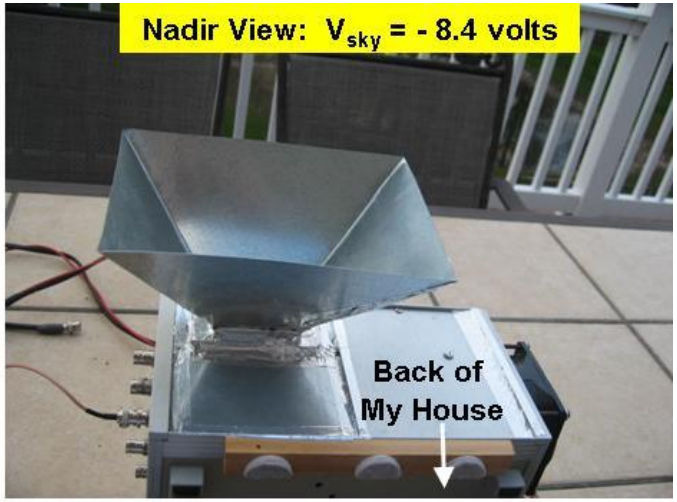

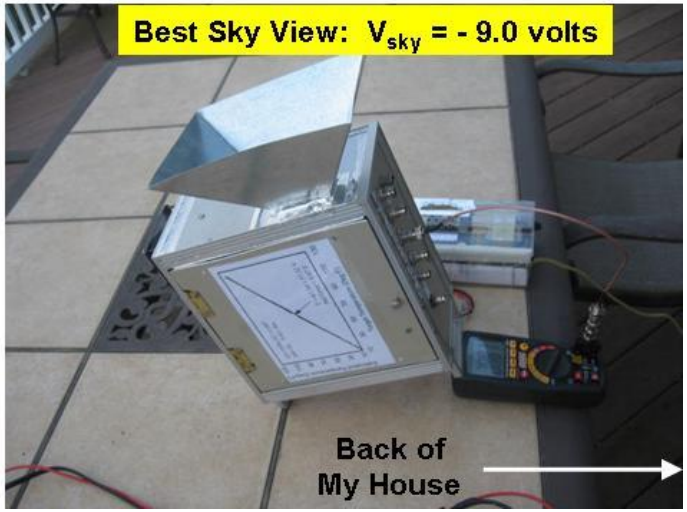

Low frequency (*i.e.*, 4 GHz) radiometers can be calibrated using clear sky measurements

Bottom-left shows 4 GHz radiometer taking sky measurements. Calibration begins by placing target over the antenna and setting radiometer output to zero volts by adjusting its fine offset (Top-Left). Top-right shows a sky measurement of -8.4v at nadir viewing while bottom-right shows it reduced to -9.0v by rotating antenna by 90 degrees and directing antenna away from my house. Target temperature is 69 ^{0}F so that assuming the sky radiation is 2.7 *K* (-455 ^{0}F), the radiometric gain becomes (455+69)/9 = 58.2 ^{0}F/V.

High frequency radiometers is best calibrated using the Tipping Curve procedure

Tipping curve absorption measurements made in 1946 by Dr. Robert Dicke along with his associates. Starting on the Left is E. Beringer, R. Kyhl, A. Vane and R. Dicke. This picture is in the MIT Rad Lab Book "Five Years". It shows Dicke holding up an absorber in front of one of his radiometers while a chart recorder on the ground plots the measurements. Measurements were made on top of an MIT building.

April 4, 2019

20.5 GHz Radiometer

Tipping Curve Procedure for Calibration and Opacity Measurements

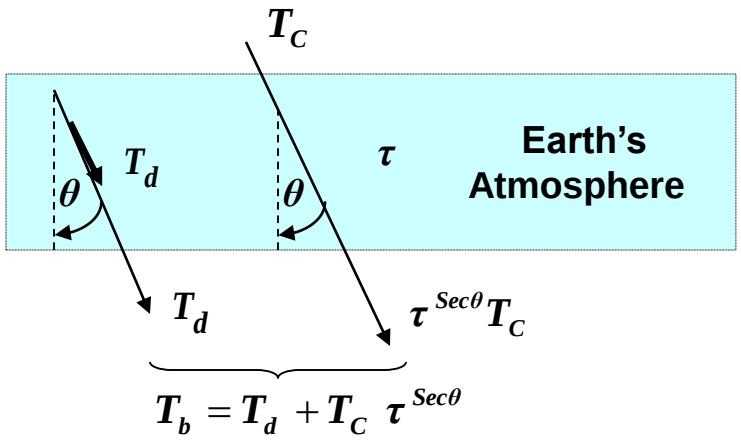

$$T_d = (1-\tau^{Sec\theta})\,T_M, \quad T_M \approx 285\ K$$

so $$T_b = (1-\tau^{Sec\theta})\,T_M + \tau^{Sec\theta} T_C$$

1. Calibration:

$$T_b = I + SV \qquad V = V_0 + V_1\ Sec\theta$$

$$T_b = T_C \ \ at\ \ V=V_0\ ,\ \ T_b = T_W \ \ at\ \ V=V_W$$

$$S = \frac{T_W - T_{CB}}{V_W - V_0}, \qquad I = T_W - S V_W$$

2. Opacity:

$$\tau = e^{-\alpha} \quad \text{so that} \quad \alpha = -\frac{d\,ln[T_M - T_b(\theta)]}{d\,Sec\theta}$$